PLASMA DYNAMICS

X. PLASMA DYNAMICS

Academic and Research Staff

Prof. William P. Allis
Prof. George Bekefi
Prof. Abraham Bers
Prof. Sanborn C. Brown
Prof. Sow-Hsin Chen
Prof. Flora Y. F. Chu
Prof. Bruno Coppi
Prof. Thomas H. Dupree
Prof. E. Victor George
Prof. Elias P. Gyftopoulos
Prof. Hermann A. Haus
Prof. Lawrence M. Lidsky
Prof. James E. McCune
Prof. Peter A. Politzer
Prof. Dieter J. Sigmar
Prof. Louis D. Smullin
Prof. Robert J. Taylor
Dr. Edward G. Apgar
Dr. Bamandas Basu
Dr. Giuseppe F. Bosia
Dr. Gradus J. Boxman
Dr. Bert C. J. M. DeKock
Dr. J. Michael Drake
Dr. Giampietro Lampis
Dr. Bernard J. Meddens
Dr. D. Bruce Montgomery*
Dr. Arnoldus A. M. Oomens
Dr. Lodewyk Ornstein
Dr. Ronald R. Parker
Dr. Francesco Pegoraro
Dr. Leonardo Pieroni
Dr. Arthur H. M. Ross
Dr. Sergio Segre
Dr. R. Van Heijningen
Dr. Gregory N. Rewoldt
Dr. Duncan C. Watson
John J. McCarthy
William J. Mulligan
Allan R. Reiman

Graduate Students

Charles T. Breuer
Leslie Bromberg
Natale M. Ceglio
Frank W. Chambers
Hark C. Chan
Franklin R. Chang
Paul W. Chrisman, Jr.
John A. Combs
Donald L. Cook
David A. Ehst
Nathaniel J. Fisch
Alan S. Fisher
Jay L. Fisher
Alan R. Forbes
Ricardo M. O. Galvao
Keith C. Garel
Ady Hershcovitch
Steven P. Hirshman
Michael K. O. Holz
James C. Hsia
Dennis J. Huber
Mark D. Johnston
David L. Kaplan
Charles F. F. Karney
Peter T. Kenyon
David S. Komm
Craig M. Kullberg
John L. Kulp, Jr.
Ping Lee
Francois Martin
Mark L. McKinstry
John L. Miller
Paul E. Morgan
Thaddeus Orzechowski
David O. Overskei
Aniket Pant
Louis R. Pasquarelli
Gerald D. Pine
Robert H. Price
Donald Prosnitz
Burton Richards
Paul A. Roth
Michael D. Stiefel
David S. Stone
Miloslav S. Tekula
David J. Tetrault
Kim Theilhaber
Alan L. Throop
Ben M. Tucker
Ernesto C. Vanterpol
Marcio L. Vianna
Yi-Ming Wang
Charles W. Werner
David M. Wildman
Stephen M. Wolfe

*Dr. D. Bruce Montgomery is at the Francis Bitter National Magnet Laboratory.

X. PLASMA DYNAMICS

A. Experimental Studies – Waves, Turbulence, and Radiation

1. NEUTRAL BEAM INJECTION SYSTEMS

U. S. Energy Research and Development Administration (Contract E(11-1)-3070)

Louis D. Smullin, Leslie Bromberg, Peter T. Kenyon

Introduction

The hopes of confined thermonuclear reactor systems are now focused primarily on Tokamak toroidal machines. The initial production and heating in these machines is done by transformer coupling of large circulating currents into the toroidal chamber. The plasma can be heated, in principle, to 2-3 keV temperatures. The limit is imposed by the rapidly increasing plasma conductivity with T_e, and by the limit on circulating current imposed by the onset of gross MHD instabilities. Thus, to achieve reactor temperatures of 5 keV or so, supplementary power sources are needed. A major candidate for this role is high-power neutral beam injection. Beams of deuterium at energies of 100-200 keV and energy fluxes corresponding to tens of amperes are required. In a full-size reactor a number of these beams would be injected into a single machine. The research reported here is aimed at developing the components necessary to produce such beams. We have concentrated on one problem, building efficient plasma sources from which to extract high-current positive ion beams (H^+ or D^+).

Such devices have been built in several laboratories and are now in experimental use. The most successful is the multifilament arc developed at Lawrence Berkeley Laboratory.[1] It has produced beams of 50 A with good focusing properties. Other schemes are the duo-PIGatron[2] and the MATS.[3] These have been limited to 5-10 A currents. The properties that make a good source are the following.

Plasma density $\approx 10^{12}$/cc over an area of 100-200 cm^2 with uniformity of ~5-10%.

Quiescent operation. The level of density fluctuations arising from oscillations or instabilities should be low ($\leq$1%) and the random transverse ion energies should be below 1-5 V.

Neutral density at the exit plane should be low in order to avoid interference with later elements of the beam systems; charge exchange cells, etc. While lower density is desirable, 5-10 mT is acceptable.

Power efficiency. The power dissipated should be low in order to simplify the problems of heating and thermal distortion of the extraction grid system.

The existing systems have specific power input of 1-5 kW per extracted beam ampere. Thus the multifilament arc requires an input power of 1/4 MW to sustain a 50 A beam. Our work has been concentrated on finding a more efficient system that meets all other criteria.

Behavior of Plasma Sources

A plasma source requires a power input system to ionize the neutral gas and sustain all of the plasma losses as well as the extracted current. Since it is desirable to sustain long pulses (>1/4 s) or dc operation, the two energy sources that we envision are electron beams or RF power. We have chosen to concentrate on hot-cathode low-pressure (1-10 mT) discharges, as have our predecessors. The factors that influence specific power input are the efficiency of energy transfer to the plasma, and the losses of plasma caused by diffusion to the walls and volume recombination (negligible because of low pressure). Since the chamber has only one wall through which ions are extracted, the other 5 walls (of a cube) represent substantial loss areas. We are studying a magnetic confinement system that substantially reduces these wall losses. Simple, axial magnetic fields are unsatisfactory because of flute instabilities that plague all plasma discharges (they appear to set limits to the performance of the MATS and duo-PIGatron sources).[3] Our system uses a multipole field to reduce lateral wall losses. This produces a radial minimum $|B|$ field that is MHD stable. In order to prevent leakage to the back wall and to launch the electron beam, we superpose a diverging solenoid field. Figure X-1 shows the basic configuration. The lateral field is produced by ceramic magnets arranged to be periodic in θ and uniform along the axis (θ-cusp). The combination of this field with that of the solenoid gives a pattern with $|B|$ increasing radially and

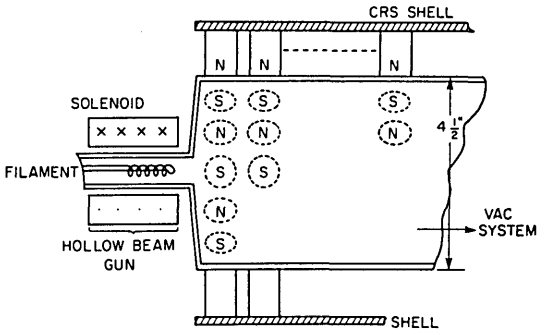

Fig. X-1. Periodic magnet discharge chamber.

toward the back – there is a broad valley toward the extraction plane. Over the area of the extraction plane the field must be small (a few gauss) so as not to interfere with the beam focusing. The high θ-periodicity (12 Indox-5 magnets (7/8 "ϕ × 1", 7" long) around the circle) gives a field that decays as r^5/a^5 and falls to 25 G within 1" of the magnet circle.

We have chosen to inject our beams from cylindrical cathodes, emitting radially as in a magnetron. We expect that relatively large emitting areas will be available from

fairly compact structures, and there may be advantages in terms of reduced ion bombardment damage. Both oxide-coated, unipotential cathodes and spiral tungsten cathodes have been used. As long as operation is in the space-charge-limited regime we see no gross qualitative differences in behavior. Oxide cathodes require only ~1 W/A of electron current at densities of 1 amp/cm^2. Tungsten requires approximately 100 W; on the other hand, it is relatively immune to poisoning and may be opened to air, and therefore has obvious experimental advantages.

We have made some preliminary tests with indirectly heated hollow cathodes and plan to study them, as well as shielded cathodes used in H_2 thyratrons. These may offer advantages in terms of resistance to ion bombardment damage, and also the possibility of operation at higher impedance levels. Thus a given power input will be achieved with higher V_a and lower I_a. If the specific power is the same as that for conventional cathodes, the cathode size needed for full-power operation, where 100-200 A of cathode current may be required from a magnetron cathode, will be reduced.

Theoretical Status

The hot-cathode low-pressure arc is still terra incognita despite Langmuir's observations and correct hypothesis in 1924. There is no closed theory that permits calculation of the V-I characteristics of such a discharge. Experiments by Druyvestyn[4] and Emeleus[5] clearly prove Langmuir's hypothesis that the coupling between the electron beam entering the plasma is by induced plasma oscillations. The nonlinear theory of the formation of the so-called meniscus and transfer of beam energy to plasma electrons is still largely unexplored. The doctoral thesis of J. A. Davis showed by numerical simulation what happens[6] and research by Vianna[7] opens up a better analytical understanding of the subject. In real geometries, with superposed magnetic fields, there is still no usable theory. The loss through magnetic cusps presents a difficult problem, and although there is an extensive literature on cusps, we have not found an easily applicable theoretical formulation.

Experimental Program

We have built two essentially identical systems (Fig. X-1). The cathode is mounted within the tube (1 3/4" diam) under the solenoid and the beam enters the chamber (4 1/2" diam). Near the cathodes an antenna picks up relatively intense oscillations in the 1-3 GHz range, depending on arc power, etc. Thus far, in our experiments we have produced plasmas up to 10^{11} cm^{-3} density in neutral gas atmospheres of 5-10 mT of H_2. The plasma, viewed from the end opposite the cathode has a relatively uniform core (~8 cm diam) surrounded by a series of sharp radial spokes going out to the center of each magnet line. Figure X-2 is a tracing of the current to a probe at the wall, as the

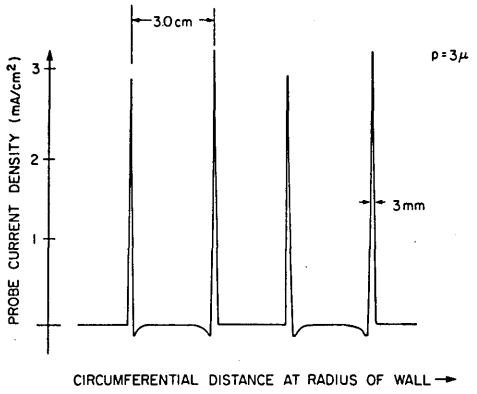

Fig. X-2.

Grounded probe current next to the wall, under permanent magnet system. Probe dimensions: length 1/8", diameter .010".

magnets are rotated past it. The sharp concentration of the plasma within the cusp is striking. The light radiated by the plasma shows the same sharp cusp geometry.

Figure X-3 is a plot of the saturated ion current to a probe moved across the plasma showing the radial variation of plasma density.

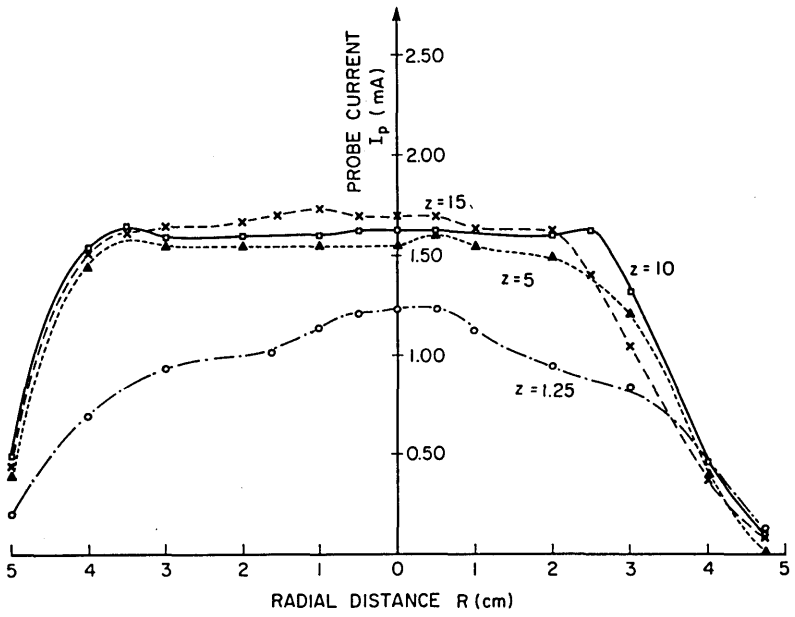

Fig. X-3. Saturated positive ion current to a 1/2 cm^2 probe at various positions (z = distance (cm) from the cathode). P = 8μ, B = 80 G, B_{SOL} = 80 G.

Figure X-4 shows the plasma density on the axis as a function of arc power for several different cathode geometries. All data represent space-charge-limited operation of the cathode. Data below 150 W represent dc operation of the arc. For higher

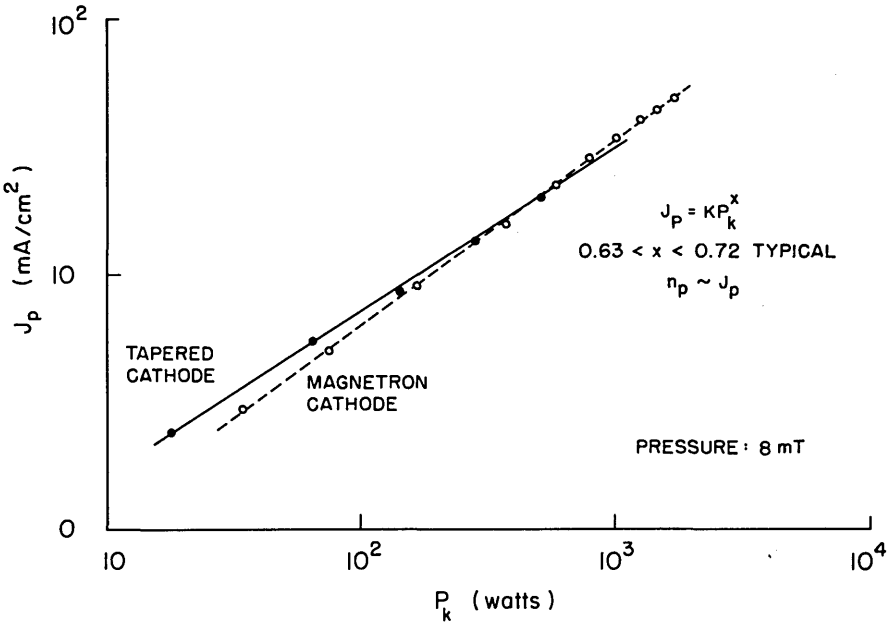

Fig. X-4. Saturated positive ion current density vs input arc power. Probe located on center line about 6" from cathode. Magnetron cathode 1/2" diam × 3/4" long. Tapered cathode D_{max} = 7/8", D_{min} = 1/2" × 1" long.

powers we used a 250 μs pulse at approximately 5 per second in order to avoid problems of power dissipation. Empirically, the various geometries show a variation $I_P \sim P_A^X$, $0.75 < X < 0.65$. If the cathode operated under constant perveance conditions, $I_A = KV_A^{3/2}$, and if $I_P \sim I_A$, we would expect $I_P \sim P_A^{0.6}$. Neither of these conditions is met precisely in our experiments, but the agreement is suggestive of a scaling law to predict operation at higher power levels and plasma densities.

In low-pressure discharges, the ionization is largely due to energetic plasma electrons rather than the relatively monoenergetic primary beams. Figures X-5 and X-6 show the V-log I plots taken from Langmuir probe curves indicating the dual-temperature nature of the plasma at varying distances from the cathode and for temperature-limited and space-charge-limited operation. The space-charge-limited operation produces a much hotter tail (30-40 eV) than does the temperature-limited condition, and the resulting plasma density is approximately twice as great for equal input powers. The applied arc voltage is ~90 V for the space-charge-limited case, but there seems to be no trace of the original primary electrons in the resulting distribution function. At greater distances from the cathode, the ratio of hot to cold electrons decreases. This is consistent with our model in which plasma heating occurs via beam-plasma oscillations in the region just outside the cathode sheath.

The self-excited beam-plasma oscillations are presumed to be responsible for the

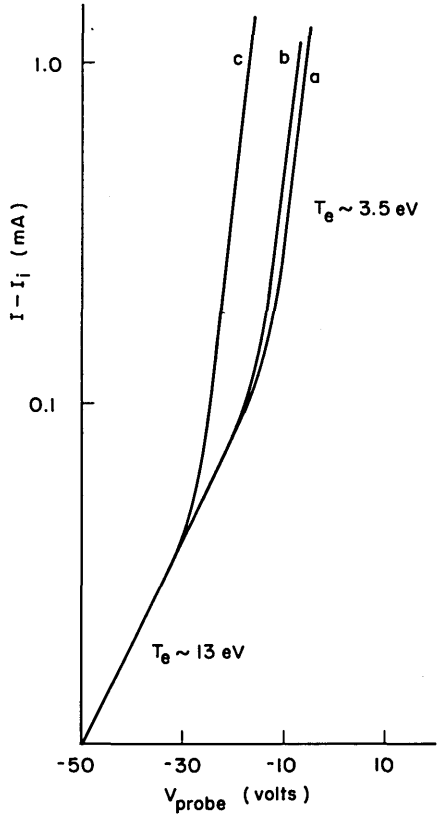

Fig. X-5.

"Electron-temperature" plot log (I_p-I_{sat}) vs V_{probe} showing two temperatures at various distances from the cathode. A temperature-limited tungsten filament was used for the cathode. Operation: 240 W, 240 mA; p = 4μ. Distance from cathode: a = 2", b = 5", c = 8".

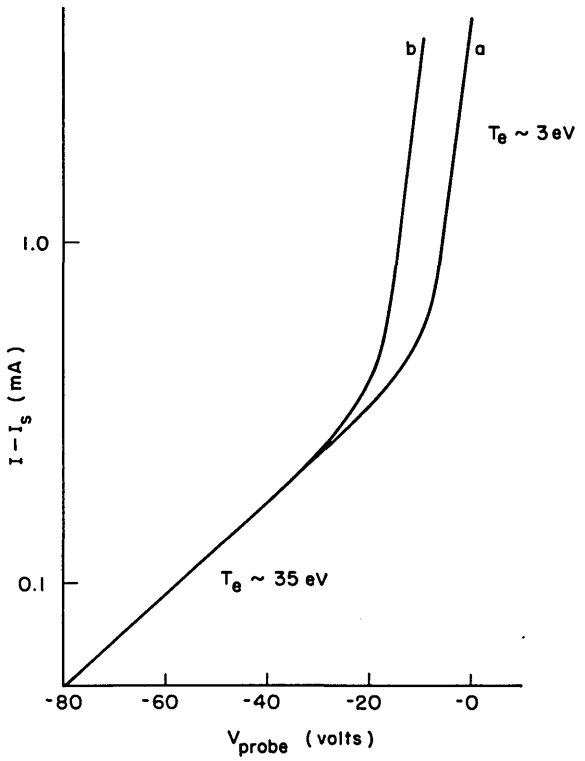

Fig. X-6.

"Electron-temperature" plot log (I_p-I_{sat}) vs V_{probe} showing two temperatures at various distances from the cathode. A space-charge-limited tungsten filament was used for the cathode. Operation: 900 mA, 90 V; p = 4μ. Distance from cathode: a = 5", b = 8".

high-voltage tail in the distribution function. A preliminary experiment was made, correlating the emitted RF spectrum with arc conditions. Figure X-7 shows the power detected by a probe near the cathode, displayed on a microwave spectrum analyzer.

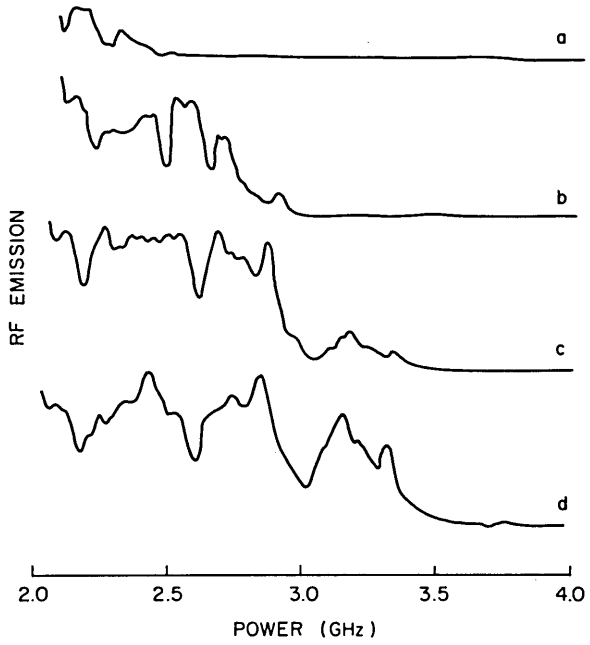

Fig. X-7. Microwave power spectrum from discharge showing increase of the upper frequency limit with increased arc power. (Image rejection preselection was not used in these tests.) Operation: a = 400 mA, 120 V; b = 600 mA, 170 V; c = 800 mA, 230 V; d = 1000 mA, 270 V.

The spectrum is complex and cannot be defined by a single emission at "ω_p". There is a more or less continuous emission up to a highest frequency. This highest frequency is seen to increase with arc power. Density measurements at the output plane scale approximately with the high-frequency cutoff of the spectrum.

References

1. K. H. Berkner et al., "Neutral Beam Development and Technology: Program Plans and Major Project Proposal," Lawrence Livermore Laboratory Proposal 115, September 1974.
2. R. C. Davis et al., "The Duo-PIGatron II Ion Source," Report ORNL-TM-4657, August 1974.
3. Proceedings of the Second Symposium on Ion Sources and Formation of Ion Beams, Berkeley, California, 1974.
4. M. J. Druyvestyn, Z. Physik 64, 790 (1930).

5. D. W. Mahaffey and K. G. Emeleus, J. Electron. Control 4, 301 (1958).

6. J. A. Davis, "Computer Models of the Beam-Plasma Interaction," Ph.D. Thesis, Department of Electrical Engineering, M. I. T., 1968; also J. A. Davis and A. Bers, "Nonlinear Aspects of the Beam-Plasma Interaction," Proceedings of the Symposium on Turbulence of Fluids and Plasmas, Polytechnic Institute of Brooklyn, April 16-18, 1968 (The Polytechnic Institute of Brooklyn Press, 1969), pp. 87-108.

7. Marcio L. Vianna, "Theory of Beam Plasma Interaction in a Longitudinal Density Gradient," Ph.D. Thesis, Department of Physics, M. I. T., May 1975.

2. EXTERNALLY INDUCED "STRONG TURBULENCE"

National Science Foundation (Grant ENG75-06242)

Ady Hershcovitch, Peter A. Politzer

Introduction

Quasi-linear theory and strong turbulence theory are used to extend Dupree's perturbation theory for strong plasma turbulence,[1] in order to include the case where turbulence is induced externally.

First, the Vlasov equation is solved for the coherent response $f_k(\underline{v}, t)$ of an infinite homogeneous magnetized plasma to an oscillating electric field E_k. Second, the diffusion coefficients arising from oscillating electric fields are computed by using quasi-linear theory to compute the diffusion coefficients from the external fields, and strong turbulence theory to compute the diffusion coefficients from the self-consistent (internal) fields. Third, the dispersion relation for a magnetized plasma in the presence of external oscillating electric fields is derived. Finally, the dispersion relation is used to investigate the possibility of experimental stabilization of instabilities in a counter-streaming electron beam system.

The physical model is the following. When an instability develops, particles are either trapped or bunched. The external turbulent fields scatter particles incoherently. If these particles are scattered at a rate that is faster than the bouncing or oscillating frequencies, the particles can be prevented from being trapped or bunched. The main difference between this case of externally induced turbulence and the case when an instability induces the turbulence is that in the former case there is no resonance broadening. Neither does there exist a possibility for threshold of the electric field which is needed to "turn on" the diffusion.[2,3] The dominating mechanism is incoherent wave-particle scattering.

Solution of the Vlasov Equation for the Coherent Response to an Oscillating Electric Field in a Turbulent Medium

Consider

(i) A plasma in a uniform magnetic field. Only one species is considered in the computation.

(ii) External and self-consistent fields. First, an expression for the coherent response is derived. This expression is valid for both the external and the self-consistent fields. Later, the following ordering is assumed: $|\phi_{ke}| \gg |\phi_{ks}|$, $\omega_{ke} \gg \omega_{ks}$, where e stands for external and s for self-consistent. But the perturbation f_{ke} caused by ϕ_{ke} is such that $f_o \gg f_{ke}$, where f_o is the unperturbed distribution function.

(iii) The external fields define a turbulent medium, and therefore provide a mechanism for stabilization through incoherent wave-particle scattering.

(iv) Mode-mode coupling is neglected.

As in previous work of Dupree and Dum,[1-5] we shall derive the response f_{k_T} ($T \Longrightarrow$ test) of a "test wave" that coexists with a set of random-phase "background waves." The effect of the background waves will be incorporated in the theory by using the perturbed trajectories of the particles moving in the turbulent media.

The Vlasov equation for particles is

$$\left[\frac{\partial}{\partial t} + \underline{v} \cdot \frac{\partial}{\partial \underline{r}} + \frac{q}{m}\underline{E} \cdot \frac{\partial}{\partial \underline{v}} + \frac{q}{m}\underline{v} \times \underline{B} \cdot \frac{\partial}{\partial \underline{v}}\right] f(\underline{r}, \underline{v}, t) = 0.$$

Expand the spatial dependence of E in a Fourier series and assume the time dependence of E to be $\exp\{-i\omega t\}$: $E(\underline{r}, t) = \sum_k E_k(t) \exp\{i\underline{k} \cdot \underline{r}\} + E_{k_T}(t) \exp\{i\underline{k} \cdot \underline{r}\}$, $f = \langle f \rangle + \sum_k f_k \exp\{i\underline{k} \cdot \underline{r}\}$, where $T \Longrightarrow$ test wave and angular brackets $\langle\ \rangle$ denote ensemble average over background waves.

With these relations, the first-order equation is

$$\left[\frac{\partial}{\partial t} + \underline{v} \cdot \frac{\partial}{\partial \underline{r}} + \frac{q}{m}\underline{v} \times \underline{B} \cdot \frac{\partial}{\partial \underline{v}}\right] f_k + \frac{q}{m} \sum_k \left[E_z(t) \exp\{i\underline{k} \cdot \underline{r}\} \frac{\partial}{\partial v_z} + \underline{E}_\perp(t) \exp\{i\underline{k} \cdot \underline{r}\} \cdot \frac{\partial}{\partial \underline{v}_\perp}\right] f_o$$

$$= -\frac{q}{m}\left[E_{z_T}(t) \exp\{i\underline{k} \cdot \underline{r}\} \frac{\partial}{\partial v_z} + \underline{E}_{\perp T}(t) \exp\{i\underline{k} \cdot \underline{r}\} \cdot \frac{\partial}{\partial \underline{v}_\perp}\right] f_o, \qquad (1)$$

where $f_o = \langle f \rangle$ is a zeroth-order quantity and f_k is a first-order quantity. Now, switch the spatial variable to guiding center coordinates $\tilde{x} = x - \frac{v_y}{\Omega}$, $\tilde{y} = y + \frac{v_x}{\Omega}$, $\tilde{z} = z$, and the velocity space coordinates to corotating coordinates $\underline{v} \rightarrow v_\perp$, Φ, v_z, where $\Phi = \theta - \Omega t$. This set of coordinates is convenient to use, since the unperturbed orbit is a helical motion about the guiding center. Also, these coordinates are slowly varying in time and therefore the diffusion coefficients describing the average perturbed orbits in terms of these coordinates can be computed. Next, a solution to Eq. 1 can be written

$$f_k = -\int_{t_o}^{t} \left\langle U(t, \tau) \left[\frac{q}{m}\left(E_{z_T}(\tau) \exp\{i\underline{k} \cdot \underline{r}\} \frac{\partial}{\partial v_z} + \underline{E}_{\perp T}(\tau) \exp\{i\underline{k} \cdot \underline{r}\} \cdot \frac{\partial}{\partial \underline{v}_\perp}\right) + \frac{\underline{E}_{\perp T}(\tau) \exp\{i\underline{k} \cdot \underline{r}\} \times \underline{B}}{B^2} \cdot \frac{\partial}{\partial \tilde{\underline{r}}_\perp}\right] f(\tilde{\underline{r}}, \underline{v}, \tau)\right\rangle d\tau + \text{i.v.}, \qquad (2)$$

where $U(t, \tau)$ is the propagator operator defined by Dupree.[6]

We assume electrostatic oscillations $\underline{E}_{kT} = -i\underline{k}\phi_k$ with $\exp\{-i\omega t\}$ time dependence. Note that $\frac{\underline{E}_\perp \times \underline{B}}{B^2} \cdot \frac{\partial}{\partial \underline{\tilde{r}}_\perp} = -i\phi_k \frac{1}{\Omega}\left[k_x \frac{\partial}{\partial \tilde{y}} - k_y \frac{\partial}{\partial \tilde{x}}\right]$, and that the rapidly varying term $\underline{E}_\perp \cdot \frac{\partial}{\partial \underline{v}_\perp} = -i\phi_k \underline{k}_\perp \cdot \underline{v}_\perp \frac{1}{v_\perp} \frac{\partial}{\partial v_\perp}$ can be written in two versions.

(i) $\underline{k}_\perp \cdot \underline{v}_\perp \exp\{i[\underline{k} \cdot \underline{r}(t-\tau) - \omega\tau]\} = i \frac{\partial}{\partial \tau} \exp\{i[\underline{k} \cdot \underline{r} - \omega\tau]\} + (\omega - k_z v_z) \exp\{i[\underline{k} \cdot \underline{r} - \omega\tau]\}$.

(ii) $\underline{k}_\perp \cdot \underline{v}_\perp \frac{1}{v_\perp} \frac{\partial}{\partial v_\perp} = \frac{k_\perp v_\perp}{2} \exp\{i[\Phi - \psi + \Omega t]\}\left(\frac{1}{v_\perp} \frac{\partial}{\partial v_\perp} - \frac{1}{iv_\perp^2} \frac{\partial}{\partial \Phi}\right) + \text{c.c.}$, where $\Phi + \Omega t - \psi$ is the angle between $\underline{k}_\perp$ and $\underline{v}_\perp$. By using the first version, f_k can be written as

$$f_k = i \int_{t_o}^{t} \left\langle U(t, \tau) \frac{q}{m} \phi_k \left\{ \exp\{i[\underline{k} \cdot \underline{r} - \omega\tau]\} k_z \frac{\partial}{\partial v_z} + \left[i \frac{\partial}{\partial \tau} \exp\{i[\underline{k} \cdot \underline{r} - \omega\tau]\} + (\omega - k_z v_z) \right.\right.\right.$$

$$\left.\left.\left. \cdot \exp\{i[\underline{k} \cdot \underline{r} - \omega\tau]\} \right] \frac{1}{v_\perp} \frac{\partial}{\partial v_\perp} + \exp\{i[\underline{k} \cdot \underline{r} - \omega\tau]\} \frac{1}{\Omega}\left(k_x \frac{\partial}{\partial \tilde{y}} - k_y \frac{\partial}{\partial \tilde{x}}\right) \right\} f(\underline{\tilde{r}}, \underline{v}, \tau) \right\rangle d\tau + \text{i.v.} \tag{3a}$$

With the second version, f_k becomes

$$f_k = i \int_{t_o}^{t} \left\langle U(t, \tau) \frac{q}{m} \phi_k \left\{ \exp\{i[\underline{k} \cdot \underline{r} - \omega\tau]\} k_z \frac{\partial}{\partial v_z} + \left[\frac{k_\perp v_\perp}{2} \exp\{i[\underline{k} \cdot \underline{r} - \omega\tau + \Phi - \psi + \Omega\tau]\} \right.\right.\right.$$

$$\left.\left.\left. \cdot \left(\frac{1}{v_\perp} \frac{\partial}{\partial v_\perp} - \frac{1}{iv_\perp} \frac{\partial}{\partial \Phi}\right) + \text{c.c.} \right] + \exp\{i[\underline{k} \cdot \underline{r} - \omega\tau]\} \frac{1}{\Omega}\left(k_x \frac{\partial}{\partial \tilde{y}} - k_y \frac{\partial}{\partial \tilde{x}}\right) \right\} f(\underline{\tilde{r}}, \underline{v}, \tau) \right\rangle d\tau + \text{i.v.} \tag{3b}$$

We make the following assumptions.

(a) U is the operator statement of f. Therefore, just as $f = \langle f \rangle + \delta f$, $U = \langle U \rangle + \delta U$. Hence $\langle UU \rangle = \langle U \rangle \langle U \rangle + \langle \delta U \delta U \rangle$ and $\langle \delta U \delta U \rangle$ is assumed to be much smaller than $\langle U \rangle \langle U \rangle$.

(b) Turbulence is stationary in time $\Longrightarrow \langle U(t, \tau) \rangle = \langle U(t-\tau) \rangle$.

(c) The integrand in (3a) and (3b) goes to zero as t becomes very large. This assumption is justified by the fact that the autocorrelation function is peaked in time. The peaking of the autocorrelation function during a time interval equal to the autocorrelation time leads to the next assumption.

(d) During a time interval T in which the integrand does make a significant contribution $\langle f \rangle$ does not change very much. This means that (i) $f(t-\tau) \approx f(t)$ and (ii) the effect of $\langle U(T) \rangle$ on $\langle f \rangle$ during an interval T can be neglected.

(e) Let $t_o = 0$, $t - \tau \equiv T$, and the upper limit on the integral $t \to \infty$. With these

assumptions (3a) and (3b) become

$$f_k = \left\{ \frac{q}{m} \phi_k Ri \left[k_z \frac{\partial}{\partial v_z} + (\omega - k_z v_z) \frac{1}{v_\perp} \frac{\partial}{\partial v_\perp} + \frac{1}{\Omega} \left(k_x \frac{\partial}{\partial \tilde{y}} - k_y \frac{\partial}{\partial \tilde{x}} \right) \right] + \frac{q}{m} \phi_k \frac{1}{v_\perp} \frac{\partial}{\partial v_\perp} \right\} \langle f \rangle \qquad (4a)$$

and

$$f_k = i \frac{q}{m} \phi_k \left\{ R \left[k_z \frac{\partial}{\partial v_z} + \frac{1}{\Omega} \left(k_x \frac{\partial}{\partial \tilde{y}} - k_y \frac{\partial}{\partial \tilde{x}} \right) \right] + R' \left[\frac{k_\perp v_\perp}{2} \left(\frac{1}{v_\perp} \frac{\partial}{\partial v_\perp} - \frac{1}{i v_\perp^2} \frac{\partial}{\partial \Phi} \right) + \text{c.c.} \right] \right\} \langle f \rangle, \qquad (4b)$$

where

$$R \equiv \exp\{-i\underline{k} \cdot \underline{r}\} \int_0^\infty dT \exp\{i\omega T\} \langle \exp\{i\underline{k} \cdot \underline{r}(-T)\} \rangle .$$

Next, we note that $\underline{r}$ is composed of a perturbed part r_t and an unperturbed part r_{up}; that is, $\underline{r} = \underline{r}_t + \underline{r}_{up}$. The unperturbed part can be expanded in a series of Bessel functions by using the identity[5] $\frac{1}{2\pi} \int_0^{2\pi} d\theta \left[\exp\{i[\underline{k} \cdot \underline{r} + \omega T - \underline{k} \cdot \underline{r}(-T)]\} = \sum_{m,n=-\infty}^{\infty} J_m \left(\frac{k_\perp v_\perp}{\Omega} \right) \cdot J_n \left(\frac{k_\perp v_\perp}{\Omega} \right) \exp\{i[\omega - k_z v_z - n\Omega] T + (n-m)(\theta - \psi)\} \right]$. Integration over θ eliminates the angular dependence. Hence m = n and, therefore, the resonance function becomes

$$R = \int_0^\infty dT \sum_{n=-\infty}^{\infty} J_n^2 \left(\frac{k_\perp v_\perp}{\Omega} \right) \exp\{i(\omega - k_z v_z - n\Omega)T\} \langle \exp\{-i\underline{k} \cdot \underline{r}_t(-T)\} \rangle . \qquad (5)$$

In R' there is an "extra" $\theta - \psi$ term. By changing the summation variable m and integrating over θ, R' reduces to R.

Equations 4a and 4b are equivalent and can be used to describe the coherent response to any oscillatory electric field whether it be external or due to unstable waves. Equation 4a is in a form that is convenient for the derivation of the dispersion relation, while Eq. 4b can be used to compute the diffusion coefficients.

Computation of the Diffusion Coefficients

The diffusion coefficients will now be computed. We are concerned with two kinds of random-phase waves, those induced externally, and those that are due to instabilities, the self-consistent fields.

Starting with the Vlasov equation and using random phase approximation, we obtain

$$\frac{d}{dt} \langle f \rangle = -\frac{q}{m} \left[\sum_{-ks} \frac{\partial}{\partial \underline{v}} \cdot \underline{E}_{ks} f_{ks} + \sum_{-ke} \frac{\partial}{\partial \underline{v}} \cdot \underline{E}_{ke} f_{ke} \right] . \qquad (6)$$

Recall that e $\Longrightarrow$ external, s $\Longrightarrow$ self-consistent. When (4b) is used to substitute for f_{ks} and f_{ke} in (6), this equation converts into a diffusion equation

$$\frac{d}{dt}\langle f\rangle = \left\{\sum_{ij} \nabla_j \cdot \underline{\underline{D}}_{sij} \cdot \nabla_i + \sum_{ij} \nabla_j \cdot D_{eij} \cdot \nabla_i\right\}.$$

For simplicity, we assume an isotropic spectrum. Therefore all cross terms in the diffusion matrices drop out, and hence the remaining coefficients are

$$D_{v_z v_z} = \sum_k \frac{q^2}{m^2} k_z^2 \phi_k \phi_{-k} R; \qquad D_{\Phi\Phi} \approx D_{v_\perp v_\perp} = \sum_k \frac{q^2}{m^2}$$

$$k_\perp^2 \phi_k \phi_{-k} R; \qquad \underline{\underline{D}}_{\perp\perp} = \sum_k \frac{\underline{k}_\perp \times \underline{B}}{B^2} \frac{\underline{k}_\perp \times \underline{B}}{B^2} \phi_k \phi_{-k} R. \tag{7}$$

But $\underline{\underline{D}}_{\perp\perp} = \sum_k \frac{1}{\Omega^2} \frac{q^2}{m^2} \underline{k}_\perp \times \hat{\ell}_z \underline{k}_\perp \times \hat{e}_z \phi_k \phi_{-k} R$; hence, $|\underline{\underline{D}}_{\perp\perp}| \approx \frac{1}{\Omega^2} D_{v_\perp v_\perp}$. There are two of each of these coefficients, one that is due to the external fields and the other to the self-consistent fields.

Our next task is to evaluate the resonant functions R_e and R_s. Since $|\phi_{ke}| \gg |\phi_{ks}|$, quasi-linear theory can be used to compute R_e. The integration is done along unperturbed orbits. Using Eq. 5 and letting $r_t = 0$, we obtain

$$R_e = \int_0^\infty dT\, J_n^2\left(\frac{k_\perp v_\perp}{\Omega}\right) \exp\{i[\omega - k_z v_z - n\Omega]T\} = \sum_{n=-\infty}^{\infty} \frac{-iJ_n^2\left(\frac{k_\perp v_\perp}{\Omega}\right)}{\omega - k_z v_z - n\Omega}. \tag{8}$$

The evaluation of R_s is much more difficult, since the perturbed part of the orbit is affected by both the externally induced turbulence and the "regular" background waves (those set by instabilities). Unlike R_e, R_s cannot be evaluated explicitly because it depends on D_s, which is a function of R_s.

In order to evaluate R_s, we expand the turbulent part of the orbit function in a cumulant series

$$\langle \exp\{i\underline{k} \cdot \underline{r}_t\}\rangle = \exp\{i\langle \underline{k} \cdot \underline{r}_t\rangle\} - \frac{1}{2!}\langle (\underline{k} \cdot \delta\underline{r}_t)^2\rangle,$$

where $\delta\underline{r}_t = \underline{r}_t - \langle \underline{r}_t\rangle$; for a Gaussian distribution, terms higher than second order vanish. Also, $\langle \underline{k} \cdot \underline{r}_t\rangle = 0$, since it is an average over the average position.[7] Since diffusion coefficients are defined in terms of the second moment of the random displacement δr_t in a time interval T during which $\langle f\rangle$ is unchanged, but which is longer than the autocorrelation time, $\langle (\underline{k} \cdot \delta\underline{r}_t)^2\rangle$ can be written in terms of diffusion coefficients. The

turbulent part of the orbit has two contributions $\underline{r}_t = \underline{r}_{ts} + \underline{r}_{te}$. Since mode-mode coupling is neglected, the diffusive effects of these two sets of random-phase waves can be superimposed. That is,

$$\left\langle (\underline{k}\cdot\delta\underline{r}_t)^2\right\rangle \approx T\left\{k_\perp^2(D_{s\perp\perp}+D_{e\perp\perp})+\frac{k_\perp^2}{\Omega^2}(D_{sv\perp v\perp}+D_{ev\perp v\perp})\right\} \equiv Tk_\perp^2(D_s+D_e), \tag{9}$$

where $D_{s,e} \equiv D_{s,ev\perp v\perp}\left(\frac{1}{\Omega^2}+1\right)$, and $D_{v\perp v\perp}$ includes $D_{\Phi\Phi}$ and is given by Eq. 7. The terms containing $D_{v_zv_z}$ are neglected, since we are interested in cases where $k_\perp \gg k_z$.

By using (5), (7), (8), and (9), R_s becomes

$$R_s = \sum_{n=-\infty}^{\infty} \frac{-iJ_n^2\left(\frac{k_\perp v_\perp}{\Omega}\right)}{\omega - k_z v_z - n\Omega + ik_\perp^2(D_s+D_e)}, \tag{10}$$

where D_e is explicitly determined by (7) and (8).

The Nonlinear Dispersion Relation

Using Poisson's equation $\nabla^2\phi_k = -\frac{\rho_k}{\epsilon_o} = \frac{-q}{\epsilon_o}\int dv\, f_k$ and Eq. 4a, we obtain a nonlinear dispersion relation with which we can study the propagation and stability characteristics of plasma modes in a turbulent medium.

$$1-\frac{\omega_p^2}{k^2}\int d\underline{v}\left\{iR_s\left[k_z\frac{\partial}{\partial v_z}+(\omega-k_zv_z)\frac{1}{v_\perp}\frac{\partial}{\partial v_\perp}+\frac{1}{\Omega}\left(k\times\frac{\partial}{\partial\tilde{y}}-k_y\frac{\partial}{\partial\tilde{x}}\right)\right]+\frac{1}{v_\perp}\frac{\partial}{\partial v_\perp}\right\}$$

$$\cdot\left\langle f(\tilde{x},\tilde{y},v_\perp,v_z,t)\right\rangle = 0, \tag{11}$$

where R_s is given by (10).

Analysis of a Counterstreaming Electron Beam System

An investigation of the possibility of stabilizing instabilities in an experimental apparatus[8] by launching a finite-width random-phase spectrum of waves into the plasma can be described by the following model.

(a) An electron gas is in a uniform constant $\underline{B}$ field composed of two counterstreaming electron beams.

(b) The beams are uniform across their cross section. Therefore constant density can be assumed with $k_\perp = \frac{2.4}{r_b}$, where r_b is the beam radius. Even though $D_{\perp\perp}$ can be large, its effect is neglected, since spatial diffusion would occur only

at the plasma boundary.

(c) The following distribution function is assumed:

$$\langle f\rangle = \frac{1}{2\pi^{3/2}V_T^3}\exp\left\{-\frac{v_\perp^2}{V_T^2}\right\}\left[\exp\left\{-\frac{(v_z-v_o)^2}{V_T^2}\right\}+\exp\left\{-\frac{(v_z+v_o)^2}{V_T^2}\right\}\right],$$

where v_o = drift velocity, V_T = thermal velocity and $V_T = V_{Tz} = V_{T\perp}$.

(d) We focus our attention at the onset of the instability. The external fields define the turbulent media, while the turbulence that is due to the self-consistent fields can be neglected. Thus $|\phi_{ke}| \gg |\phi_{ks}|$, and hence $D_e \gg D_s$. Also, at the onset time V_T corresponds to the temperature of the cathode.

(e) The turbulence is launched with a center frequency of $n\Omega e$. Therefore, it couples resonantly to the plasma; hence, the contribution of the resonant denominator R_e is π, since $\sum_{n=-\infty}^{\infty} J_n^2\left(\frac{k_\perp v_\perp}{\Omega}\right) = 1$. Using this value of R_e, we determine D_e from Eq. 7.

With these assumptions and using Eq. 11, we obtain a dispersion relation for the system. The procedure to be followed is similar to that for the linear analysis of the $\Omega/2$ frequency instability.[7,8] After performing the velocity integration and keeping only the n = 0, -1 modes, we obtain

$$\epsilon = \left(\frac{kV_T}{\omega_p}\right)^2 + 4 + \sum_{n=-1}^{0}\exp\{-b\}\, I_n(b)\sum_{\pm} Z\left(\frac{\omega \pm k_z v_o + n\Omega}{k_z V_T} + i\,\frac{k_\perp^2 D_e}{k_z V_T}\right) = 0, \qquad (12)$$

where $b = \frac{1}{2}\frac{k_\perp^2 V_T^2}{\Omega^2}$. The Z functions are expanded about the point $\frac{\omega}{\Omega} = \frac{k_z v_o}{\Omega} = \frac{1}{2}$ in the ω-k plane. In the case of marginal stability $\gamma = \frac{I_m \epsilon}{\frac{\partial}{\partial\omega} R_e \epsilon}$. Now γ can be calculated from (12) in terms of D_e. Since we are interested in the case $\gamma = 0$, the value of D_e needed for stabilization is determined. Since $D_e \approx \frac{q^2}{m^2}\frac{k_\perp^2 |\phi_{rms}|^2}{\Omega^2}$, and T = 0.1 eV, $k_\perp = 2.4 \times 10^3\ m^{-1}$, $\Omega \equiv \left|\frac{q_e B}{m_e}\right|$, and $B = 10^{-2}$ tesla; therefore, $\phi_{rms} \approx 10\ \mu V$.

References

1. T. H. Dupree, "A Perturbation Theory for Strong Plasma Turbulence," Phys. Fluids 9, 1773-1782 (1966).
2. T. H. Dupree, "Nonlinear Theory of Drift-Wave Turbulence and Enhanced Diffusion," Phys. Fluids 10, 1049-1055 (1967).
3. T. H. Dupree, "Nonlinear Theory of Low-Frequency Instabilities," Phys. Fluids 11, 2680-2694 (1968).
4. C. T. Dum, "Nonlinear Stabilization and Enhanced Diffusion of a Turbulent Plasma in a Magnetic Field," Ph.D. Thesis, Department of Physics, M.I.T., May 10, 1968.

5. C. T. Dum and T. H. Dupree, "Nonlinear Stabilization of High-Frequency Instabilities in a Magnetic Field," Phys. Fluids 13, 2064-2081 (1970).

6. T. H. Dupree, Phys. Fluids 9, 1773 (1966), see Eqs. 3.2 and 3.3.

7. T. H. Dupree, Private communication, 1975.

8. A. Hershcovitch, "Time Evolution of Beam Instabilities," S.M. Thesis, Department of Nuclear Engineering, M.I.T., November 1974.

9. A. Hershcovitch and P. A. Politzer, "Linear Analysis of the 'One-Half Cyclotron Frequency' Instability," Quarterly Progress Report No. 111, Research Laboratory of Electronics, M.I.T., October 15, 1973, pp. 41-46.

X. PLASMA DYNAMICS

B. General Theory

1. PARAMETRIC EXCITATION OF ELECTROSTATIC ION CYCLOTRON MODES WITH ARBITRARY $k_\perp a_i$

U.S. Energy Research and Development Administration (Contract E(11-1)-3070)

Charles F. F. Karney, Abraham Bers

Introduction

The problem of parametrically exciting electrostatic ion cyclotron (EIC) modes has been considered in previous reports[1-3] in which we used a fluid description for the EIC modes. The fluid description is only valid in the limit $k_\perp a_i \ll 1$ (a_i is the ion gyro radius, $a_i = \frac{(T_i/m_i)^{1/2}}{\Omega_i}$). In this report we relax the restriction on $k_\perp a_i$ by using a kinetic description for the ions. We shall see that if we allow $k_\perp a_i > 1$, then lightly damped EIC modes exist when $\frac{k_\parallel}{k_\perp} < \sqrt{\frac{m_e}{m_i}}$. The importance of this observation lies in the fact that we shall now be able to excite EIC modes by using an electrostatic wave close to the lower hybrid frequency (ω_{LH}). This leads in turn to a more complete transfer of power from the pump to the EIC modes (as a consequence of the Manley-Rowe relations) and raises the possibility of more efficient heating of ions in a Tokamak by using RF energy near the lower hybrid frequency.

Linear Dispersion Relation for EIC Modes

We start with the Harris dispersion relation for a Maxwellian plasma

$$K = 1 + \chi_i + \chi_e = 0, \tag{1}$$

where

$$\chi = \frac{\omega_p^2}{k^2 v_T^2}\left[1 + \zeta_o \sum_{n=-\infty}^{\infty} \Gamma_n Z_n\right] \tag{2}$$

for the electrons and ions, and $v_T^2 = T/m$; $\zeta_n = \frac{\omega - n\Omega}{k_\parallel \sqrt{2}\, v_T}$; $Z_n = Z(\zeta_n)$; $\Gamma_n = e^{-\lambda} I_n(\lambda)$; $\lambda = \left(\frac{k_\perp v_T}{\Omega}\right)^2 = k_\perp^2 a^2$. Here I_n is the modified Bessel function. We shall look for roots to (1) in the range $\Omega_i < \omega < 2\Omega_i$.

If $\zeta_{oe} \ll 1$ and $\lambda_e \ll 1$, then the electrons behave adiabatically and

$$\chi_e \approx \frac{\omega_{pe}^2}{k^2 v_{Te}^2}. \tag{3}$$

If $k^2 v_{Te}^2/\omega_{pe}^2 = k^2\lambda_{De}^2 \ll 1$, (1) reduces to

$$K = \chi_i + \chi_e = 0. \tag{4}$$

In order to avoid ion Landau and ion cyclotron damping we demand that $\zeta_{ni} \gg 1$, for all n. (A sufficient condition is that $\zeta_{1i} \gg 1$. In cases of interest ω is closer to Ω_i than to $2\Omega_i$ and so ion cyclotron damping from the fundamental is the most important.) We may then use the asymptotic expansion for Z in evaluating Z_{ni}, so $Z_{ni} \approx -1/\zeta_{ni}$. Neglecting all terms in the sum in (2) except for the n = 0 and n = 1 terms, we obtain

$$\chi_i = \frac{\omega_{pi}^2}{k^2 v_{Ti}^2}\left[1 - \Gamma_{oi} - \frac{\zeta_{oi}}{\zeta_{1i}}\Gamma_{1i}\right] = \frac{\omega_{pi}^2}{k^2 v_{Ti}^2}\left[1 - \Gamma_o - \frac{\omega}{\omega - \Omega_i}\Gamma_1\right]. \tag{5}$$

(Hereafter we shall omit the subscript i from Γ_n and λ.) The neglect of the n = 2 term is justifiable because $\Gamma_2 < \Gamma_1$, for all λ and $\zeta_2 > \zeta_1$, as long as $\omega - \Omega_i < 2\Omega_i - \omega$. The neglect of the other terms follows in a similar manner.

Using (3) and (5) in (4), we obtain

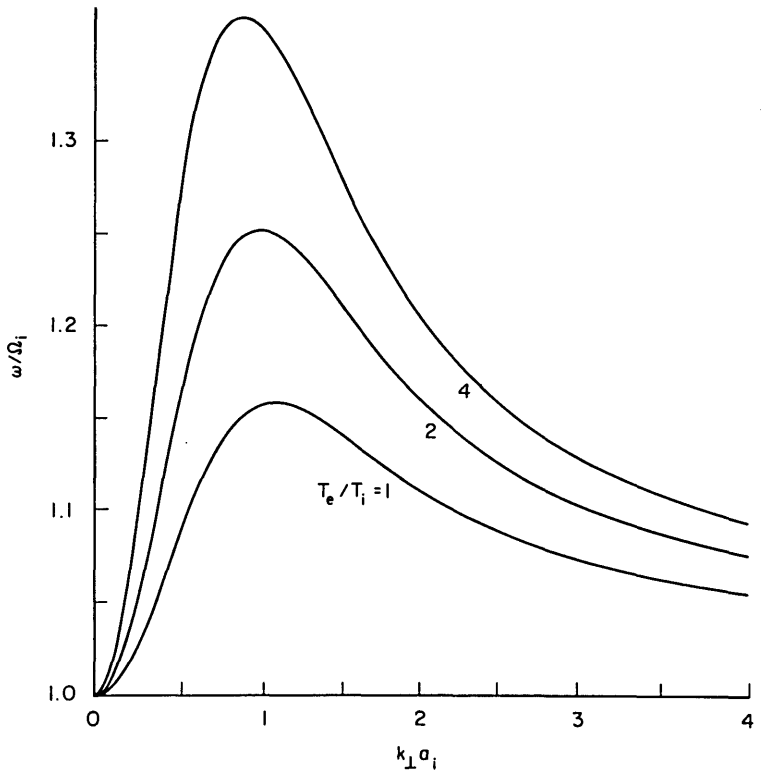

Fig. X-8. Dispersion relation for electrostatic ion cyclotron modes.

$$K = \frac{\omega_{pe}^2}{k^2 v_{Te}^2} + \frac{\omega_{pi}^2}{k^2 v_{Ti}^2}\left[1 - \Gamma_o - \frac{\omega}{\omega - \Omega_i}\Gamma_1\right] = 0. \tag{6}$$

Solving for ω, we obtain

$$\omega = \Omega_i \frac{1}{1 - \Gamma_1 \Big/ \left(1 + \frac{T_i}{T_e} - \Gamma_o\right)}. \tag{7}$$

This is plotted in Fig. X-8 as a function of $k_\perp a_i$ for $T_e/T_i = 1$, 2, and 4. Note that our assumption $\omega - \Omega_i < 2\Omega_i - \omega$ is justified for these temperature ratios. Using this, we may rewrite (7) as

$$\omega \approx \Omega_i \left[1 + \frac{\frac{T_e}{T_i}\Gamma_1}{1 + \frac{T_e}{T_i}[1-\Gamma_o]}\right]. \tag{8}$$

In the limit $\lambda \ll 1$, $\Gamma_o \approx 1$ and we recover the familiar dispersion relation $\omega \approx \Omega_i\left[1 + \frac{T_e}{T_i}\Gamma_1\right]$.

Conditions of Validity of the Dispersion Relation

Having obtained the dispersion relation, we must go back and check the approximations.

A. $k^2 v_{Te}^2/\omega_{pe}^2 \ll 1$ or $k_\perp^2 a_i^2 \frac{T_e}{T_i} \ll \frac{\omega_{pi}^2}{\Omega_i^2}$

under the assumption $k \approx k_\perp$. For the ranges of T_e/T_i that we are considering and the typical values of ω_{pi}/Ω_i encountered in Tokamaks (approximately 20) this is a relatively mild condition on the parameter $k_\perp a_i$.

B. $\lambda_e \ll 1$ or $k_\perp^2 a_i^2 \frac{T_e}{T_i} \ll \frac{m_i}{m_e}$.

This is normally implied by A.

C. $\zeta_{oe} \ll 1$ or $k_\perp a_i \gg \frac{k_\perp}{k_\parallel}(m_e/m_i)^{1/2}(T_i/T_e)^{1/2}$

under the assumption $\omega \sim \Omega_i$.

D. $\zeta_{1i} \gg 1$ or $k_\perp a_i \ll \frac{k_\perp}{k_\parallel} \frac{\omega - \Omega_i}{\Omega_i}$.

Combining C and D, we obtain

$$(T_i/T_e)^{1/2} \frac{1}{k_\perp a_i} \ll \frac{k_\parallel}{k_\perp} (m_i/m_e)^{1/2} \ll (m_i/m_e)^{1/2} \frac{1}{k_\perp a_i} \frac{(\omega-\Omega_i)}{\Omega_i}. \tag{9}$$

The inequalities in (9) show that when $k_\perp a_i > 1$ we can choose $k_\parallel/k_\perp$ to be less than $(m_e/m_i)^{1/2}$. For example, when $T_e/T_i = 1$ and $k_\perp a_i$ = from 1 to 3, $\frac{\omega - \Omega_i}{\Omega_i} \sim 0.1$ and for an H plasma (9) becomes $\frac{1}{k_\perp a_i} \ll \frac{k_\parallel}{k_\perp} (m_i/m_e)^{1/2} \ll \frac{4}{k_\perp a_i}$. Note that we are not well able to satisfy these inequalities and, for that reason, it is important to find the damping rate for these waves. Note that the inequalities in (9) serve two purposes: They allow us to expand the Z-function and so obtain a simple dispersion relation, and they are the condition that the damping rate is small. When the inequalities break down, we are primarily interested in the magnitude of the damping rate.

Damping Rate

As long as the damping rate γ is small, it may be obtained from

$$\gamma = \frac{\text{Im (K)}}{\partial K/\partial \omega}. \tag{10}$$

To evaluate $\partial K/\partial\omega$, we use (6), and to find Im (K) we include the imaginary part of the Z-function. Keeping only the largest contributions, those from Z_{oe} and Z_{1i}, we find

$$\text{Im (K)} = \frac{\omega_{pe}^2}{k^2 v_{Te}^2} \zeta_{oe} \sqrt{\pi} + \frac{\omega_{pi}^2}{k^2 v_{Ti}^2} \zeta_{oi} \sqrt{\pi}\, \Gamma_1 \exp\left(-\zeta_{1i}^2\right). \tag{11}$$

From this we obtain

$$\frac{\gamma}{\Omega_i} = \frac{\sqrt{\pi} \left[\frac{T_i}{T_e} \zeta_{oe} + \zeta_{oi} \Gamma_1 \exp\left(-\zeta_{1i}^2\right)\right]}{\Gamma_1 \Omega_i^2/(\omega-\Omega_i)^2}, \tag{12}$$

where ω is given by (7). This is plotted in Fig. X-9. Note that even for $T_e = T_i$ there are waves with $\gamma < 0.1\ \Omega_i$ and $k_\parallel/k_\perp < (m_e/m_i)^{1/2}$.

Energy Density and Group Velocity

The energy density for electrostatic modes is given by

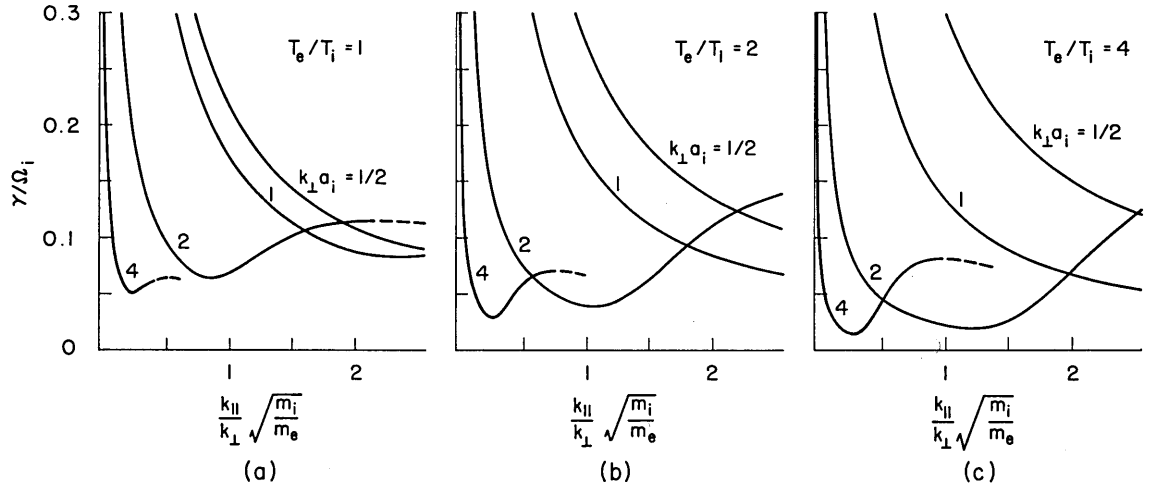

Fig. X-9. Damping rate, γ, for electrostatic ion cyclotron modes.

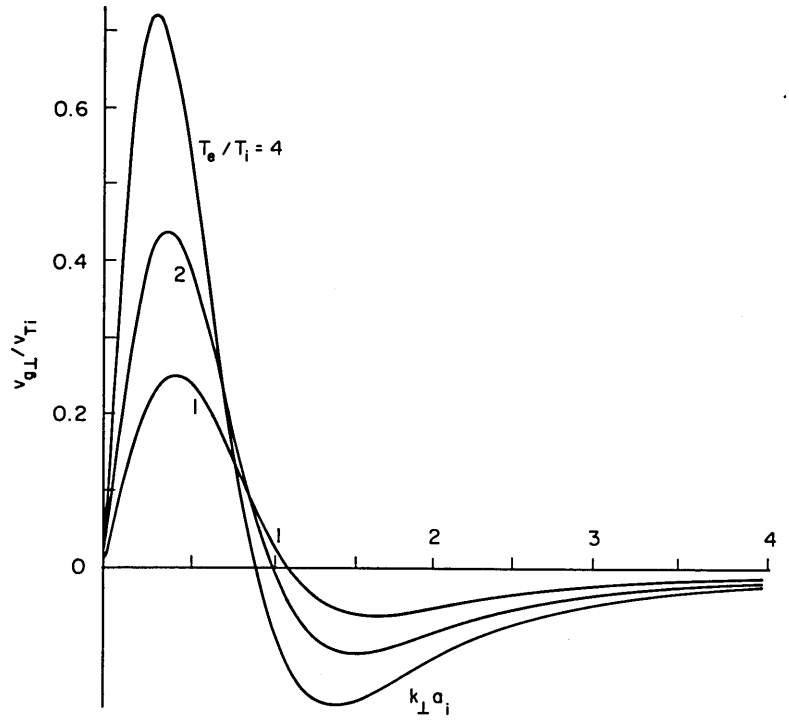

Fig. X-10. Group velocity, $v_{g\perp}$, for electrostatic ion cyclotron modes.

$$W = \frac{1}{4}\epsilon_o |E|^2 \omega \frac{\partial K}{\partial \omega}. \tag{13}$$

We evaluate (13) using (6) to obtain

$$W = \frac{1}{4}\epsilon_o |E|^2 \frac{\omega_{pi}^2}{k^2 v_{Ti}^2} \frac{\omega\Omega_i}{(\omega-\Omega_i)^2} \Gamma_1, \tag{14}$$

where ω is given by (7).

The group velocity $\bar{v}_g$ is given by

$$v_{g\alpha} = \frac{\partial \omega}{\partial k_\alpha} = -\frac{\partial K/\partial k_\alpha}{\partial K/\partial \omega}, \tag{15}$$

where α is $\perp$ or $\parallel$. Since, from (6), K is independent of $k_\parallel$, $v_{g\parallel}$ is approximately zero. Evaluating (15) with $\alpha = \perp$ and making use of the identities: $\Gamma_n' = -\Gamma_n[1+n/\lambda] + \Gamma_{n-1}$ and $\Gamma_{-1} = \Gamma_1$, where prime indicates differentiation with respect to λ, we find

$$\frac{v_{g\perp}}{v_{Ti}} = 2k_\perp a_i \left(\frac{\omega-\Omega_i}{\Omega_i}\right) \frac{\left[\Gamma_o - \Gamma_1 - \frac{\omega}{\Omega_i}\frac{\Gamma_1}{\lambda}\right]}{\Gamma_1}, \tag{16}$$

where ω is given by (7). This is plotted in Fig. X-10.

Parametric Coupling from Lower Hybrid Waves

We have established that when $k_\perp a_i > 1$ there exist lightly damped EIC modes for which $k_\parallel/k_\perp < (m_e/m_i)^{1/2}$. We wish to excite these modes parametrically using a pump and idler that are lower hybrid modes with the dispersion relation

$$\omega^2 = \omega_{pi}^2 \left[1 + \frac{m_i}{m_e}\cos^2\theta\right]. \tag{17}$$

(For simplicity, we take $\omega_{LH} \approx \omega_{pi}$; this is true for most Tokamak plasmas for which $\Omega_e^2 \gg \omega_{pe}^2$.) The ω and $\bar{k}$ matching conditions or resonance conditions can be satisfied easily in this instance by choosing the $k_\perp$ and the $k_\parallel$ for all three modes to be roughly the same. For example, if we choose $k_\perp a_i$ for the EIC mode to be 4, then from Fig. X-9 we see that this wave is least damped at $\frac{k_\parallel}{k_\perp} \approx \frac{1}{4}(m_e/m_i)^{1/2}$. Using this value in (17), we have $\omega \approx 1.12\ \omega_{pi}$. Thus we can utilize pumps at all frequencies above the lower hybrid frequency.

Accessibility Conditions

Having found that waves close to ω_{LH} can excite EIC modes, we must next check

that these waves can be linearly excited from the exterior. The most important condition is the "accessibility condition" on $n_{||}$ (=kc/ω). This is the condition that the pump be propagating (as opposed to evanescent) all the way through the density gradient except for a very narrow region at low densities. Golant[4] gives this condition as

$$n_{||} > 1 + \frac{\omega_{pe}^2}{\Omega_e^2}. \tag{18}$$

This condition is derived by using cold-plasma theory. In most cases (18) reduces to $n_{||} > 1$.

The inclusion of warm-plasma effects introduces two new effects, (i) electron Landau damping, and (ii) linear wave conversion to an outward traveling mode before the lower hybrid resonance is reached.

Landau Damping for Lower Hybrid Modes

The relevant quantity to examine when considering the effect of Landau damping in k_{xi} (the imaginary part of k_x) is

$$k_{xi} = -\frac{\text{Im (K)}}{\partial K/\partial k_x}, \tag{19}$$

where x is the direction of the density gradient. The major contribution to Im (K) comes from electron Landau damping parallel to the magnetic field so that

$$\text{Im (K)} = \sqrt{\pi}\,\frac{k_{||}^2}{k^2}\,\zeta_{oe}^3\,2\,\frac{\omega_{pe}^2}{\omega^2}\exp\left(-\zeta_{oe}^2\right). \tag{20}$$

Using $\partial K/\partial k_x = \frac{k_{||}^2}{k^3}\,2\,\frac{\omega_{pe}^2}{\omega^2}$, we find

$$k_{xi} = \sqrt{\pi}\,\zeta_{oe}^3\exp\left(-\zeta_{oe}^2\right)k. \tag{21}$$

We use the fact that we are interested in pumps for which $k_\perp a_i \sim 1$, and consider a plasma with B_o = 50 kG, $n_o = 10^{14}$ cm^{-3}, T_e = 2 keV, and T_i = 1 keV, then $a_i \sim 1$ mm. For a machine with minor radius a = 1 m we demand that k_{xi} as given by (21) be less than 1 (m^{-1}). This means that $\zeta_{oe} > 3.5$ and $n_{||} = \frac{c}{\sqrt{2}\,v_{Te}\zeta_{oe}} < 3.2$. This figure for ζ_{oe} is insensitive to most of the parameters in the problem, and so the upper limit on $n_{||}$ scales as $1/\sqrt{T_e}$.

Linear Wave Conversion

The problem of linear mode conversion has been extensively studied by Simonutti.[5] His results indicate that wave conversion occurs at a density given by

$$\frac{\omega_{pi}^2}{\omega^2} \approx 1 - \frac{2k_{\|}}{\omega}(3T_i/m_e)^{1/2} = 1 - 2n_{\|}\frac{(3T_i/m_e)^{1/2}}{c}. \tag{22}$$

For T_i = 1 keV the quantity $\frac{(3T_i/m_e)^{1/2}}{c} = \frac{1}{16}$. From this we have $1 < n_{\|} < 3.2$, and therefore mode conversion occurs for frequencies $1.1\,\omega_{pi} < \omega < 1.2\,\omega_{pi}$, under the assumption that we wish to utilize the full range of the $n_{\|}$. These results indicate that in order to avoid linear mode conversion we have to choose $\omega > 1.2\,\omega_{pi}$. This number increases as the ions become hotter.

Resonance Conditions

We must now check that lower hybrid waves lying in the accessible range of the $n_{\|}$ have $\bar{k}$ comparable to those of the EIC waves discussed in the first part of this report. To do this we observe from Fig. X-9 that the product $\frac{k_{\|}}{k_{\perp}}(m_i/m_e)^{1/2} \times k_{\perp}a_i$ lies in the range 1-2 when the EIC modes are lightly damped. With the same plasma parameter as before, $\frac{k_{\|}\ \text{pump}}{k_{\|}\ \text{EIC}} \sim 0.5$ to 2.

To summarize these results: From the outside of the plasma we are able to excite lower hybrid waves inside the plasma with the $n_{\|}$ lying in the range 1-3 and frequencies of $1.2\,\omega_{pi}$ or above. These waves have the $\bar{k}$ that are comparable to the $\bar{k}$ of EIC modes propagating closely perpendicular to the magnetic field and so the resonance conditions for the parametric interaction are satisfied.

Coupling Coefficient and Growth Rate

Since the electrons in these kinetic EIC modes behave in the same way as in the fluid limit (viz. adiabatically), and since the electrons provide the major contribution to the coupling coefficient, the form of the coupling coefficient is the same for coupling to the fluid EIC modes as reported previously.[1] Using this and the energy density given by (14), we obtain the following expression for the growth rate, γ_o, of the EIC mode:

$$\frac{\gamma_o}{|\omega_b\omega_n|^{1/2}} = \frac{\sqrt{2}\sqrt{\Gamma_1}\,c_s/v_{Ti}}{1 + \frac{T_e}{T_i}[1-\Gamma_o]}\sqrt{\frac{\omega_n}{\Omega_i}}\frac{\omega_{pe}}{\omega_a}\sin\psi\,\frac{v_{ae\perp}}{4v_{Te}}, \tag{23a}$$

where subscripts a, b, and n denote the pump, idler, and EIC mode; ψ is the angle between the projections of $\bar{k}_a$ and $\bar{k}_b$ on the x-y plane; and $v_{ae\perp} = E_a/B_o$ is the $\bar{E} \times \bar{B}$ velocity of the electrons in the pump field.

If we take $\omega_b \approx \omega_a$, then (23) can be rewritten

$$\frac{\gamma_o}{\Omega_i} = \left\{ \frac{\sqrt{\Gamma_1}\sqrt{T_e/T_i}}{1 + \frac{T_e}{T_i}[1-\Gamma_o]} \frac{\omega_n}{\Omega_i} (\omega_{pi}/\omega_a)^{1/2} \right\} \frac{\sqrt{2}}{4} (\omega_{pi}/\Omega_i)^{1/2} \frac{v_{ae\perp}}{c_s} \sin\psi$$

$$= C \frac{\sqrt{2}}{4} (\omega_{pi}/\Omega_i)^{1/2} \frac{v_{ae\perp}}{c_s} \sin\psi. \qquad (23b)$$

We assume $\theta_n = \theta_a$ and that for a given θ_n, $k_{\perp n} a_i$ and hence ω_n are determined by $k_{\parallel n}/k_{\perp n} (m_i/m_e)^{1/2} = \frac{1}{k_{\perp n} a_i}$, to avoid damping on the EIC mode. Then the factor C in (23a) contains the terms that are related to the pump frequency, ω_a. In Fig. X-11 the quantity is plotted against ω_a for various T_e/T_i. Note that the growth rate is maximum near $\omega_a \sim 1.5\ \omega_{pi}$ (or $k_{\perp n} a_i \sim 1$). In fact, the maximum growth rate may occur for

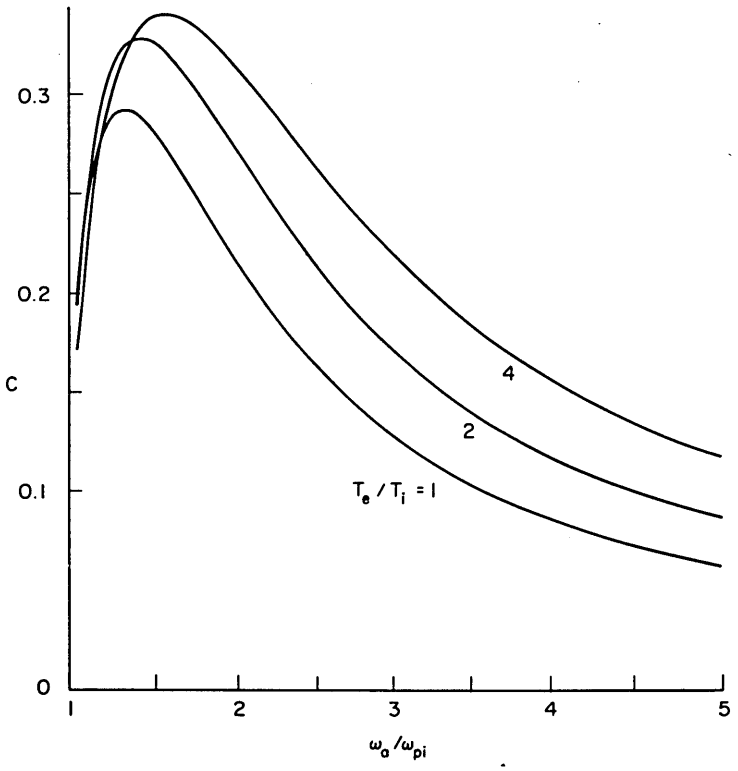

Fig. X-11. Dependence of growth rate, γ_o, on pump frequency ω_a. (C is defined by Eq. 23b.)

somewhat lower pump frequencies (higher $k_{\perp n}a_i$), since, by the WKB field enhancement,[2] $v_{ae\perp}$ tends to increase as we approach lower hybrid resonance.

As an example, consider a plasma with B_o = 50 kG, $n_o = 10^{14}$ cm^{-3}, T_e = 2 keV, T_i = 1 keV, $\omega_a \approx \omega_{pi}$, E_a = 10 kV/cm, which corresponds to a wall field of ~1 kV/cm at the wall,[3] and $k_{\perp n}a_i = 2$, then $\gamma_o \approx 0.2\ \Omega_i$. Since the linear damping rate for the EIC modes is approximately $0.1\ \Omega_i$ and the damping of the idler is typically far less than for the EIC mode, this figure for γ_o easily exceeds normal threshold $\gamma_o^2 = \gamma_n\gamma_b$.

Thresholds Attributable to Plasma Nonuniformity

The threshold condition just mentioned is the condition that there be growth of the modes in a uniform plasma in the presence of a uniform pump. The effect of nonuniformity of the plasma is to introduce a position-dependent k mismatch into the parametric interaction. If we assume that the k mismatch is a linear function of x, the direction of nonuniformity, then the idler and the EIC modes grow and saturate[6] with a gain of $e^{\pi\lambda}$ where λ is given by

$$\lambda = \frac{\gamma_o^2}{\kappa v_{bx} v_{nx}}. \tag{24}$$

Here κ is $d[k_a+k_b-k_n]/dx$, and v_b and v_n are the group velocities of the idler and the EIC mode. The threshold condition that this introduces is $e^{\pi\lambda} \gg 1$. If this condition is satisfied, noise is greatly amplified and some other saturating effect may well be important.

Effect of Density Gradient

We shall consider two types of nonuniformity: a density gradient, and a magnetic field gradient. When exciting waves in a Tokamak we must inevitably consider the propagation of waves in the density gradient. After a while, however, the waves will reach a central region where the density can be assumed constant. The situation is different with the magnetic field gradient, since it is present throughout the plasma and must be accounted for even in the central homogeneous part of the plasma.

In both cases we assume a slab model in which x is the direction of nonuniformity. The justification for this is that the wavelength of the modes under consideration is much less than the minor radius of the Tokamak, so that effects of the cylindrical or toroidal nature of the geometry are unimportant.

The density gradient causes the dispersion relation for the pump and the idler to be functions of position. (The dispersion relation for the EIC mode does not depend on density.) For simplicity, we assume $\omega_a^2 \gg \omega_{pi}^2$, the <u>local</u> ion plasma frequency, so that $\omega_{a,b} = \omega_{pe} \cos\theta_{a,b}$. (Remember that the local ω_{pi} in the density gradient is less than that in the center of the plasma, and that we choose $\omega_a \approx \omega_{pi,\,center}$.) κ is given by

$$\kappa \approx \frac{1}{2} k_{\perp a} \frac{1}{n} \frac{dn}{dx}. \tag{25}$$

Thus taking $v_{bx} \sim \omega_a / k_{\perp a}$ and $v_{nx} \sim c_s$, we have

$$\lambda \sim \frac{\gamma_o^2 L_n}{\omega_a c_s}, \tag{26}$$

where $L_n = \frac{1}{n} \frac{dn}{dx} \sim a$, the minor radius of the Tokamak. Using $\gamma_o = 0.2\, \Omega_i$ and the plasma parameter used before, $\lambda \sim 1.5\ (m^{-1})\ a$.

In present Tokamaks a ~ 10 cm and the density gradient effectively prevents the parametric interaction from occurring anywhere except in the central homogeneous region. In the larger machines envisaged for the future a ~ 1 m and the parametric interaction will cause only moderate gain ($\sim e^{\pi}$) of the noise present in the density gradient.

Effect of Magnetic Field Gradient

The main (toroidal) magnetic field in a Tokamak has a 1/R dependence, where R is the distance to the axis of the machine. Only the dispersion relation for the EIC mode is sensitive to the magnetic field. In this case κ is given by

$$\kappa \approx \frac{\partial k_{\perp n}}{\partial \Omega_i} \frac{\partial \Omega_i}{\partial x} \sim \frac{\partial k_{\perp n}}{\partial \Omega_i} \frac{\Omega_i}{R_o}, \tag{27}$$

where R_o is the major radius, and $\partial k_{\perp n} / \partial \Omega_i$ has a singularity at one point, but $v_{nx} = \partial \omega / \partial k_{\perp n}$ goes to zero at the same point and λ remains finite, given by

$$\lambda = \frac{\gamma_o^2}{(\Omega_i / R_o) \frac{\partial \omega_n}{\partial \Omega_i} v_{bx}}, \tag{28}$$

where $\partial \omega_n / \partial \Omega_i$ is very close to unity, since $\omega_n \sim \Omega_i$. We take $v_{bx} = \omega_a / k_{\perp b}$, with $k_{\perp b} = 2a_i^{-1}$. This is an overestimate of v_{bx} if ω_a is close to ω_{pi}. Then $\lambda \approx 4(m^{-1})\ R_o$. We see that in present machines ($R_o \sim$ I m), and to a lesser extent in future machines ($R_o \sim 5$ m) magnetic field inhomogeneity may play a role in saturating the parametric instability in the central, homogeneous density region of the plasma.

In this work we have not considered the effect of the magnetic field gradient on the linear behavior of the EIC modes. The work of Sperling and Perkins[7] indicates that this may lead to stronger damping of the EIC modes.

Effect of Finite Pump Extent

An array of waveguides at the wall of a Tokamak[8] can excite a narrow ray of lower hybrid waves which travel nearly parallel to the magnetic field. We can conveniently

treat the problem of the pulse response for the parametric interaction in such a system by looking at its two-dimensional analogue. Ignoring the y-dimension and assuming, for convenience, that the pump ray is parallel to the z axis, the equations for the pulse response are

$$\left[\frac{\partial}{\partial t} + v_{x1}\frac{\partial}{\partial x} + v_{z1}\frac{\partial}{\partial z}\right] a_1 = \gamma_o a_2 + \delta(x, y, z) \tag{29}$$

$$\left[\frac{\partial}{\partial t} - v_{x2}\frac{\partial}{\partial x} + v_{z2}\frac{\partial}{\partial z}\right] a_2 = \gamma_o^* a_1, \tag{30}$$

where 1 and 2 are the decay products of the parametric interaction, a is the mode amplitude normalized to the action density, and $\bar{v}$ is the group velocity. (Note that we define $\bar{v}_2 = -v_{x2}\bar{x} + v_{z2}\bar{z}$.) We take the boundaries of the pump ray to be at x = 0 and x = ℓ.

We distinguish two cases: First, if $v_{x1}v_{x2} < 0$, then both edges of the pulse travel out of the pump ray in the same direction. The total amplification, A, of the pulse will be approximately $\exp\left[\frac{2\gamma_o}{|v_{x1}| + |v_{x2}|}\right]$. The threshold criterion would then be that $A \gg 1$, as calculated in previous reports.[2,9]

The second case is $v_{x1}v_{x2} > 0$. In this case there is the possibility of pulse growth similar to that occurring in a one-dimensional backward wave oscillator. We transform (29) and (30) to the coordinate system

$$\left.\begin{aligned} t' &= t \\ x' &= x \\ z' &= z - ut - \alpha x \end{aligned}\right\} \tag{31}$$

where $\alpha = (v_{z1} - v_{z2})/(v_{x1} + v_{x2})$ and $u = v_{z1} - \alpha v_{x1}$. Note that z' = 0 gives the line along which the pulse response is nonzero for an infinite system. We use (31), and (29) and (30) become

$$\left(\frac{\partial}{\partial t'} + v_{x1}\frac{\partial}{\partial x'}\right) a_1 = \gamma_o a_2 + \delta(x', z', t'), \tag{32}$$

$$\left(\frac{\partial}{\partial t'} - v_{x2}\frac{\partial}{\partial x'}\right) a_2 = \gamma_o^* a_1. \tag{33}$$

If $v_{x1}, v_{x2} > 0$, the boundary conditions are $a_1(0) = a_2(\ell) = 0$. If z' = 0, then (32) and (33) are the one-dimensional equations solved by Bobroff and Haus.[10] Elsewhere, for z' = 0, the pulse response is zero. Using the results of Bobroff and Haus and reversing the transformation (31), we obtain the following description of the pulse response: Initially the pulse grows as it would in a pump of infinite extent.[11] This continues until one of the edges of the pulse (traveling at $\bar{v}_1$ or $\bar{v}_2$) meets the boundary. Although the boundaries in this problem are nonreflecting, the fact that the edge of one mode has propagated out of the system is mathematically reflected as a discontinuity in some derivative on

the other mode which carries it back along the line of the pulse. After a few reflections the 'normal mode' solution is established. This is the same as the normal mode solution in one dimension, except that the wave packets in this case propagate along the ray with velocity u. The normal mode grows as long as ℓ exceeds the threshold length:

$$\ell_{th} = \frac{\pi}{2} \frac{\sqrt{v_{1x}v_{2x}}}{\gamma_o}. \tag{34}$$

The growth rate for the mode is

$$\gamma = \beta \frac{\gamma_o \sqrt{v_{1x}v_{2x}}}{(v_{1x}+v_{2x})/2}, \tag{35}$$

where β is the largest root of $\beta \tan\left(\sqrt{1-\beta^2}\,\frac{\pi}{2}\,\frac{\ell}{\ell_{th}}\right) + \sqrt{1-\beta^2} = 0$. As $\ell \to \infty$, $\beta \to 1$, with $\beta \approx 0.8$ when $\ell = 2.5\,\ell_{th}$.

The threshold condition for this case is less strict than when $v_{1x}v_{2x} < 0$, since normally the x-directed group velocity of an EIC mode is much less than that of a lower hybrid idler, so $\sqrt{v_{1x}v_{2x}} \ll (v_{1x}+v_{2x})/2$.

A limit on the eventual growth of an unstable normal mode is set either by nonlinear effects, or by the magnetic field gradient which introduces a t'-varying mismatch into the right-hand sides of (32) and (33). Finally, there is the possibility that the pulse will continue to grow until the pump ray leaves the plasma.

References

1. C. F. F. Karney, A. Bers, and J. L. Kulp, Quarterly Progress Report No. 110, Research Laboratory of Electronics, M.I.T., July 15, 1973, pp. 104-117.
2. C. F. F. Karney and A. Bers, Quarterly Progress Report No. 113, Research Laboratory of Electronics, M.I.T., April 15, 1974, pp. 105-112.
3. A. Bers and C. F. F. Karney, Quarterly Progress Report No. 114, Research Laboratory of Electronics, M.I.T., July 15, 1974, pp. 123-131.
4. V. E. Golant, Sov. Phys. – Tech. Phys. 16, 1980 (1972).
5. M. D. Simonutti, Ph.D. Thesis, Department of Electrical Engineering, M.I.T., 1971.
6. C. S. Liu, M. N. Rosenbluth, and R. B. White, Phys. Rev. Letters 31, 697 (1973).
7. J. L. Sperling and F. W. Perkins, MATT 1126, Plasma Physics Laboratory, Princeton University, 1975.
8. S. Bernabei, M. A. Heald, W. M. Hooke, and F. J. Paoloni, Phys. Rev. Letters 34, 866 (1975).
9. A. Bers, C. F. F. Karney, and K. Theilhaber, Progress Report No. 115, Research Laboratory of Electronics, M.I.T., January 1975, pp. 184-204.
10. D. L. Bobroff and H. A. Haus, J. Appl. Phys. 38, 390 (1967).
11. A. Bers and F. W. Chambers, Quarterly Progress Report No. 113, Research Laboratory of Electronics, M.I.T., April 15, 1974, pp. 112-116.

2. PARAMETRIC DOWNCONVERSION FROM LOWER HYBRID WAVES TO KINETIC ION CYCLOTRON HARMONIC WAVES

U.S. Energy Research and Development Administration (Contract E(11-1)-3070)

Duncan C. Watson, Abraham Bers

Introduction

Recently Bers and Karney[1] proposed a scheme for the RF heating of Tokamak plasmas that depends on parametric downconversion occurring in the central, relatively homogeneous region of the plasma. Downconversion to warm-fluid modes has already been investigated.[2,3] Downconversion to kinetic modes is considered in this report.

The form of the required coupling coefficients is derived in Section X-B.5. Here the computations are carried through to an estimation of the growth rate for a Bernstein wave signal and Bernstein wave idler driven by a lower hybrid wave pump. The growth rate compares favorably with growth rates for unstable downconversion to fluid modes.[3]

In the Bers and Karney scheme for heating the central region of a Tokamak plasma, microwave radiation beamed at the plasma surface is only attenuated slightly by evanescence in a thin surface layer, beyond which it converts to an electron-plasma wave.[4] The microwave frequency is chosen so that this plasma wave then propagates inward to the central region of the plasma without further linear conversion.[5] The component of the wavevector parallel to the steady magnetic field remains constant as the energy travels inward, and the perpendicular component greatly increases.[4] The frequency is near the value of the lower hybrid resonance at the center of the plasma,[1] so that the electron plasma wave there may appropriately be termed a lower hybrid wave.

The actual heating takes place as follows. Linear WKB theory predicts that the amplitude of the wave, which we shall call the pump wave, is markedly increased in the denser region of the plasma column. The pump amplitude may then be chosen so that only in the central region it exceeds the threshold for parametric downconversion into other waves. The unstable coupling causes the decay products to grow until these decay waves are capable of heating the ions by nonlinear processes.

The growth rate of the decay products depends on the coupling coefficient for the coherent three-wave interaction that is considered. Karney, Bers, and Kulp[2] have computed the coupling coefficient in three cases of downconversion of the lower hybrid pump wave: (i) downconversion into two ion-acoustic waves, (ii) downconversion into another lower hybrid wave and an electrostatic ion cyclotron wave, and (iii) downconversion into another lower hybrid wave and a magnetosonic wave. In these three cases fluid modes were considered, and so a fluid model of the plasma dynamics suffices for the computation of the coupling coefficient.

The possibility exists that the pump wave may downconvert into modes that cannot

be described by the fluid model and then the corresponding coupling coefficient must be computed from Vlasov theory. This introduces a new feature. We recall that in linear theory fluid waves are undamped, whereas Vlasov waves, when causality is included properly, display Landau damping. In nonlinear theory the wave-wave coupling coefficient computed from fluid theory is completely symmetric in all three interacting waves,[6] whereas the wave-wave coupling coefficient computed from Vlasov theory, when causality is included properly, is in general not symmetric. The asymmetry disappears if the waves possess no resonant particles. This point is enlarged upon in Section X-B.5.

Physical Parameters of Interacting Waves

There are two principal possibilities for downconverting a lower hybrid pump wave into Vlasov modes. The first is to downconvert into two electrostatic ion cyclotron harmonic (EICH) waves. This is the Vlasov model version of the downconversion into two ion acoustic waves; indeed the EICH waves mark the appearance of kinetic effects in the ion acoustic regime of wavevector and frequency. This first possibility entails the computation of the coupling between modes that have very different kinematics; the pump has $k_{\|}v_{Te} \ll \omega$ but the decay waves have $k_{\|}v_{Te} \gg \omega$. A problem arises when computing the electron contribution to the coupling coefficient according to Eq. 25 of Section X-B.5, since each of the three terms in that contribution must be evaluated by using a different set of physical approximations. Furthermore, we shall find that the resulting coupling coefficient does not satisfy the usual symmetries, and must be recomputed for each choice of driven and driving modes.

The second possibility is to downconvert into two Bernstein waves. This possibility entails the computation of coupling between modes all of which have $k_{\|}v_{Te} \ll \omega$. This means that the three terms in the electron contribution to the coupling coefficient can be evaluated in identical fashion. Furthermore, the near absence of resonant particles allows us to use the computed result for any choice of driven and driving modes, since the usual coupling coefficient symmetry is approximately satisfied.

We shall look at the validity of the further approximations

$$k_{\|} = 0 \tag{1}$$

$$k_{\perp}v_{Ti}/\Omega_i \geq 1 \tag{2}$$

as applied to all three interacting modes (the pump wave and the two decay waves). These approximations will enable asymptotic methods to be used in computing the ion contribution to the coupling coefficient. The limit on $k_{\perp}a_i$ for the pump wave is set by the onset of cold-mode to warm-mode conversion. Results of Simonutti[5] indicate that this conversion occurs at a position in the plasma density gradient such that

$$\frac{\omega_{pi}^2(x)}{\omega_{pump}^2} \cong 1 - 2\sqrt{2}\,\frac{k_{\|}v_{Te}}{\omega_{pump}}\,(T_i/T_e)^{1/2}. \tag{3}$$

The cold-fluid mode dispersion relation is

$$\omega^2 = \omega_{pi}^2\left(1 + \frac{m_e}{m_i}\cos^2\theta\right). \tag{4}$$

By combining (3) and (4), we have

$$\frac{k_{\|}^2}{k^2} \cong \frac{m_e}{m_i}\left(\frac{2\sqrt{2}\,\frac{k_{\|}v_{Te}}{\omega}\,(T_i/T_e)^{1/2}}{1 - 2\sqrt{2}\,\frac{k_{\|}v_{Te}}{\omega}\,(T_i/T_e)^{1/2}}\right). \tag{5}$$

For the ingoing pump wave to avoid Landau damping

$$k_{\|}v_{Te} \ll \omega \tag{6}$$

and T_i/T_e is of order unity. Thus (5) may be approximated by setting the denominator of the right-hand side equal to unity. Then the squared ratio of ion Larmor radius to perpendicular wavelength becomes

$$k_{\perp}^2 a_i^2 = (T_i/T_e)^{1/2}\,\frac{k_{\|}v_{Te}}{\omega}\,\frac{\omega^2}{\Omega_i^2}\,\frac{1}{2\sqrt{2}}. \tag{7}$$

To avoid Landau damping effectively

$$\omega/k_{\|}v_{Te} \gtrsim 2.5. \tag{8}$$

The pump frequency lies roughly at the 13^{th} harmonic in the Bers-Karney heating scheme.[1] Thus we may attain a value of the parameter (7) as large as

$$k_{\perp}^2 a_i^2 \cong 25(T_i/T_e)^{1/2}. \tag{9}$$

Hence asymptotic evaluation of the ion contribution to the coupling coefficient, based on the largeness of (9), is worth considering.

Having thus justified approximation (2) let us look at (1). Detailed justification of (1) awaits computation of the coupling coefficient; but we should at least check that $k_{\|}/k_{\perp}$ is small before using approximation (1). According to (5), at the conversion point in the plasma density gradient

$$\frac{k_{\|}}{k_{\perp}} \cong (T_i/T_e)^{1/4}\,(m_e/m_i)^{1/2}\left(\frac{k_{\|}/v_{Te}}{\omega}\right)^{1/2} 2^{3/4}. \tag{10}$$

We deduce that we can attain

$$\frac{k_{\parallel}}{k_{\perp}} \lesssim (m_e/m_i)^{1/2}, \tag{11}$$

so that (1) may be used at least as a first approximation.

Evaluation of Bernstein Coupling Coefficient

For the purpose of evaluating the ion part of the Bernstein wave coupling coefficient (Eq. 35 in Sec. X-B.5) in the limit (2), we assume a Maxwellian distribution, and rewrite in terms of half-angles as

$$\begin{aligned}\frac{\phi_a(\rho_{b,c}+\rho_{c,b})}{\epsilon_o} = &-\frac{q\omega_p^2}{m\Omega^2}\phi_a\phi_b\phi_c k_{a\perp}k_{b\perp}k_{c\perp}\frac{k_{c\perp}}{\sin\frac{\pi\omega_a}{\Omega}\sin\frac{\pi\omega_b}{\Omega}}\int_{-\pi/\Omega}^{\pi/\Omega}\int_{-\pi/\Omega}^{\pi/\Omega} ds\,dt \\ &\cdot \exp[i(\omega_a s+\omega_b t)]\cos\frac{\Omega s}{2}\cos\frac{\Omega t}{2}\sin\left(\frac{\Omega s}{2}-\theta_{ca}\right)\sin\left(\frac{\Omega t}{2}+\theta_{bc}\right) \\ &\cdot \exp\left\{-\frac{2k_{a\perp}^2 v_T^2}{\Omega}\cos^2\frac{\Omega s}{2}-\frac{2k_{b\perp}^2 v_T^2}{\Omega^2}\cos^2\frac{\Omega t}{2}\right. \\ &\left.-\frac{4k_{a\perp}k_{b\perp}v_T^2}{\Omega^2}\cos\frac{\Omega s}{2}\cos\frac{\Omega t}{2}\cos\left(\frac{\Omega s}{2}-\frac{\Omega t}{2}+\theta_{ab}\right)\right\} \\ &+ 2 \text{ more terms obtained by cyclic permutation of subscripts a,b,c.}\end{aligned} \tag{12}$$

The angle θ_{ab} is defined as the angle through which $\vec{k}_{a\perp}$ must be rotated (in clockwise direction as seen by an observer looking in the positive z direction) in order to lie along $\vec{k}_{b\perp}$.

As the asymptotic parameters $|k_{\perp}v_T/\Omega|$ become very large, the final exponential factor becomes very small except where its exponent is zero. The last occurrence then determines those parts of the range of integration whose contributions dominate as $|k_{\perp}v_T/\Omega| \to \infty$.

The final exponent is negative semidefinite. It is zero at the corners of the square forming the region of integration. At the corners the trigonometrical functions preceding the final exponential go to zero. The final exponent is also zero at the point determined by the equations

$$k_{a\perp}\cos\frac{\Omega s}{2} = k_{b\perp}\cos\frac{\Omega t}{2} \tag{13}$$

$$\frac{\Omega s}{2}-\frac{\Omega t}{2} = -\theta_{ab}+\pi+2n\pi, \tag{14}$$

where n is chosen so that (s, t) lies within the region of integration. That is,

$$0 < \theta_{ab} < \pi \Longrightarrow \frac{\Omega s}{2} - \frac{\Omega t}{2} = -\theta_{ab} + \pi \tag{15}$$

$$-\pi < \theta_{ab} < 0 \Longrightarrow \frac{\Omega s}{2} - \frac{\Omega t}{2} = -\theta_{ab} - \pi. \tag{16}$$

At this point, say (s_c, t_c), the trigonometrical functions preceding the final exponential are not zero. Therefore, as the asymptotic parameters $|k_\perp v_T/\Omega| \to \infty$, the contributions from the neighborhoods of the corners of the region of integration are outweighed by the contribution from the neighborhood of the point (s_c, t_c). This point may be located from (13)-(16) by using the trigonometry of the triangle formed by $\vec{k}_{a\perp}$, $\vec{k}_{b\perp}$, and $\vec{k}_{c\perp}$.

Take $0 < \theta_{ab}, \theta_{bc}, \theta_{ca} < \pi$ without loss of generality. Then

$$\frac{\Omega s_c}{2} = \theta_{ca} - \frac{\pi}{2} \tag{17}$$

$$\frac{\Omega t_c}{2} = -\theta_{bc} + \frac{\pi}{2}. \tag{18}$$

Standard asymptotic methods now yield an estimate for (12) in the form

$$\frac{\phi_a(\rho_{b,c} + \rho_{c,b})}{\epsilon_o} = \frac{q\omega_p^2}{m\Omega^2}\,\phi_a\phi_b\phi_c(k_{a\perp}k_{b\perp}k_{c\perp})^{1/2}\,\frac{(2\pi)^{1/2}}{v_T^2}$$

$$\cdot\,\frac{k_{c\perp}^{1/2}\,\exp\left[\frac{i\omega_a}{\Omega}(2\theta_{ca}-\pi)\right]\exp\left[-\frac{i\omega_b}{\Omega}(2\theta_{bc}-\pi)\right]}{\sin\frac{\pi\omega_a}{\Omega}\sin\frac{\pi\omega_b}{\Omega}}\,\sin\theta_{ca}\,\sin\theta_{bc}$$

$$\cdot\,\exp\left\{\frac{-(k_{a\perp}\omega_b\cos\theta_{ca} + k_{b\perp}\omega_a\cos\theta_{bc})^2 - k_{a\perp}k_{b\perp}\omega_c^2}{2(k_{a\perp}k_{b\perp}k_{c\perp})\,k_{c\perp}v_T^2}\right\} + \underset{\text{cyclically}}{\circlearrowleft\,(a,b,c)} \tag{19}$$

This dominant contribution can cease to be dominant if the propagation vectors become collinear. Then the factor $\sin\theta_{ca}\,\sin\theta_{bc}$ goes to zero and the estimate (19) must be supplemented by estimates of the contribution from the corners of the region of interaction. This collinear case has been studied exhaustively by Coppi, Rosenbluth, and Sudan;[7] it will not be pursued further here.

Expression (19) is still more complicated than we would like. It may be simplified if we regard the largeness of the asymptotic parameters $|k_\perp v_T/\Omega|$ as resulting from the largeness of $k_\perp v_T$, with frequencies Ω and ω fixed. Then the parameters $|k_\perp v_T/\omega|$

also become large and the final exponential becomes unity. Including the subscript-permuted terms explicitly, we have the coupling coefficient for noncollinearly propagating waves:

$$\frac{\phi_a(\rho_{b,c}+\rho_{c,b})}{\epsilon_o} = \frac{q\omega_p^2}{m\Omega^2}\,\phi_a\phi_b\phi_c(k_{a\perp}k_{b\perp}k_{c\perp})^{1/2}\,\frac{(2\pi)^{1/2}}{v_T^2}$$

$$\left\{ k_{c\perp}^{1/2}\,\frac{\sin\theta_{ca}\,\sin\theta_{bc}}{\sin\frac{\pi\omega_a}{\Omega}\,\sin\frac{\pi\omega_a}{\Omega}}\,\exp\left[\frac{i\omega_a}{\Omega}(2\theta_{ca}-\pi)-\frac{i\omega_b}{\Omega}(2\theta_{bc}-\pi)\right]\right.$$

$$+\,k_{a\perp}^{1/2}\,\frac{\sin\theta_{ab}\,\sin\theta_{ca}}{\sin\frac{\pi\omega_b}{\Omega}\,\sin\frac{\pi\omega_c}{\Omega}}\,\exp\left[\frac{i\omega_b}{\Omega}(2\theta_{ab}-\pi)-\frac{i\omega_c}{\Omega}(2\theta_{ca}-\pi)\right]$$

$$\left.+\,k_{b\perp}^{1/2}\,\frac{\sin\theta_{bc}\,\sin\theta_{ab}}{\sin\frac{\pi\omega_c}{\Omega}\,\sin\frac{\pi\omega_a}{\Omega}}\,\exp\left[\frac{i\omega_c}{\Omega}(2\theta_{bc}-\pi)-\frac{i\omega_a}{\Omega}(2\theta_{ab}-\pi)\right]\right\}. \tag{20}$$

Thus the ion contribution to the normalized coupling coefficient depends on the physical magnitudes of the problem as follows:

$$C_i \sim \frac{q_i\omega_{pi}^2}{m_i\Omega_i^2}\,\frac{1}{k_\perp v_{Ti}^2}. \tag{21}$$

Now we examine the electron contribution. Assume a Maxwellian distribution and take the electron Larmor radius to be small compared with the wavelength. Since the Bernstein coupling coefficient is known from Eq. 35 in Section X-B.5 to be symmetric in all three modes, this coupling coefficient may be calculated from Eq. 25 in Section X-B.5, with all three terms having the same sign and the same intervals of integration, and with the imaginary parts of $\omega_a, \omega_b, \omega_c$ chosen merely to ensure convergence. Then the electron contribution to the coupling coefficient to zero order in the electron Larmor radius is just the cold-fluid result of Eq. 29 in Section X-B.5 with all $k_{\parallel}$ set to zero:

$$\frac{\phi_a(\rho_{b,c}+\rho_{c,b})}{\epsilon_o} = \frac{q\omega_p^2}{m}\,\phi_a\phi_b\phi_c k_{a\perp}k_{b\perp}k_{c\perp}\,\frac{k_{c\perp}}{4}\left[\frac{\exp(i\theta_{ca})}{\omega_a(\omega_a-\Omega)}+\frac{\exp(-i\theta_{ca})}{\omega_a(\omega_a+\Omega)}\right]$$

$$\cdot\left[\frac{\exp(i\theta_{bc})}{\omega_b(\omega_b+\Omega)}+\frac{\exp(-i\theta_{bc})}{\omega_b(\omega_b-\Omega)}\right]+\begin{array}{c}\circlearrowright\\ a\to b\to c\end{array}\ \text{cyclically}. \tag{22}$$

Thus the electron contribution to the normalized coupling coefficient depends on the physical magnitudes of the problem as follows:

$$C_e \cong \frac{q_e \omega_{pe}^2}{m_e \Omega_e^2} \frac{k_\perp}{\omega^2}. \tag{23}$$

Comparing this with the ion contribution (21), we see that

$$\text{ion contribution : electron contribution} \cong 1 : \frac{k_\perp^2 v_{Ti}^2}{\Omega_i^2} \frac{\Omega_i^2}{\omega^2}. \tag{24}$$

From (7) this leads to the conclusion that the ion and electron contributions to the coupling coefficient are comparable.

Unstable Growth Rates for Parametric Downconversion

Expressions (20) and (22) are unnormalized couplings between Bernstein modes. To obtain coupling coefficients normalized to modes of unit electric field strengths, divide by $\phi_a \phi_b \phi_c k_{a\perp} k_{b\perp} k_{c\perp}$. Let the normalized ion and electron coupling coefficient contributions be C_i, C_e, respectively. Then the growth rate for very small waves a, b in the presence of a much larger, and hence effectively undepleted, pump wave c is given by

$$\gamma^2 = \frac{|C_i + C_e|^2 \, |E_c|^2}{(\partial \epsilon_a/\partial\omega)(\partial \epsilon_b/\partial\omega)}. \tag{25}$$

The linear dispersion function for an ion Bernstein wave is approximately

$$\epsilon = 1 + \frac{\omega_{pe}^2}{\Omega_e^2} - \frac{\omega_{pi}^2}{k_\perp^2 v_{Ti}^2} \sum \frac{2n^2 \Omega_i^2}{\left(\omega^2 - n^2 \Omega_i^2\right)} \Gamma_{ni}, \tag{26}$$

where

$$\Gamma_{ni} = I_n\left(\frac{k_\perp^2 v_{Ti}^2}{\Omega_i^2}\right) \exp\left(-\frac{k_\perp^2 v_{Ti}^2}{\Omega_i^2}\right). \tag{27}$$

For fixed $k_\perp$, (26) determines how near the cyclotron harmonic the frequency ω lies. As $k_\perp \to 0$ or $k_\perp \to \infty$ the function $\Gamma_{ni} \to 0$ and $\omega \to n\Omega_i$, where n indexes the particular harmonic that is being considered. We keep only this near-resonant harmonic term,

$$\epsilon \cong 1 + \frac{\omega_{pe}^2}{\Omega_e^2} - \frac{\omega_{pi}^2}{k_\perp^2 v_{Ti}^2} \frac{2n^2\Omega_i^2}{\omega^2 - n^2\Omega_i^2} \Gamma_{ni}. \tag{28}$$

Further approximation is possible, since the resonant denominator can be factored and $\omega \cong n\Omega_i$. Also $\omega_{pe} \ll \Omega_e$ so that

$$\epsilon \cong 1 - \frac{\omega_{pi}^2}{\Omega_i^2} \frac{n\Omega_i}{\omega - n\Omega_i} X_{ni}, \tag{29}$$

where

$$\left.\begin{aligned} X_{ni} &= I_n(\Lambda)\, e^{-\Lambda}/\Lambda \\ \Lambda &= k_\perp^2 v_{Ti}^2/\Omega_i^2 \end{aligned}\right\} \tag{30}$$

From (29)

$$\frac{\partial\epsilon}{\partial\omega} \cong \frac{\omega_{pi}^2}{\Omega_i^2} \frac{n\Omega_i}{(\omega - n\Omega_i)^2} X_{ni}. \tag{31}$$

But the derivative is taken at $\epsilon = 0$, and therefore

$$\frac{\partial\epsilon}{\partial\omega} \cong \frac{1}{\omega - n\Omega_i}. \tag{32}$$

Substituting in (25) and using (21) with the resonant sine-function denominators from (20), we get

$$\gamma \cong \Omega_i \frac{q_i E_c^{peak}/2m_i\omega_c}{v_{Ti}} \frac{\omega_{pi}^2}{\Omega_i^2} \frac{\omega_c}{\Omega_i} \frac{\Omega_i}{(k_{a\perp}k_{b\perp})^{1/2} v_{Ti}} \frac{\Omega_i}{\pi^2 \sqrt{(\omega_a - n_a\Omega_i)(\omega_b - n_b\Omega_i)}} \tag{33}$$

for growth dominated by ion coupling to decay modes near harmonics of the ion cyclotron frequency. Substituting in (25) and using (23), we get

$$\gamma \cong \frac{k_{c\perp} E_c^{peak}}{2B_o} \frac{\omega_{pi}^2}{\Omega_i^2} \frac{\Omega_i^2}{\omega_a\omega_b} \frac{\sqrt{(\omega_a - n_a\Omega_i)(\omega_b - n_b\Omega_i)}}{\Omega_i} \tag{34}$$

for growth dominated by electron coupling. In general (33) and (34) should both be evaluated and the square root of the sum of their squares used as a guide to the strength of the interaction.

Furthermore, for ion Bernstein waves

$$\omega \sim \left(n + \frac{1}{2}\right) \Omega_i \tag{35}$$

so that the estimates (33) and (34) may be simplified to

$$\gamma \cong \Omega_i \cdot \frac{v_i^{pump}}{v_i^{thermal}} \cdot \frac{\omega_{pi}^2}{\Omega_i^2} \cdot \frac{\omega_c}{\Omega_i} \cdot \frac{2}{\pi^2} \cdot \frac{\Omega_i}{\sqrt{k_{a\perp} k_{b\perp}}\, v_{Ti}} \tag{36}$$

for ion-dominated coupling and

$$\gamma \cong k_{c\perp} v_e^{E \times B \text{ drift}} \cdot \frac{\omega_{pi}^2}{\Omega_i^2} \cdot \frac{\Omega_i^2}{\omega_a \omega_b} \cdot \frac{1}{2} \tag{37}$$

for electron-dominated coupling.

Comparison with Fluid-Mode Coupling

The most promising result found by Karney and Bers (Sec. X-B.1) is the growth rate for unstable downconversion of the lower hybrid pump to a lower hybrid idler and an electrostatic ion cyclotron (EIC) signal. This growth rate is

$$\gamma_o \cong \Omega_i \frac{v_e^{E \times B \text{ drift}}}{v_{Ti}} \frac{T_i}{4T_e} \sqrt{\frac{\omega_{pi}}{\Omega_i}} \frac{\omega_{EIC}}{\Omega_i} \left(\frac{\omega_{EIC} - \Omega_i}{\Omega_i}\right) \sqrt{\frac{2}{\Gamma_{1i}}} \tag{38}$$

and is dominated by electron coupling. The EIC wave is found, for values of $k_\perp v_{Ti}/\Omega_i$ around 5 or 6, to have the parameters

$$\omega_{EIC} \sim 1.1\, \Omega_i \tag{39}$$

$$\Gamma_{1i} \sim 0.2. \tag{40}$$

Taking the Tokamak parameters envisaged by Bers and Karney, for equal electron and ion temperatures we find roughly

$$\gamma_o \cong \Omega_i \cdot \frac{v_e^{E \times B \text{ drift}}}{v_{Ti}} \cdot \frac{1}{2}. \tag{41}$$

Similarly, for the electron-dominated Bernstein downconversion (37) we find

$$\gamma_o \cong \Omega_i \cdot \frac{v_e^{E \times B \text{ drift}}}{v_{Ti}} \cdot \frac{k_{c\perp} v_{Ti}}{\Omega_i} \cdot 2, \tag{42}$$

where the subscript c denotes the pump. Recall that the choice of the factors $k_{c\perp}/\omega_a\omega_b$ in the estimate of the electron-dominated Bernstein coupling coefficient (34) is based on the assumption that the three wavevectors are comparable. Should the pump wavevector be markedly smaller than the decay wavevectors, the estimate (42) can be revised to

$$\gamma_o \cong \Omega_i \cdot \frac{v_e^{E\times B \text{ drift}}}{v_{Ti}} \cdot \frac{k_{a\perp} v_{Ti}}{\Omega_i}, \tag{43}$$

and we still reach the following conclusion. As we allow the ratio of the wavelength to the ion Larmor radius to become large for any of the three interacting waves, the downconversion from a lower hybrid pump to Bernstein decay products acquires a higher growth rate. The downconversion into a lower hybrid decay wave and an electrostatic ion cyclotron wave acquires no such higher growth rate. As the parameter $k_\perp v_{Ti}/\Omega_i$ increases, therefore, the Bernstein downconversion becomes more advantageous as a route to the final goal of plasma heating.

References

1. A. Bers and C. F. F. Karney, Quarterly Progress Report No. 114, Research Laboratory of Electronics, M.I.T., July 15, 1974, pp. 123-131.
2. C. F. F. Karney, A. Bers, and J. L. Kulp, Quarterly Progress Report No. 110, Research Laboratory of Electronics, M.I.T., July 15, 1973, pp. 104-117.
3. C. F. F. Karney and A. Bers, Quarterly Progress Report No. 111, Research Laboratory of Electronics, M.I.T., October 15, 1973, pp. 71-84.
4. R. R. Parker, Quarterly Progress Report No. 102, Research Laboratory of Electronics, M.I.T., July 15, 1971, pp. 97-111.
5. M. D. Simonutti, Jr. and R. R. Parker, Quarterly Progress Report No. 110, Research Laboratory of Electronics, M.I.T., July 15, 1973, pp. 79-86; M. D. Simonutti, Jr., Ph.D. Thesis, Department of Electrical Engineering, M.I.T., September 1974.
6. See, for example, D. C. Watson and A. Bers, Progress Report No. 115, Research Laboratory of Electronics, M.I.T., January 1975, pp. 172-183; D. C. Watson, Ph.D. Thesis, Department of Electrical Engineering and Computer Science, M.I.T., January 1975.
7. B. Coppi, M. N. Rosenbluth, and R. N. Sudan, Ann. Phys. (N.Y.) 55, 207-270 (1969).

3. WHISTLER WAVE FIELD STRUCTURE INSIDE A LINEAR DENSITY PROFILE

U.S. Energy Research and Development Administration (Contract E-(11-1)-3070)

Kim S. Theilhaber, Abraham Bers

Introduction

In a previous report[1] we examined accessibility conditions for the penetration of whistler waves into a magnetized plasma with a transverse density gradient. The exciting structure for the waves was an array of waveguides with electric fields at the apertures transverse to both the external field B_o and the density gradient (Fig. X-12). We decomposed the fields imposed at the boundary into a spectrum of $\exp(-ik_o n_z z)$ components, and found that only a narrow "window" of n_z components could penetrate into the plasma without excessive attenuation. We shall continue the work carried out in the previous report by examining the whistler wave field structure inside the plasma resulting from a source of finite extent at the boundary. We shall use explicit solutions to the wave equation for propagation in a linear density gradient. First, we consider the propagation of a single n_z component into the density gradient. Then the fields corresponding to a narrow spectrum of n_z components will be obtained by integral superposition.

Penetration of a Single n_z Component

The geometry for the penetration of the waves is illustrated in Fig. X-12. With a space-time dependence $\exp(i(\omega t - k_z z))$ the complete wave equation is

$$ik_z \frac{dE_z}{dx} + k_o^2\left(K_\perp - n_z^2\right) E_x - k_o^2 K_x E_y = 0 \tag{1a}$$

$$\frac{d^2E_y}{dx^2} + k_o^2 K_x E_x + k_o^2\left(K_\perp - n_z^2\right) E_y = 0 \tag{1b}$$

$$\frac{d^2E_z}{dx^2} + ik_z \frac{dE_x}{dx} + k_o^2 K_\parallel E_z = 0, \tag{1c}$$

where the K are elements of the cold-plasma dielectric tensor[1] and $n_z \equiv \frac{k_z}{k_o} = \frac{ck_z}{\omega}$.

In a homogeneous medium, for which we can write $\frac{d}{dx} = -ik_x$, Eqs. 1 describe two independent modes of propagation, a "slow" electrostatic wave with a resonance in k_x at $K_\perp = 0$, and a "fast" electromagnetic wave that is a whistler wave in the regime of interest.

In a weak density gradient, Eqs. 1 still describe the independent propagation of slow

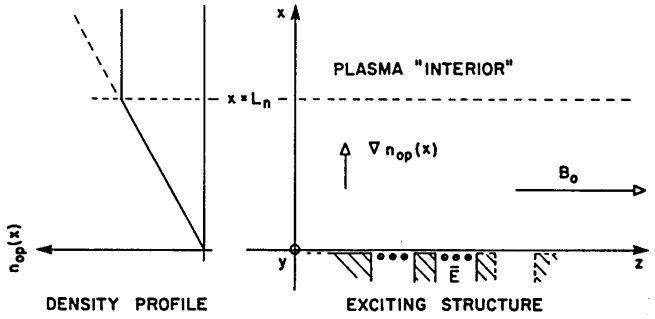

Fig. X-12. Geometry for wave penetration into the linear density profile with input field polarizations.

and fast waves. By neglecting $ik_z \frac{dE_z}{dx}$ in (1a) and eliminating E_x between (1a) and (1b) (an approximation that will be justified later), we obtain an equation for the fast wave:

$$\frac{d^2E_y}{dx^2} + k_o^2 n_x^2(x)\, E_y = 0, \tag{2}$$

where

$$n_x^2(x) = \frac{|K_x(x)|^2}{\left(n_z^2 - K_\perp(x)\right)} - \left(n_z^2 - K_\perp(x)\right). \tag{3}$$

To solve (2), we make the simplifying assumptions: (i) the linear density profile extends to infinity, (ii) the boundary condition at x = 0 is $\underline{E}(x=0, n_z) = \hat{y}E_{yo}(n_z)$ where $E_{yo}(n_z)$ is a component of the unperturbed waveguide fields at x = 0 (that is, the fields maintained in a waveguide with no termination), and (iii) $E_y(x, n_z)$ is an outgoing wave at $x = \infty$.

The following quantities are also useful for gauging and comparing the scale lengths that are involved:

$$\bar{n}(x) = \frac{\omega_{pi}^2(x)}{\omega^2}\left(1 - \frac{\omega^2}{\Omega_e\Omega_i}\right) = \frac{\omega_{pi}^2(x)}{\omega_{pi}^2(x_{LH})} \tag{4a}$$

$$\beta = \frac{\omega_{pi}^2(x_{LH})}{\omega\Omega_i}, \tag{4b}$$

where $\omega_{pi}^2(x_{LH})$ denotes ω_{pi}^2 at the lower hybrid resonance density. In Fig. X-12, $x = L_n$ denotes the point where the "interior" of the plasma (flat density profile) begins. The parametric downconversion scheme contemplated previously[1] requires

$\omega_{pi}^2(L_n) < \omega_{pi}^2(x_{LH})$. In general we shall have $\omega_{pi}^2(L_n) \approx \omega_{pi}^2(x_{LH})$, which maximizes the accessibility "window," and $\beta = \mathcal{O}(10)$. Using the definitions (4), we have

$$K_\perp(x) = 1 - \bar{n}(x) \tag{5a}$$

$$K_x(x) = i\beta\bar{n}(x). \tag{5b}$$

Cutoff for the fast wave ($n_x = 0$ in (3)) occurs at an $x = x_c$ that is given by

$$x_c = \frac{n_z^2 - 1}{\beta\bar{n}(L_n)} L_n \tag{6}$$

so that $x_c/L_n \sim \mathcal{O}(10^{-1})$ and there are many cutoff lengths in the density profile.

Letting $\xi = x/x_c$, we obtain a normalized form of (2):

$$\frac{d^2E_y}{d\xi^2} + a^2 \left\{ \frac{\xi^2 - (1+\xi/\beta)^2}{(1+\xi/\beta)} \right\} E_y = 0, \tag{7}$$

where $a = k_o x_c \sqrt{n_z^2 - 1}$. To solve (7), we delineate the density profile into two overlapping regions: region 1, with $0 < x \ll L_n$, and region 2, with $x_c \ll x < L_n$. In region 1 we have $\xi \ll \beta$ so that the coefficient of E_y in (7) can be approximated by $a^2(\xi^2-1)$. An exact solution can then be obtained for this equation. With the boundary condition $E_y(x=0) = E_{yo}$, we get

$$E_y^{(1)}(x) = E_{yo} \frac{\left\{ W\left(\frac{a}{2}, \sqrt{2a}\,\frac{x}{x_c}\right) - i\kappa W\left(\frac{a}{2}, -\sqrt{2a}\,\frac{x}{x_c}\right) \right\}}{W\left(\frac{a}{2}, 0\right) \cdot (1-i\kappa)}, \tag{8}$$

where $\kappa = (1+e^{\pi a})^{1/2} - \exp\left(\frac{1}{2}\pi a\right)$. The W denote parabolic cylinder functions.[2] We can now calculate from (8) the input impedance for whistler waves. From Faraday's law, $H_z(x) = \frac{i}{\eta_o k_o} \frac{dE_y(x)}{dx}$, where $\eta_o = (\mu_o/\epsilon_o)^{1/2} = 377\ \Omega$. Thus we have

$$\eta = \frac{E_y}{H_z}(x=0) = i\eta_o\left(\frac{1-i\kappa}{1+i\kappa}\right) \frac{\sqrt{2a}\; W^2\left(\frac{a}{2}, 0\right)}{\left(n_z^2-1\right)^{1/2}}. \tag{9}$$

Here, $W^2\left(\frac{a}{2}, 0\right)$ is given by

$$W^2\left(\frac{a}{2}, 0\right) = \frac{1}{2^{3/2}} \left| \frac{\Gamma\left(\frac{1}{4} + i\frac{a}{4}\right)}{\Gamma\left(\frac{3}{4} + i\frac{a}{4}\right)} \right| \sim (e/2)^{1/2} \left[(1+a^2)\left(1 + \frac{a^2}{9}\right) \right]^{-1/8} \exp\left(-\frac{a}{4} \tan^{-1} \frac{2a}{3 + a^2} \right). \tag{10}$$

The expansion is asymptotic to W^2 as $a \to \infty$ but remains fairly accurate down to $a \to 0$ (within a 20% error). For $a = 0$, we have angle $(\eta) = +48°$, so that the reactive part of the impedance is inductive and remains so for $a > 0$.

We now solve (7) for region 2. The WKB solution is

$$E_y^{(2)}(\xi) = \frac{A}{\left[\frac{\xi^2 - \left(1 + \frac{\xi}{\beta}\right)^2}{\left(1 + \frac{\xi}{\beta}\right)} \right]^{1/4}} \cdot \exp[-i\psi_2(\xi)], \tag{11}$$

where the phase function is given by

$$\psi_2(\xi) = a \int^{\xi} \frac{\left[t^2 - \left(1 + \frac{t}{\beta}\right)^2 \right]^{1/2}}{\left(1 + \frac{t}{\beta}\right)^{1/2}} dt + K_2. \tag{12}$$

The constant of integration K_2 accounts for the effect of the lower limit of integration in (12), left undefined. Both A and K_2 are to be determined by asymptotic matching to the solution of region 1. First, we find an approximate expression for ψ_2. By factoring t^2 from the radical in the integrand of (12), expanding it in powers of $\left(1 + \frac{t}{\beta}\right)^2/t^2$, and integrating successive terms we get

$$\psi_2(\xi) \cong a \left\{ 2\beta^2 \left[\frac{1}{3}\left(1 + \frac{\xi}{\beta}\right)^{3/2} - \left(1 + \frac{\xi}{\beta}\right)^{1/2} \right] \right.$$

$$\left. - \frac{1}{2} \left[\frac{2}{3}\left(1 + \frac{\xi}{\beta}\right)^{3/2} + 2\left(1 + \frac{\xi}{\beta}\right)^{1/2} + \log \frac{\left(1 + \frac{\xi}{\beta}\right)^{1/2} - 1}{\left(1 + \frac{\xi}{\beta}\right)^{1/2} + 1} \right] + \mathcal{O}(1/\beta^2) \right\} + K_2. \tag{13}$$

In the matching region $x_c \ll x \ll L_n$, $\xi/\beta \ll 1$ and we can expand (13) in powers of ξ/β. We then neglect terms of $\mathcal{O}(\xi/\beta)$. Similarly, we can expand the parabolic cylinder functions in (8) in the limit $\xi \gg 1$ to obtain an asymptotic expression for $E_y^{(1)}(x)$. This expression for $E_y^{(1)}(x)$ is in the form of an outgoing wave. By matching the asymptotic forms of $E_y^{(1)}$ and $E_y^{(2)}$ (Eqs. 8 and 11), we obtain the complete solution for region 2:

$$E_y^{(2)}(x) = \frac{E_{yo}}{(n_x(x))^{1/2}} \frac{\sqrt{\kappa}}{1 - i\kappa} \frac{(2/a)^{1/4}}{W\left(\frac{a}{2}, 0\right)} \left(n_z^2 - 1\right)^{1/4} \exp[-i\psi_2(x)], \tag{14}$$

where $\psi_2(x)$ is given by (13) with

$$K_2 = a\left\{\frac{4}{3} + \frac{4}{3}\beta^2 - \frac{1}{2}\log(4\beta)\right\} + \frac{\pi}{4} + \frac{1}{2}\phi_2 - \frac{a}{4}\log(2a). \tag{15}$$

Eventually we shall use a greatly simplified form of Eq. 13. By retaining only the leading term of order β^2 and performing some expansions, we obtain

$$\psi(x) \cong \frac{1}{2} k_o \frac{x^2 \omega_{pe}^2(L_n)}{\omega \Omega_e L_n} \cdot \frac{1}{\left(n_z^2 - K_\perp(x)\right)^{1/2}}. \tag{16}$$

In the regime $x \gg x_c$, the field amplitude is given by

$$|E_x(x)| \cong |E_{yo}(n_z)| \frac{\left(n_z^2 - 1\right)\left(n_z^2 - K_\perp\right)^{-3/4}}{(1+e^{\pi a})^{1/4} (2a)^{1/4} W\left(\frac{a}{2}, 0\right)} |K_{\tilde{x}}(x)|^{1/2}. \tag{17}$$

In the limit $a \gg 1$, the exponential tunneling factor caused by wave evanescence near the x = 0 boundary is evident.

$$|E_x(x)| = |E_{yo}| \cdot |K_x(x)|^{1/2} \left(n_z^2 - 1\right)\left(n_z^2 - K_\perp\right)^{-3/4} \exp\left(-\frac{\pi}{4} a\right). \tag{18}$$

The factor $\exp\left(-\frac{\pi}{4} a\right)$ is essentially identical to e^{-a}, which was used in deriving accessibility curves in the previous report.[1] Qualitative plots of the fields as the wave penetrates into the density profile are displayed in Fig. X-13.

Finally, let us comment on the validity of the approximation made in deriving (2). In region 2 both fast and slow waves have short wavelengths, and the effect of the density gradient, with scale length L_n, is small. Taking $d/dx = -ik_x$ and using the polarizations of a homogeneous medium, we get

$$\left| \frac{ik_z dE_z/dx}{k_o^2 K_x E_y} \right| \sim \frac{n_{x\ fast}^2}{n_{x\ slow}^2} \ll 1, \tag{19}$$

where $n_{x\ fast}^2$ is given by (3) and $n_{x\ slow}^2 = -\frac{K_\parallel}{K_\perp}\left(n_z^2 - K_\perp\right) \gg n_{x\ fast}^2$. Thus the approximation appears valid in region 2.

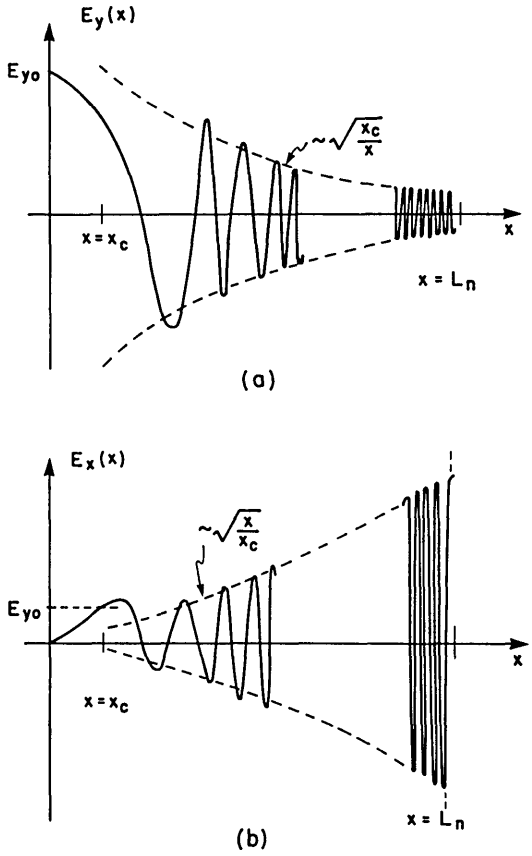

Fig. X-13. Plots of the fields as they penetrate into the density profile. (a) $E_y(x)$, (b) $E_x(x)$.

In region 1 the analysis is more complex at least in the vicinity of the slow-wave cutoff $\left(x_c = \frac{\omega^2}{\omega_{pe}^2(L_n)} L_n\right)$, $|n_{x\ fast}| \sim |n_{x\ slow}|$, and slow and fast waves are coupled together. Equation 2 is no longer valid; it must be replaced by a single fourth-order equation in one field component. Tang and Wong[3] have considered solutions to this equation for arbitrary boundary conditions at x = 0. Their "TE excitation" corresponds to ours; the electric field at x = 0 is transverse to both $\underline{B}_o$ and the density gradient. The analytical details of their calculations are rather complicated, so we merely quote their

results. If we define

$$\lambda_o^2 = -\left(n_z^2 - 1\right) \left.\frac{dK_{\parallel}(x)}{k_o dx}\right|_{x=x_c \text{ slow}} \tag{20}$$

then the ratio of the powers coupled into the slow and fast waves is of order

$$\frac{P_{x \text{ slow}}}{P_{x \text{ fast}}} = \mathcal{O}\left(\lambda_o^{-4/3}\right) \sim \mathcal{O}(10^{-2}). \tag{21}$$

This result corresponds to the case of pure TE excitation at the boundary. Thus the fast wave will exchange little energy with the slow wave as it tunnels through the region of narrow evanescence. While coupling between the waves may be nonnegligible in the evanescence region, it occurs over a region of such small extent that it has little effect on the fast wave once it has reached region 2. Consequently, we shall assume that (2) has approximate validity even down in region 1.

Superposition of a Spectrum of n_z Components

We have just examined the propagation of a single n_z component into the density profile. This case corresponds to an infinite sinusoidal excitation along the x = 0 boundary. We shall now investigate the effect of a source of finite extent at the boundary, one that corresponds to a whole spectrum of n_z components. As explained in the previous report,[1] evanescence in the density profile results in a "filtering" process, in which only a narrow portion of the n_z spectrum propagates all the way into the interior of the plasma. Now we consider only n_z components in this narrow frequency range. We refer to the field at x = 0 corresponding to the narrow n_z spectrum as the "filtered" field $E_{yf}(z)$. We model the filtered spectrum by two rectangular pulses each of 2δ width and $1/(2\delta)$ height, centered about $n_z = \pm n_o$. For a given case the parameters n_o and δ are determined from the accessibility conditions given previously.[1] In this simple approximation, the filtered field is

$$E_{yf}(z) = 2 \cos(k_o z n_o) \cdot \frac{\sin(k_o z \delta)}{k_o z \delta}. \tag{22}$$

The filtered field and its transform are illustrated in Fig. X-14. The halfwidth of the envelope of $E_{yf}(z)$, Δz_e, and the period of the carrier of the waveform, Δz_c, are given by

$$\Delta z_e = \pi / k_o \delta \tag{23a}$$

$$\Delta z_c = 2\pi / k_o n_o. \tag{23b}$$

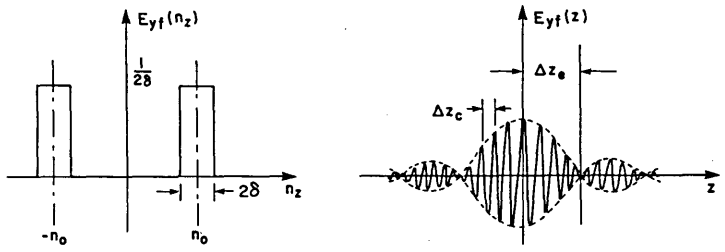

Fig. X-14. Filtered field at x = 0 and its corresponding spectrum. $n_{1,2} = n_o \pm \delta$.

Equations 16 and 17 can be written

$$E_x(x, n_z) = \phi(x, n_z) \exp[-i\psi(x, n_z)], \tag{24}$$

where $\phi(x, n_z) = |E_x(x, n_z)|$, with $E_{yf}(n_z)$ replacing $E_{yo}(n_z)$ in the expression for $|E_x|$. We can now use integral superposition on the entire E_{yf} spectrum. The contribution from the $n_z > 0$ components is

$$E_x(x, z) = \int_{n_1}^{n_2} \phi(x, \eta) \exp\left[-iA\left(\eta + \frac{B}{\left(\eta^2 - K_\perp\right)^{1/2}}\right)\right] d\eta, \tag{25}$$

where we have defined the quantities

$$A = k_o z \tag{26a}$$

$$B = \frac{1}{2} \frac{\omega_{pe}^2(L_n)}{\omega \Omega_e L_n} \cdot \frac{x^2}{z}. \tag{26b}$$

The contribution from the $n_z < 0$ components, as expressed by an integral similar to (25), is identical to (25), with z in B replaced by (-z). As a first simplification of (25), we note that to maximize the accessibility window we must have $\omega_{pi}^2(L_n) \approx \omega_{pi}^2(x_{LH})$, for which $K_\perp \approx 0$. Therefore we neglect $K_\perp$ in the exponent of the integrand in (25). The dominant contribution to the integral will then come from the stationary-phase points of the integrand, if they are included inside the range of integration. The stationary-phase points occur for

$$\frac{d}{d\eta}\psi(x, \eta) = 1 - \frac{B}{\eta^2} = 0. \tag{27}$$

For a given η, $n_1 \leq \eta \leq n_2$, this requires a z such that

$$z = \frac{1}{2} \frac{\omega_{pe}^2(L_n)}{\omega\Omega_e} \frac{1}{\eta^2} = z_{ray}(\eta), \tag{28}$$

where $z_{ray}(\eta)$ is the formula for the ray trajectory of the n_z component given in the previous report.[1] Thus at a given x, the dominant contribution to the integral in (25) will occur whenever $z_{ray}(\eta_2) \leq z \leq z_{ray}(\eta_1)$.

To further evaluate (25), we approximate $\phi(\eta) \approx \phi(n_o)$ and take this factor out of the integrand. We also define the following integrals:

$$F_1(u, \mathcal{M}) = \int_0^u \cos\left(\mathcal{M}\left[\left(t + \frac{1}{t}\right) - 2\right]\right) dt. \tag{29}$$

F_2 is defined similarly with sine replacing cosine in the integrand. Finally, let $z_R \equiv z_{ray}(n_z = n_R)$ with R = 0, 1, 2. Then, with $\hat{E}_x(x,z) \equiv \text{Re}\, E_x(x,z)$, we obtain

$$\hat{E}_x(x,z) = \phi(n_o, x)\, \mathcal{F}(z,x),$$

where

$$\mathcal{F}(z,x) = n_o(z_o/z)^{1/2} \left\{ \cos\left(2k_o n_o (z z_o)^{1/2}\right) F_1\left((z/z_R)^{1/2}, k_o n_o (z z_o)^{1/2}\right) \Bigg|_{R=1}^{R=2} \right.$$

$$\left. - \sin\left(2k_o n_o (z z_o)^{1/2}\right) F_2\left((z/z_R)^{1/2}, k_o n_o (z z_o)^{1/2}\right) \Bigg|_{R=1}^{R=2} \right\}. \tag{30}$$

This complicated expression can be simplified in two complementary regimes. Let $\Delta z_R(x) \equiv z_1(x) - z_2(x) \equiv \frac{4\delta}{n_o} z_o(x)$ denote the separation of the ray trajectories of the extreme n_z components in the right-hand pulse of Fig. X-14. There are two cases of interest.

Case 1. $\Delta z_R(L_n) < \Delta z_e$

The field in the interior ($x = L_n$) is the filtered field multiplied by an amplification factor

$$E_x(x,z) = (x/x_{co})^{1/2} \left[\left(1 + e^{\pi a_o}\right)^{1/4} (2a_o)^{1/4}\, W\left(\frac{a_o}{2}, 0\right)\right]^{-1}$$

$$\cdot \frac{\sin\left(k_o \delta (z - z_o)\right)}{k_o \delta (z - z_o)} \cdot \cos\left(k_o z n_o\right), \tag{31}$$

where the subscript o indicates evaluation at $n_z = n_o$. The waveform at x = 0 has

simply propagated as a single n_z component at $n_z = n_o$, following the ray trajectory of that component. For $\omega \approx \omega_{LH}$, we have $L_n/x_{co} \sim \mathcal{O}(10\text{-}100)$ and the overall amplification of the fields may be as large as $\mathcal{O}(10)$.

The case $\Delta z_R < \Delta z_e$ is illustrated in Fig. X-15a. $|\mathcal{F}(z, L_n)|^2$ is plotted against z/z_o with the following parameters: $L_n = 50$ cm, $B_o = 10$ T, $n_{op}(L_n) = 10^{13}$ cm^{-3}, $n_o = 1.2$, and $\delta = 0.15$.

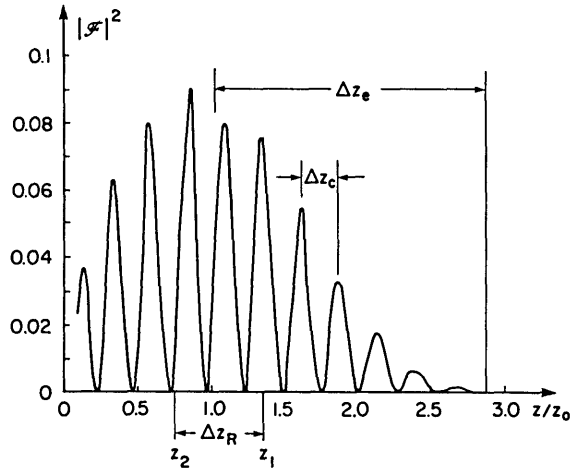

(a)

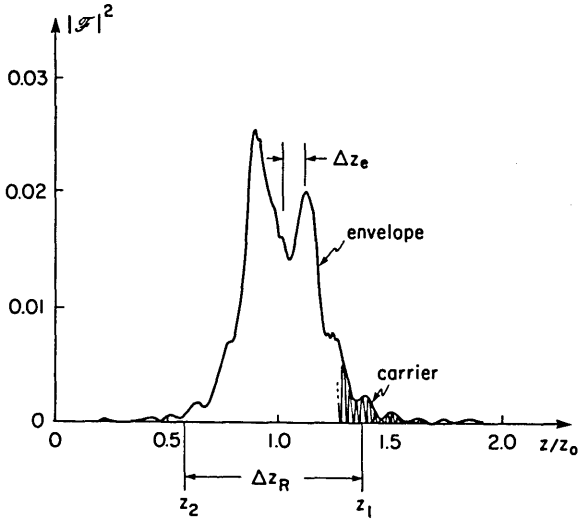

(b)

Fig. X-15. (a) Case 1 plot of $|\mathcal{F}(z,x)|^2$ at $x = L_n$.
(b) Case 2 plot of $|\mathcal{F}(z,x)|^2$ at $x = L_n$.

Case 2. $\Delta z_R(L_n) > \Delta z_e$

Here the differences in the propagation of individual n_z components become important. Interference effects spread out the waveform so that it extends at $x = L_n$ over the range $z_2(L_n) \lesssim z \lesssim z_1(L_n)$. In this range we can write

$$\langle \hat{E}_x^2(x,z) \rangle \approx \frac{\pi}{2} \frac{\left(n_o^2 - 1\right)^{1/2}}{n_o} \frac{|E_{yf}(n_o)|^2}{k_o x} \left(\frac{z_o}{z}\right)^{3/2} \cdot \left[\left\{ C(\nu) \Big|_{R=1}^{R=2} \right\}^2 + \left\{ S(\nu) \Big|_{R=1}^{R=2} \right\}^2 \right], \tag{32}$$

where $\nu = (2/\pi)^{1/2} (k_o n_o z_o)^{1/2} (z/z_o)^{1/2} \{(z/z_R)^{1/2} - 1\}$, the angular brackets denote averaging over a period of the "carrier" frequency $k_o n_o$, and C and S refer to Fresnel integrals of the form[4]

$$C(\nu) = \int_0^\nu \cos\left(\frac{\pi}{2} t^2\right) dt. \tag{33}$$

The case $\Delta z_R > \Delta z_e$ is illustrated in Fig. X-15b with the following parameters: $L_n = 50$ cm, $B_o = 10$ T, $n_{op}(L_n) = 10^{14}$ cm^{-3}, $n_o = 1.4$, and $\delta = 0.2$. The Fresnel integrals in (32) exhibit interference fringes about $\nu = 0$. The width, Δz_f, of these fringes is typically

$$\frac{\Delta z_f}{z_o} = \left(\frac{2\pi}{k_o n_o z_o}\right)^{1/2}. \tag{34}$$

These fringes are clearly visible in Fig. X-15b. They contribute to the irregularities in the envelope of the waveform for the range $z_2 \lesssim z \lesssim z_1$. Finally, the maximum amplification of the fields will be of order

$$\frac{|E_x|}{|E_{yo}|} \sim \frac{1}{\delta (k_o L_n)^{1/2}} = \mathcal{O}(1\text{-}10). \tag{35}$$

The problem of parametric downconversion from various possible field structures that have been obtained is being investigated.

References

1. A. Bers, C. F. F. Karney, and K. Theilhaber, "Whistler Wave Excitation and Its Parametric Downconversion to Electrostatic Ion Cyclotron Waves," Progress Report No. 115, Research Laboratory of Electronics, M.I.T., January 1975, pp. 184-204.
2. M. Abramowitz and Irene A. Stegun, Handbook of Mathematical Functions with Formulas, Graphs and Mathematical Tables (Dover Publications, New York, 1964), p. 685.
3. T. W. Tang and K. C. Wong, "RF Coupling and Mode Conversion at the Lower Hybrid Resonance," University of Massachusetts, January 1975.
4. M. Abramowitz and I. A. Stegun, op. cit., p. 300.

4. ANOMALOUS RF EMISSION AND ION HEATING BY MICROINSTABILITIES IN TOKAMAKS

U.S. Energy Research and Development Administration (Contract E(11-1)-3070)

Abraham Bers, Miloslav S. Tekula

Introduction

Recent experiments on Alcator have produced several interesting results.[1] In these experiments Alcator was operated in a low-density (1×10^{13}/cc) and high-drift velocity ($\langle v_D/v_{Te} \rangle \triangleq \langle J/env_{Te} \rangle \approx 0.3-1$) regime. Other plasma parameters are listed in Table X-1. Under these conditions, microwave radiation ranging from the ion plasma

Table X-1. Alcator parameters in the low-density, high-drift velocity regime. Major radius ≈ 0.5 m, plasma radius ≈ 0.12.

$n = 1 \times 10^{13}$/cc	$\omega_{pi} = 4.1 \times 10^9$/s (650 MHz)
$B_o = 40$ kG	$\nu_{ei} = 2.4 \times 10^4$/s
$T_i = 0.2$ keV	$\nu_{ei}^{eff}(r = a_p/2) = 2.2 \times 10^5$/s
$T_e = 1.0$ keV	$\nu_{ii}^{eff}(r = a_p/2) = 5.6 \times 10^4$/s
$\langle J/env_{Te} \rangle \triangleq \langle v_{De}/v_{Te} \rangle = 0.3$	$\omega_{be}(r = a_p/2) = 4.6 \times 10^6$/s
$m_i/m_e = 1836$	$\omega_{bi}(r = a_p/2) = 4.8 \times 10^4$/s
$\Omega_i = 3.8 \times 10^8$/s	

frequency to a fraction of the electron plasma frequency and heating of the ions from 0.2 keV to 1 keV were observed. From soft and hard x-ray measurements we found that an electron energy tail extending from several kilovolts to hundreds of kilovolts was present. From soft x-rays there is also some evidence that a bump in the electron energy distribution function near 4 keV may have been present. We shall address ourselves to explaining the microwave radiation and ion heating. We assume that the energy source for the discharge phenomenon resides in an anisotropic electron velocity distribution function arising from the applied electric field. We also assume that this drives instabilities in the core of the plasma where the plasma may be assumed to be homogeneous, and trapped electron effects are negligible. Since the electron distribution functions parallel to $\bar{B}_o$ are unknown, we shall study several simple models to see whether any of them is consistent with the available data. The radiation that is generated in such instabilities in the quasi-homogeneous core of the plasma can only be detected if it can propagate out through the density gradient to the plasma wall. We therefore begin with a study of such wave propagation.

Wave Propagation in a Density Gradient

The microwave spectrum that was detected outside Alcator is shown schematically in Fig. X-16. In order to explain it we note that the detection of microwave signals at the outside of the plasma is the inverse of the problem of wave propagation from the outside for lower hybrid heating experiments.[2,3]

We use the cold-plasma approximation to study the propagation of low-frequency electrostatic plasma waves (LFEPW) out of the plasma that is immersed in a uniform magnetic field possessing a density gradient. The more exact warm-plasma theory will not change the arguments significantly. For the sake of simplicity, we use a linear density profile as shown in Fig. X-17. We have singled out three densities, $n_1(x_1)$, $n_2(x_2)$, $n_3(x_3)$. To each of these there corresponds a lower hybrid frequency which in the case of Alcator is approximately equal to the ion plasma frequency $\left(\omega_{lh}^2 = \omega_{pi}^2 = e^2 n(x)/m_i \epsilon_o\right)$. According to cold-plasma theory, a wave with $\omega^2 = \omega_{lh}^2$, and a fixed parallel wave number

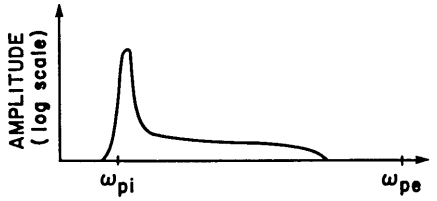

Fig. X-16. Spectrum of microwave radiation.

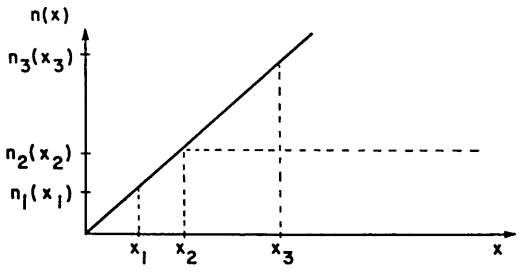

Fig. X-17. Density profile.

($k_{\parallel}$), starting off with $k_{\perp}^2 \gg k_{\parallel}^2$ inside the plasma, will propagate outward. This is shown schematically in Fig. X-18 where curves 1,2,3 correspond to the different densities considered. We pick $k_{\parallel}$ to satisfy the condition of accessibility and avoid electron Landau damping, $v_{Te} \ll \frac{\omega}{k_{\parallel}} \ll c$. Wave 1 is evanescent for very low densities $n < n_1(x_{c1})$ and also for densities greater than $n_1(x_1)$; similarly for the other two waves. We are now ready to construct the plasma model. We assume that the core of the plasma is homogeneous but the periphery has a linear density profile. That is, in Fig. X-17 it is assumed that for $x > x_2$ the density profile is flat (dashed line). We pick n_2 to correspond to a density of 10^{13}/cc, which corresponds to an ion plasma frequency of 650 MHz. The fact that the profile is flat for $x > x_2$ means that in Fig. X-18 curve 3 now becomes curve 4 beyond $n_2(x_2)$. We further assume that the waves leaving the plasma are generated in this homogeneous core. The reason for this will become clear eventually. If this is indeed the case, then the waves for $\omega^2 \gg \omega_{pi}^2 = e^2 n_2(x_2)/m_i \epsilon_o$ will propagate out of the plasma (curves 3,4 in Fig. X-18), while waves having frequencies less than this have to go through a large region of evanescence between $n_2(x_2)$ and whatever their resonant density $n(x) < n_2(x_2)$ is before they start to propagate (see curve 1 in Fig. X-18).

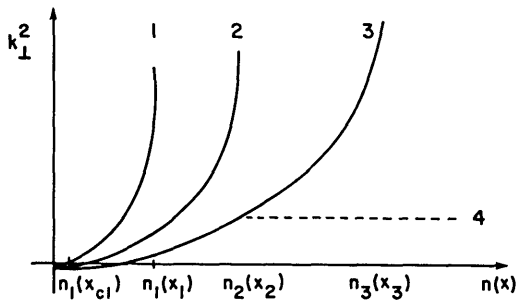

Fig. X-18. Perpendicular wave number as a function of density.

Recall that in the low-density region all waves become evanescent (Fig. X-18). The higher frequency waves are evanescent starting at higher densities. In the case with the plasma core homogeneous, the density $n(x_c)$ at which each of the waves becomes evanescent is given by

$$\frac{n(x_c)}{n(x_2)} = \cos^2 \theta, \tag{1}$$

where θ is the angle of propagation of the wave at the core of the plasma. For the lower hybrid wave $\cos^2 \theta \cong m_e/m_i$. This wave corresponds to wave 2 in Fig. X-18. The reason that no waves are observed at the electron plasma frequency can be inferred from Eq. 1. For these waves $\cos^2 \theta \cong 1$, and hence they are evanescent at $n(x_c) = n(x_2)$.

The detailed solution of the wave propagation problem is complicated when $k_\perp$ approaches zero. The effects of trapped particles may also be important in the density gradient.

Excitation of Low-Frequency Electrostatic Plasma Waves

We have seen that low-frequency electrostatic plasma (LFEPW) waves generated in the core of the plasma can propagate out of the plasma. We shall now study these waves in more detail. The dispersion relation for the LFEPW in a homogeneous magnetoplasma is given[4] by

$$\omega^2 \cong \omega_{pi}^2 \left[1 + \frac{m_i}{m_e} \cos^2 \theta\right]. \tag{2a}$$

This can be obtained by modeling the ions and electrons as cold $\frac{\omega}{k_\parallel} \gg v_{Te}$ and taking $k^2 v_{Te}^2/\omega_{pe}^2 \ll 1$, $k_\perp^2 v_{Te}^2/\Omega_e^2 \ll 1$, and $k_\perp^2 v_{Ti}^2/\Omega_i^2 \ll 1$. Since we are assuming $\Omega_e \gg \omega_{pe}$, we need only assume $k^2 v_{Te}^2/\omega_{pe}^2 \ll 1$. We use the symbols $\omega, k_\parallel, k_\perp, v_{Te}, \omega_{pe}, \Omega_e$ for frequency, parallel and perpendicular wave numbers, electron thermal velocity, electron plasma frequency and electron cyclotron frequency, respectively. Equation 2a simplifies into

$$\omega \cong \omega_{pi} \tag{2b}$$

when $|\theta - \pi/2|^2 \ll m_e/m_i$, which is the lower hybrid wave (LHW), and

$$\omega \cong \omega_{pe} \cos\theta \tag{2c}$$

when $|\theta - \pi/2|^2 \gg m_e/m_i$, which is the electron plasma wave (EPW) (Gould-Trivelpiece mode). These waves are virtually undamped because of their fast parallel phase velocities. Three types of anisotropic electron distribution functions destabilize these waves: drifted, runaway tail, and bump on tail distribution functions. We shall examine each one separately.

a. Electron Drift

Since these waves (Eqs. 2b and 2c) have very fast parallel speeds, the drift velocity necessary to destabilize these waves would have to be larger than the electron thermal speed. (See Fig. X-19.) This would lead to a Buneman-type instability.[4] We shall not examine this instability further, since the conditions necessary to drive it are not likely to prevail.

b. Runaway Tail

In this case (Fig. X-20) the waves (LFEPW) (Eqs. 2b and 2c) are maintained by the bulk of the electron distribution function. The runaway tail is a Maxwellian distribution

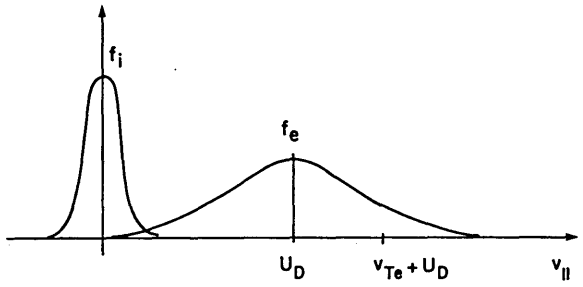

Fig. X-19. Distribution function with large relative drifts ($U_D > v_{Te}$).

in the perpendicular direction with a temperature that is smaller than the bulk temperature but flat in the parallel direction. The total number of particles in the tail is $n_T \ll n_o$, where n_o is the number of particles in the bulk. Since the distribution function in the tail is flat, we can only have cyclotron-driven instabilities[4] and for the LFEPW this produces a growth rate of

$$\frac{\gamma}{\omega} = \frac{\pi}{16} \frac{\omega_{pt}^2}{\Omega_e^2} \frac{k_\perp^2}{k^2} \frac{\Omega_e}{|k_\parallel|} f_{oT}[\Omega_e/k_\parallel], \tag{3a}$$

where

$$f_{oT}[\Omega_e/k_\parallel] = \frac{1}{v_{max} - v_{min}} \approx \frac{1}{v_{max}} = \frac{1}{\alpha c} \tag{3b}$$

with $\alpha \leq 1$, and c the speed of light. We have picked $v_{min} < \omega/k_\parallel < v_{max}$ for all of the LFEPW. Let us now see what v_{max} has to be in order to excite the LFEPW.

Let us consider first the lower hybrid wave with $\omega \cong \omega_{pi}$. To excite these waves, we require that $k_\parallel^2 < \omega^2/v_{Te}^2 \approx \omega_{pi}^2/v_{Te}^2$ be satisfied, which automatically satisfies the requirements $k^2 < \omega_{pe}^2/v_{Te}^2$ and $k_\perp^2 < \Omega_e^2/v_{Te}^2$. Thus for the lower hybrid wave we get

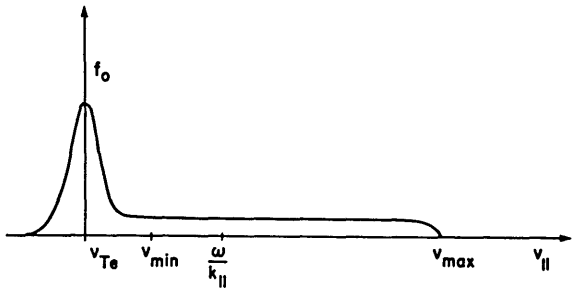

Fig. X-20. Electron distribution function with a runaway tail.

$$\frac{\Omega_e}{k_{\|}c} \gg \frac{\Omega_e}{\omega_{pi}} \frac{v_{Te}}{c} \gg 1. \tag{4a}$$

Since $\Omega_e/k_{\|}c \gg 1$, this implies that the particles that destabilize this wave have velocities near the speed of light. This means that the relativistic mass correction should be used in Eqs. 3. These superfast particles are not likely to be confined very long. Thus we assume that the tail is unlikely to drive the lower hybrid waves.

Let us now consider the electron plasma waves $\omega \cong \omega_{pe} \cos\theta$. Again, we require $k_{\|}^2 < \omega^2/v_{Te}^2 \approx \omega_{pe}^2 \cos^2\theta/v_{Te}^2$, which automatically satisfies $k^2 < \omega_{pe}^2/v_{Te}^2$ and $k_{\perp}^2 < \Omega_e^2/v_{Te}^2$. We get

$$\frac{\Omega_e}{k_{\|}c} \geq \frac{\Omega_e}{\omega_{pe}} \frac{v_{Te}}{c} \frac{1}{\cos\theta}. \tag{4b}$$

From this we can obtain an upper bound on the velocities of the electrons that drive these waves. In the case of Alcator, runaway electrons with energies of several hundred kilovolts were observed. Picking 300 keV as an upper bound, we find that $v_{\|}^{max}/c \approx 0.78$. When using a relativistic mass correction this means that $k_{\| min} \cong \Omega_e/1.2\,c$. This implies that $\cos\theta \geq 0.2$ in Eq. 4b. For these maximum values the growth rate in Eq. 3a is given by $\gamma/\omega_{pi} \cong 0.1\, n_T/n_o \alpha$, which for $n_T/n_o = 0.2$ and $\alpha \cong 0.8$ reduces to $\gamma/\omega_{pi} \approx 2.5 \times 10^{-2}$. As another example, for $\omega \approx \omega_{pe}/2$, and $\Omega_e/k_{\|}c \approx 0.5$, $\alpha = 0.8$ and $n_T/n_o = 0.2$, we get $\gamma/\omega_{pi} \approx 0.015$. We can also find the velocities of the slowest particles that can destabilize these waves. From Eq. 4b we see that $\Omega_e/k_{\|}c$ is smallest when $\cos\theta \approx 1$, which corresponds to $v_{\|}^{min}/c \approx 0.25$. But we note from Eq. 3a that this leads to a zero growth rate. This is consistent with the Alcator observations where no radiation was observed near ω_{pe}.

c. Bump on Tail

We assume that the LFEPW waves are maintained by the bulk electron distribution function (Fig. X-21). Thus if we consider a Maxwellian bump with unequal parallel and perpendicular temperatures containing a total of $n_b \ll n_o$ particles, the growth rate of the LFEPW is

$$\frac{\gamma}{\omega} = \frac{1}{8}\sqrt{\frac{\pi}{2}} \frac{n_b}{n_o} \frac{\omega_{pe}^2}{k^2 v_{Te}^2} (T_e/T_{b\|})^{3/2} (U_b/v_{Te} - \omega/k_{\|}v_{Te}) \exp(-T_e/2T_{b\|})[\omega/k_{\|}v_{Te} - U_b/v_{Te}]^2, \tag{5a}$$

where $T_{b\|}$ is the parallel temperature of the bump, and T_e is the temperature of the bulk electrons. For instability we require $U_b > \omega/k_{\|}$, while to establish the waves we require

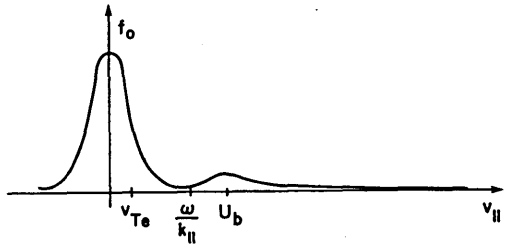

Fig. X-21. Bump on tail electron distribution function.

$k_{||} < \omega/v_{Te}$. These conditions are met both for the lower hybrid waves and the electron plasma waves.

We have not yet imposed any restrictions on the bump, but it has to be made consistent with the experimental evidence. With this in mind we shall require that the bump carry all the measured current (I)

$$I = en_b U_b A, \tag{5b}$$

where n_b, U_b are the homogeneous bump density and velocity. The toroidal effects have been lumped into the area A, which may be different from πr_c^2, the estimated current channel area. To relate n_b, U_b to experimentally measured quantities, we now define the parameter

$$\left\langle \frac{v_D}{v_{Te}} \right\rangle = \left(\frac{I}{\pi r_c^2} \right) \left(\frac{1}{en_{eo} v_{Teo}} \right) \left(\frac{S_1}{S_2} \right), \tag{5c}$$

where I is the measured current, n_{eo} and v_{Teo} are the central electron density and temperature, and S_1 and S_2 are integrals that involve the electron density and temperature profiles. In deriving Eq. 5b it was assumed that the resistivity was classical (proportional to $T_e(r)^{-3/2}$) and the electric field was constant across the cross section. Combining (5b) and (5c), we get

$$\frac{n_b}{n_{eo}} = \left\langle \frac{v_D}{v_{Te}} \right\rangle \left(\frac{\pi r_c^2}{A} \right) \left(\frac{S_2}{S_1} \right) \left(\frac{v_{Teo}}{U_b} \right). \tag{5d}$$

In the case of Alcator, S_1/S_2 is typically equal to 2. From the experiment when $\langle v_D/v_{Te} \rangle = 0.3$ the soft x-ray spectrum indicates the possible presence of a bump at $\sim U_b/v_{Teo} = 2$. In this case, the total number of electrons in the bump and the runaway tail may be inferred to have been 30% of the total. Assuming these values, we then must take $A = \pi r_c^2/4$.

We can now evaluate the growth rate in (5a) for LFEPW. Maximizing the growth rate, we find $\omega/k_{||}v_{Te} = U_b/v_{Te} - \sqrt{T_{b||}/T_e}$. Then for both the lower hybrid and the

electron plasma waves, $k^2 v_{Te}^2/\omega_{pe}^2 = \left(U_b/v_{Te} - \sqrt{T_{b\parallel}/T_e}\right)^{-2}$. Taking into account electron Landau damping, and picking $T_{b\parallel}/T_e \approx 1/4$, we find that the maximum growth rate for $n_b/n_o = 0.3$ is $\gamma/\omega = 0.09$.

The distribution functions considered thus far lead to a variety of other instabilities which we shall consider in connection with ion heating.

Ion Heating

It was observed during the course of the Alcator experiments that the ion temperatures changed from 0.2 keV to 1 keV. This requires an energy input of (3/2 nΔT) of ~1700 J/m^3. We shall now discuss the amount of energy that is available in each of the distribution functions that we have discussed.

a. Electron Drift

We have seen that it is unlikely that the LFEPW would be excited by this mechanism. Let us consider, however, some of the low-frequency electrostatic ion waves that may be destabilized. These are the ion acoustic (IA) and ion cyclotron harmonic waves (EICHW).[5] It has been shown recently that with trapped particle effects taken into account the slow magnetosonic waves ($\omega = k_\parallel c_s$) would essentially be inhibited except very close to the center ($r/R < m_e/m_i$) of the plasma.[6] It is speculated that the IA and EICHW may also be inhibited, since they are destabilized too by slow electrons that may be trapped. If that is not the case, however, we can tap some energy from the drift (for Alcator, $\langle v_D/v_{Te} \rangle \sim 0.3 - 1$). The complete flattening of the electron distribution in one dimension (Fig. X-22) provides us with approximately 5 J/m^3; for example, some

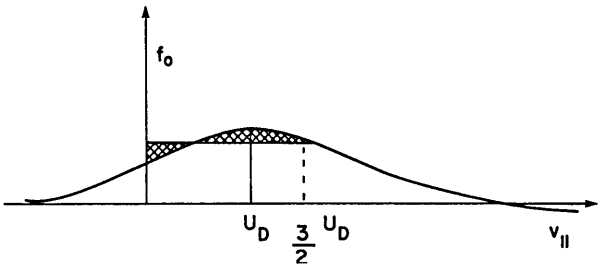

Fig. X-22. Energy available in the electron drift velocity ($U_D < v_{Te}$).

of this energy could be transferred into the ion tail through resonance broadening.[7] Since the isotropization time for the electrons is $\sim \nu_{ee}^{-1} \approx 0.05$ ms, and for the ions $\nu_{ii}^{-1} \approx 0.2$ ms, we would expect this would happen several times in the course of the experiment. Still, the amount of energy available is far from what we require, and the energy is fed mainly into the tail.

b. Runaway Tail

The runaway tail can also be used to excite the IA and ESICH. We assume that the waves are maintained by the bulk electron and ion distribution functions. We shall calculate the amount of growth provided by a tail such as was shown in Fig. X-20 except that now $v_{Ti} \ll \omega/k_{\|} \ll v_{Te}$. This implies that for these waves we need

$$\frac{\Omega_e}{\omega_{pi}} \frac{v_{Ti}}{c} \ll \frac{\Omega_e}{k_{\|}c} \ll \frac{\Omega_e}{\omega_{pi}} \frac{v_{Te}}{c} \tag{6a}$$

for $\omega = k(T_e/m_i)^{1/2} \sim \omega_{pi}/2$ and $k^2 v_{Te}^2/\omega_{pe}^2 \ll 1$. We are neglecting the effects of ion cyclotron damping. In the case of Alcator, Eq. 6a reduces to

$$0.1 \ll \Omega_e/k_{\|}c \ll 11.0. \tag{6b}$$

Thus the tail can extend from $0.1 < v_{\|}/c < 1$. The growth rate of the IA waves because of the tail is given by

$$\frac{\gamma}{\omega} = \frac{\pi}{16} \frac{\omega^2}{\omega_{pi}^2} \frac{\omega_{pt}^2}{\Omega_e^2} \frac{k_{\perp}^2}{k^2} \frac{\Omega_e}{|k_{\|}|} f_{oT}[\Omega_e/k_{\|}]. \tag{6c}$$

As an example, consider Alcator parameters, and $\Omega_e/k_{\|}c = 0.2$, $\omega = \omega_{pi}/2$, $\cos\theta = 0.5$, $v_{max} = ac$ with $a \leq 1$. Then Eq. 6c leads to

$$\frac{\gamma}{\omega_{pi}} = 1.3 \times 10^{-4} \frac{n_t}{n_o} \frac{1}{a}. \tag{6d}$$

Furthermore, letting $a = 1$, $n_T/n_o = 0.2$ leads to $\gamma/\omega_{pi} = 0.2 \times 10^{-4}$, which is rather small. In fact, this is not even large enough to overcome the damping of the wave that has been neglected in Eq. 6c. Thus it is necessary to have some other mechanism whereby these waves are driven unstable at least marginally. Such a mechanism would be the drift of the electron distribution. In the case of Alcator, for a $\langle v_D/v_{Te} \rangle \sim 0.3$ and $\omega \sim \omega_{pi}/2$, we get a growth rate of $\gamma/\omega_{pi} \approx 0.05$. Since the tail is not likely to produce substantial growth of the ion waves, we do not expect the tail to be a large source of energy to the ions through these instabilities.

We shall not discuss the energy that may be available to the lower hybrid wave, since the tail is not likely to excite this wave.

c. Bump on Tail

In this case the only unstable wave in which the ions participate is the lower hybrid wave. Let us now calculate the amount of energy available for heating the ions. A bump that has both perpendicular and parallel temperatures much smaller than those of the

bulk has a kinetic energy of $\sim n_b m U_b^2/2$, where n_b and U_b are the bump number density and velocity, respectively. The total energy in the bump is approximately

$$E_b \cong 1400 \frac{n_b}{n_o} \frac{U_b^2}{v_{Te}^2} \text{ J/m}^3. \tag{7}$$

A fraction ξ of this energy may be transferred to the ions through nonlinear mechanisms. Recall that we required that the bump have $U_b/v_{Te} = 2$ and $n_b/n_{eo} = 0.3$, as inferred from measurements. For these numbers we find that the amount of energy going into the ions is 1700ξ J/m^3. Since the efficiency of energy transfer from the bump to the ions is unlikely to be even 50%, the bump on tail instability alone cannot heat the ions to their observed temperature.

Summary and Conclusion

We have been concerned with explaining the observed microwave radiation and ion heating in some recent experiments on Alcator. The detection of microwaves at the outside wall of the device has two parts. First, it is necessary to find waves that propagate out through the density gradient. We found that low-frequency electrostatic plasma waves (LFEPW) which include the lower hybrid wave and the electron plasma waves are a good candidate. Second, it is necessary to find the kind of anisotropic electron distribution functions that destabilize the LFEPW. To do this we considered 3 model distribution functions for the electrons: a drifted Maxwellian, a Maxwellian with a runaway tail, and a Maxwellian with a bump on tail. Besides driving the LFEPW, these distribution functions lead to various other microinstabilities that could heat the ions.

First, we considered the drifted Maxwellian distribution function. We found that in order to excite the LFEPW, the drift velocity of the electron distribution function has to be greater than the electron thermal speed. Since this was unlikely to happen, this mechanism for exciting the LFEPW was abandoned. On the other hand, if it is possible to neglect the effects of trapped particles, then much smaller drift velocities could destabilize the ion acoustic and ion cyclotron harmonic waves. We found, however, that the amount of energy available from the flattening of the electron distribution function is far below what is needed to explain the observed ion heating.

Next, we considered the runaway tail distribution function, and found that in order to destabilize the lower hybrid waves it was necessary to have electrons with a speed close to that of light. Since these electrons are unlikely to be confined long enough to destabilize the lower hybrid wave, we abandoned this as a mechanism for exciting the lower hybrid wave. We found, however, that the electron plasma waves could be destabilized by particles having velocities $0.25 < v_{||}/c < 0.78$ with the upper bound corresponding to experimentally observed electrons having energy of ~300 keV. But the

runaway tail would not be able to drive either the ion acoustic or the ion cyclotron harmonic waves with large growth rates. Thus the runaway tail was useful only in destabilizing the electron plasma waves.

Finally, we considered a bump on tail distribution function. We found that neither the ion acoustic nor ion cyclotron harmonic waves would be destabilized but that both the lower hybrid and the electron plasma waves would. Since this did not put much of a constraint on the bump, we then looked for other mechanisms that might affect the bump. The requirement that the bump carry all of the plasma current led us to place the bump at $U_b/v_{Te} \approx 2$ (to be consistent with the soft x-ray spectrum) which led to $n_b/n_o \approx 0.30$. However, the amount of energy available in the bump was not sufficient to heat the ions to the observed temperature unless a complete transfer of energy was assumed.

We conclude with a brief remark about some of the nonlinear effects that may account for the energy transfer in the various cases. In the cases of the ion acoustic and the ion cyclotron harmonic waves the energy transfer mechanism is probably resonance broadening.[7] In the case of the bump-driven lower hybrid wave the transfer probably occurs through a nonlinear distortion of the ion orbits which has been studied for $k_{||} = 0$.[8,9] Finally, it is also possible that there may be parametric downconversion from the electron plasma waves[10] to low-frequency ion waves. This would be useful for two reasons; it would help account for the observed peak (at $\omega \sim \omega_{pi}$) in the microwave spectrum and would also make some of the tail energy available to the ions. The electron plasma waves probably account for the quasi-linear scattering[11] of the runaway tail electrons and this leads to an inhibition of the runaway tail.

References

1. "High and Low Current Density Plasma Experiments within the M.I.T. Alcator Program," U. Ascoli-Bartoli et al., to appear in Proc. Fifth Conference on Plasma Physics and Controlled Nuclear Fusion Research, Tokyo, Japan, November 11-15, 1974. (International Atomic Energy Agency, Vienna).
2. R. R. Parker, Quarterly Progress Report No. 102, Research Laboratory of Electronics, M.I.T., July 15, 1971, pp. 97-111.
3. M. D. Simonutti, Ph.D. Thesis, Department of Electrical Engineering, M.I.T., September 1974.
4. A. B. Mikhailovskii, Theory of Plasma Instabilities (Consultants Bureau, New York, 1974).
5. A. Bers, B. Coppi, T. Dupree, R. Kulsrud, and F. Santini, in Plasma Physics and Controlled Nuclear Fusion Research 1971, Vol. II (International Atomic Energy Agency, Vienna, 1971), pp. 247-263.
6. R. D. Hazeltine and F. L. Hinton, Res. Report FRCR #74, University of Texas, Austin, February 1974.
7. M. Z. Caponi and R. C. Davidson, Phys. Rev. Letters 31, 86 (1973).
8. R. E. Aamodt and S. E. Bodner, Phys. Fluids 12, 1471 (1969).
9. D. J. Sigmar and J. D. Callen, Phys. Fluids 14, 1423 (1971).
10. A. Bers and C. F. F. Karney, Quarterly Progress Report No. 114, Research Laboratory of Electronics, M.I.T., July 15, 1974, pp. 123-131.
11. B. B. Kadomtsev and O. P. Pogutse, Sov. Phys. – JETP 26, 1146 (1968).

5. COHERENT WAVE-WAVE COUPLING IN MAGNETIZED VLASOV PLASMA

National Science Foundation (Grant ENG75-06242)

Duncan C. Watson, Abraham Bers

Introduction

The coupling coefficients characterizing nonlinear wave-wave coupling in homogeneous magnetized Vlasov plasma are displayed here in a form that is more convenient for computation than forms found elsewhere.[1-3] This form is used in Section X-B.2 to compute growth rates for unstable parametric downconversion from a lower hybrid pump wave to ion cyclotron harmonic decay waves.

Review of Linear Results

Electrostatic modes in magnetized Vlasov plasma satisfy

$$\frac{\partial f_1}{\partial t} + \vec{v} \cdot \frac{\partial f_1}{\partial \vec{x}} + \vec{v} \times \frac{q\vec{B}_o}{m} \cdot \frac{\partial f_1}{\partial \vec{v}} = - \frac{q\vec{E}_1}{m} \cdot \frac{\partial f_o}{\partial \vec{v}}. \tag{1}$$

We shall not go through the Laplace transform method of solution in detail. We merely note that the correct dispersion relation, with causality taken into account, is obtained by solving (1) for a growing wave and analytically continuing to a damped wave as required. We assume therefore that $\vec{E}_1$ and f_1 go to zero sufficiently rapidly as $t \to -\infty$, then we may integrate (1) along its characteristic or "free-particle orbit" to obtain

$$f_1(\vec{x}, \vec{v}, t) = - \int_{-\infty}^{t} dt' \frac{q\vec{E}_1'}{m} \cdot \frac{\partial f_o}{\partial \vec{v}'}, \tag{2}$$

where the primed quantities are evaluated at the points $(\vec{x}', \vec{v}', t')$ lying on the free-particle trajectory through the points $(\vec{x}, \vec{v}, t)$. The first-order plasma response to an electric field with wavevector and frequency $(\vec{k}_a, \omega_a)$ is given by

$$f_1(\vec{x}, \vec{v}, t) = f_a(\vec{v}) \exp(i\vec{k}_a \cdot \vec{x} - i\omega_a), \tag{3}$$

where

$$f_a(\vec{v}) = - \int_{-\infty}^{t} dt' \frac{q\vec{E}_a}{m} \exp[i\vec{k}_a \cdot (\vec{x}' - \vec{x}) - i\omega_a(t' - t)] \cdot \frac{\partial}{\partial \vec{v}'} f_o(\vec{v}'). \tag{4}$$

We now follow Catto and Baldwin.[4] The charge-density response is

$$\rho_a = \frac{n_o q^2 \phi_a}{m} \int d^3\vec{v} \int_{-\infty}^{t} dt' \, i\vec{k}_a \cdot \frac{\partial}{\partial \vec{v}} f_o(\vec{v}') \exp[i\vec{k}_a \cdot (\vec{x}' - \vec{x}) - i\omega_a(t' - t)]. \tag{5}$$

Interchange the order of integrations and change the variable of integration in the velocity-space integral. Thus

$$\rho_a = \frac{n_o q^2 \phi_a}{m} \int_{-\infty}^{t} dt' \int d^3\vec{v}' \left| \frac{\partial \vec{v}}{\partial \vec{v}'} \right| i\vec{k}_a \cdot \frac{\partial}{\partial \vec{v}'} f_o(\vec{v}') \exp[i\vec{k}_a \cdot (\vec{x}'-\vec{x}) - i\omega_a(t'-t)]. \tag{6}$$

The determinant of the Jacobian is unity. Also,

$$\vec{x} - \vec{x}' = \begin{pmatrix} \frac{\sin \Omega(t-t')}{\Omega} & \frac{1-\cos \Omega(t-t')}{\Omega} & 0 \\ \frac{-1+\cos \Omega(t-t')}{\Omega} & \frac{\sin \Omega(t-t')}{\Omega} & 0 \\ 0 & 0 & 0 \end{pmatrix} \vec{v}',$$

$$\equiv \vec{\vec{M}}(t-t')\,\vec{v}' \tag{7}$$

say, where $\Omega = qB_o/m$ and $\vec{B}_o$ lies along z. In terms of the Fourier-transformed velocity distribution function

$$F_o(\vec{\beta}) \equiv \int d^3\vec{v}' \exp(-i\vec{\beta} \cdot \vec{v}')\, f_o(\vec{v}'), \tag{8}$$

expression (6) for the charge-density response of the plasma may be written

$$\frac{\rho_a}{\epsilon_o} = -\phi_a \omega_p^2 \int_{-\infty}^{t} dt' \exp[-i\omega_a(t'-t)]\, \vec{k}_a \cdot \vec{\vec{M}}(t-t')\, \vec{k}_a F_o\left(\vec{\vec{M}}^T(t-t')\,\vec{k}_a\right). \tag{9}$$

This is as far as we need go to illustrate the methods used in the nonlinear calculations. The result (9) for the linear charge density excited by a single potential wave may be substituted in Poisson's equation to obtain a linear dispersion relation. Similarly, results that we shall obtain for the second-order charge density may be substituted in Poisson's equation to obtain equations describing mode-mode coupling. These additional steps are well known and will not be repeated here.

Derivation of the Coupling Coefficient

We continue to use the same methods to find the second-order response of a magnetized Vlasov plasma to two potential waves.

The first-order response of a magnetized Vlasov plasma satisfies

$$\frac{\partial f_1}{\partial t} + \vec{v} \cdot \frac{\partial f_1}{\partial \vec{x}} + \vec{v} \times \frac{q\vec{B}_o}{m} \cdot \frac{\partial f_1}{\partial \vec{v}} = -\frac{q\vec{E}_1}{m} \cdot \frac{\partial f_o}{\partial \vec{v}}. \tag{10}$$

The second-order response satisfies a similar equation:

$$\frac{\partial f_2}{\partial t} + \vec{v} \cdot \frac{\partial f_1}{\partial \vec{x}} + \vec{v} \times \frac{q\vec{B}_o}{m} \cdot \frac{\partial f_2}{\partial \vec{v}} = - \frac{q\vec{E}_1}{m} \cdot \frac{\partial f_1}{\partial \vec{v}} . \tag{11}$$

Thus it may be computed in the same way by integrating along the characteristic:

$$f_2(\vec{x}, \vec{v}, t) = - \int_{-\infty}^{t} dt' \frac{q\vec{E}_1'}{m} \cdot \frac{\partial f_1}{\partial \vec{v}'} \tag{12}$$

(cf. (2)). The second-order plasma response to two electric fields with wavevectors and frequencies $(\vec{k}_b, \omega_b)$, $(\vec{k}_c, \omega_c)$ is given by

$$f_2(\vec{x}, \vec{v}, t) = (f_{b,c}(\vec{v}) + f_{c,b}(\vec{v})) \exp(i(\vec{k}_b + \vec{k}_c) \cdot \vec{x} - i(\omega_b + \omega_c) t), \tag{13}$$

where

$$f_{b,c}(\vec{v}) = - \int_{-\infty}^{t} dt' \frac{q\vec{E}_b}{m} \exp[i\vec{k}_b \cdot (\vec{x}' - \vec{x}) - i\omega_b(t'-t)] \frac{\partial}{\partial \vec{v}'} f_c(\vec{v}') \exp[i\vec{k}_c \cdot (\vec{x}' - \vec{x}) - i\omega_c(t'-t)] \tag{14}$$

(cf. (3), (4)). Here $f_c(\vec{v}')$ is the linear response to the electric field at $(\vec{k}_c, \omega_c)$. We use again the technique of Catto and Baldwin[4] and write the second-order charge-density response as

$$\rho_{b,c} = \frac{n_o q^2 \phi_b}{m} \int_{-\infty}^{t} dt' \int d^3\vec{v}' \left| \frac{\partial \vec{v}}{\partial \vec{v}'} \right| i\vec{k}_b \cdot \frac{\partial}{\partial \vec{v}'} f_c(\vec{v}') \exp[i(\vec{k}_b + \vec{k}_c) \cdot (\vec{x}' - \vec{x}) - i(\omega_b + \omega_c)(t'-t)] \tag{15}$$

(cf. (6)). The determinant of the Jacobian is unity, and again

$$\vec{x} - \vec{x}' = \vec{\vec{M}}(t-t') \vec{v}'. \tag{16}$$

In terms of the Fourier-transformed first-order perturbation in the velocity distribution

$$F_c(\vec{\beta}) = \int d^3\vec{v}' \exp(-i\vec{\beta} \cdot \vec{v}') f_c(\vec{v}'), \tag{17}$$

we have

$$\frac{\rho_{b,c}}{\epsilon_o} = -\phi_b \omega_p^2 \int_{-\infty}^{t} dt' \exp[-i(\omega_b + \omega_c)(t-t')] (\vec{k}_b + \vec{k}_c) \cdot \vec{\vec{M}}(t-t') \vec{k}_b F_c\left[\vec{\vec{M}}^T(t-t')(\vec{k}_b + \vec{k}_c) \right] \tag{18}$$

(cf. (8), (9)). The next step is to express $F_c(\vec{\beta})$ in terms of F_o. From (4) we have

$$f_c(\vec{u}) = \frac{q\phi_c}{m} \int_{-\infty}^{s} ds' \exp[-i\omega_c(s'-s)] \exp[i\vec{k}_c \cdot (\vec{y}' - \vec{y})] i\vec{k}_c \cdot \frac{\partial}{\partial \vec{u}'} f_o(\vec{u}') \tag{19}$$

$$F_c(\vec{\beta}) = \frac{q\phi_c}{m} \int_{-\infty}^{s} ds' \exp[-i\omega_c(s'-s)] \int d^3\vec{u} \exp(-i\vec{k}_c \cdot \vec{\vec{M}}(s-s')\vec{u}')$$

$$\cdot \exp(-i\vec{\beta} \cdot \vec{u}) \, i\vec{k}_c \cdot \frac{\partial}{\partial \vec{u}'} f_o(\vec{u}'). \tag{20}$$

Also

$$\vec{u} = \begin{pmatrix} \cos \Omega(s-s') & \sin \Omega(s-s') & 0 \\ -\sin \Omega(s-s') & \cos \Omega(s-s') & 0 \\ 0 & 0 & 1 \end{pmatrix} \vec{u}'$$

$$\equiv \vec{\vec{N}}(s-s') \vec{u}', \text{ say.} \tag{21}$$

Therefore (20) may be written

$$F_c(\vec{\beta}) = -\frac{q\phi_c}{m} \int_{-\infty}^{s} ds' \exp[-i\omega_c(s'-s)]$$

$$\cdot \left[\vec{k}_c \cdot \vec{\vec{M}}(s-s') \vec{k}_c + \vec{\beta} \cdot \vec{\vec{N}}(s-s') \vec{k}_c\right] F_o\left[\vec{\vec{M}}^T(s-s') \vec{k}_c + \vec{\vec{N}}^T(s-s') \vec{\beta}\right]. \tag{22}$$

Substitute (22) in (18) and make use of definitions (7) and (21). We then have the expression for one piece of the second-order charge density (13) in terms of the Fourier transform (8) of the unperturbed velocity distribution function.

$$\frac{\rho_{b,c}}{\epsilon_o} = \phi_b \phi_c \frac{\omega_p^2 q}{m} \int_{-\infty}^{s} \int_{-\infty}^{t} ds'dt' \exp[-i\omega_c(s'-s) - i(\omega_b+\omega_c)(t'-t)]$$

$$\cdot \left[(\vec{k}_b+\vec{k}_c) \cdot \vec{\vec{M}}(t-t') \vec{k}_b\right]\left[-\vec{k}_b \cdot \vec{\vec{M}}(s-s') \vec{k}_c + (\vec{k}_b+\vec{k}_c) \cdot \vec{\vec{M}}(s-s'+t-t') \vec{k}_c\right]$$

$$\cdot F_o\left[-\vec{\vec{M}}^T(s-s') \vec{k}_b + \vec{\vec{M}}^T(s-s'+t-t')(\vec{k}_b+\vec{k}_c)\right]. \tag{23}$$

The Fourier transform of the unperturbed velocity distribution in a magnetic field has the same symmetry as the distribution itself:

$$\left.\begin{aligned} f_o(\vec{v}) &\equiv f_o\left(v_\perp^2, v_\parallel\right) \\ F_o(\vec{\beta}) &\equiv F_o\left(\beta_\perp^2, \beta_\parallel\right) \end{aligned}\right\} \tag{24}$$

We use this fact and the explicit form (7) for the matrix $\vec{\vec{M}}$. After some manipulation of the ranges and variables of integration we obtain

$$\frac{\phi_a(\rho_{b,c}+\rho_{c,b})}{\epsilon_o} = \frac{q\omega_p^2}{m}\phi_a\phi_b\phi_c$$

$$\left\{\int_{-\infty}^{0}\int_{0}^{\infty} dsdt\, \exp[i(\omega_a s+\omega_b t)]\right.$$

$$\left\{\frac{1}{\Omega}[(\vec{k}_c\times\vec{k}_a)_{\parallel}(1-\cos\Omega s)+\vec{k}_{c\perp}\cdot\vec{k}_{a\perp}\sin\Omega s]+k_{c\parallel}k_{a\parallel}s\right\}$$

$$\left\{\frac{1}{\Omega}[(\vec{k}_b\times\vec{k}_c)_{\parallel}(1-\cos\Omega t)-\vec{k}_{b\perp}\cdot\vec{k}_{c\perp}\sin\Omega t]-k_{b\parallel}k_{c\parallel}t\right\}$$

$$F_o\left\{\frac{2}{\Omega^2}[(\vec{k}_c\times\vec{k}_a)_{\parallel}\sin\Omega s-(\vec{k}_b\times\vec{k}_c)_{\parallel}\sin\Omega t-(k_a\times k_b)_{\parallel}\sin\Omega(s-t)\right.$$

$$\left.-\vec{k}_{c\perp}\cdot\vec{k}_{a\perp}(1-\cos\Omega s)-\vec{k}_{b\perp}\cdot\vec{k}_{c\perp}(1-\cos\Omega t)-\vec{k}_{a\perp}\cdot\vec{k}_{b\perp}(1-\cos\Omega(s-t))],k_{a\parallel}s+k_{b\parallel}t\right\}$$

$$-\int_{0}^{\infty}\int_{0}^{\infty} dsdt\, \exp[i(\omega_b s+\omega_c t)]$$

$$\left\{\frac{1}{\Omega}[(\vec{k}_a\times\vec{k}_b)_{\parallel}(1-\cos\Omega s)+\vec{k}_{a\perp}\cdot\vec{k}_{b\perp}\sin\Omega s]+k_{a\parallel}k_{b\parallel}s\right\}$$

$$\left\{\frac{1}{\Omega}[(\vec{k}_c\times\vec{k}_a)_{\parallel}(1-\cos\Omega t)-\vec{k}_{c\perp}\cdot\vec{k}_{a\perp}\sin\Omega t]-k_{c\parallel}k_{a\parallel}t\right\}$$

$$F_o\left\{\frac{2}{\Omega^2}[(\vec{k}_a\times\vec{k}_b)_{\parallel}\sin\Omega s-(\vec{k}_c\times\vec{k}_a)_{\parallel}\sin\Omega t-(\vec{k}_b\times\vec{k}_c)_{\parallel}\sin\Omega(s-t)\right.$$

$$\left.-\vec{k}_{a\perp}\cdot\vec{k}_{b\perp}(1-\cos\Omega s)-\vec{k}_{c\perp}\cdot\vec{k}_{a\perp}(1-\cos\Omega t)-\vec{k}_{b\perp}\cdot\vec{k}_{c\perp}(1-\cos\Omega(s-t))],k_{b\parallel}s+k_{c\parallel}t\right\}$$

$$+\int_{0}^{\infty}\int_{-\infty}^{0} dsdt\, \exp[i(\omega_c s+\omega_a t)]$$

$$\left\{\frac{1}{\Omega}[(\vec{k}_b\times\vec{k}_c)_{\parallel}(1-\cos\Omega s)+\vec{k}_{b\perp}\cdot\vec{k}_{c\perp}\sin\Omega s]+k_{b\parallel}k_{c\parallel}s\right\}$$

$$\left\{\frac{1}{\Omega}[(\vec{k}_a\times\vec{k}_b)_{\parallel}(1-\cos\Omega t)-\vec{k}_{a\perp}\cdot\vec{k}_{b\perp}\sin\Omega t]-k_{a\parallel}k_{b\parallel}t\right\}$$

$$F_o\left\{\frac{2}{\Omega^2}[(\vec{k}_b\times\vec{k}_c)_{\parallel}\sin\Omega s-(\vec{k}_a\times\vec{k}_b)_{\parallel}\sin\Omega t-(\vec{k}_c\times\vec{k}_a)_{\parallel}\sin\Omega(s-t)\right.$$

$$\left.\left.-\vec{k}_{b\perp}\cdot\vec{k}_{c\perp}(1-\cos\Omega s)-\vec{k}_{a\perp}\cdot\vec{k}_{b\perp}(1-\cos\Omega t)-\vec{k}_{c\perp}\cdot\vec{k}_{a\perp}(1-\cos\Omega(s-t)),k_{c\parallel}s+k_{a\parallel}t\right\}\right\}$$

(25)

The wavevector and frequency $(\vec{k}_a, \omega_a)$ are defined by

$$(\vec{0}, 0) = (\vec{k}_a, \omega_a) + (\vec{k}_b, \omega_b) + (\vec{k}_c, \omega_c). \tag{26}$$

The right-hand side of (25) becomes the coupling coefficient normalized to modes of unit electric field strength $\vec{e} \cdot \vec{j}/\epsilon_o\omega$ when divided by $\phi_a\phi_b\phi_c k_a k_b k_c$. It is almost symmetric in the three subscripts a, b, c, with the symmetry broken by a reversed interval of integration and a reversed sign, both of which are associated with the subscript a. It will be shown that this formal asymmetry can only lead to genuine asymmetry of the coupling coefficient if at least one of the three modes has a Doppler-shifted cyclotron resonance $\omega - k_{||}v_{||} = n\Omega$, n integer at a parallel velocity lying within the velocity distribution function. The energy of particles resonant with a mode is not included physically in the energy of that mode, and yet it must enter into the total energy conservation of the system. This is why particles with resonant parallel velocities destroy the symmetry of the mode-mode coupling coefficient. The form (25) has the advantage that in case the modes do possess many resonant particles, the coupling between them can still be dealt with correctly. These points will now be illustrated further in the course of specializing the form (25) to particular distribution functions and particular directions of propagation.

Special Forms of Coupling Coefficient

The simplest form of zero-order velocity distribution that may be considered is that corresponding to a cold beam. For later convenience, we index the beam by α and write

$$f_o(\vec{v}) = \delta^2(\vec{v}_\perp)\, \delta(v_{||} - v_{o\alpha}). \tag{27}$$

The Fourier transform of this is

$$F_o(\vec{\beta}) = \exp(-i\beta_{||}v_{o\alpha}). \tag{28}$$

The result of substituting (28) in (25) is

$$\frac{\phi_a(\rho_{b,c}+\rho_{c,b})}{\epsilon_o} = -\frac{q\omega_{p\alpha}^2}{m}\phi_a\phi_b\phi_c \left\{\frac{i\Omega(\vec{k}_c \times \vec{k}_a)_{||}}{\omega_{a\alpha}\left(\Omega^2 - \omega_{a\alpha}^2\right)} + \frac{\vec{k}_{c\perp} \cdot \vec{k}_{a\perp}}{\Omega^2 - \omega_{a\alpha}^2} - \frac{k_{c||}k_{a||}}{\omega_{a\alpha}^2}\right\}$$

$$\left\{\frac{i\Omega(\vec{k}_b \times \vec{k}_c)_{||}}{\omega_{b\alpha}\left(\Omega^2 - \omega_{b\alpha}^2\right)} - \frac{\vec{k}_{b\perp} \cdot \vec{k}_{c\perp}}{\Omega^2 - \omega_{b\alpha}^2} + \frac{k_{b||}k_{c||}}{\omega_{b\alpha}^2}\right\}$$

$$+ \text{2 further terms generated by cyclic interchange of subscripts a, b, c.} \tag{29}$$

Here $\omega_{a\alpha} \equiv \omega_a - k_{a\parallel} v_{o\alpha}$, and so on.

This cold-beam coupling coefficient is totally symmetric in the three modes, as expected for a system lacking resonant particles. It agrees with previous cold-fluid calculations[5] and is included to clarify later discussion of the effect of resonant particles on the coupling coefficient.

Another simple form of velocity distribution is the beam that only possesses perpendicular temperature. For such a beam

$$f_o(\vec{v}) = f_{\perp\alpha}\left(v_\perp^2\right) \delta(v_\parallel - v_{o\alpha}). \tag{30}$$

The Fourier transform of this is

$$F_o(\vec{\beta}) = F_{\perp\alpha}\left(\beta_\perp^2\right) \exp(-i\beta_\parallel v_{o\alpha}). \tag{31}$$

The result of substituting (31) in (25) is

$$\frac{\phi_a(\rho_{b,c} + \rho_{c,b})}{\epsilon_o} = \frac{q\omega_{p\alpha}^2}{m} \phi_a\phi_b\phi_c \frac{4}{\sin\frac{\pi\omega_{a\alpha}}{\Omega} \sin\frac{\pi\omega_{b\alpha}}{\Omega}} \int_{-\pi/\Omega}^{\pi/\Omega} \int_{-\pi/\Omega}^{\pi/\Omega} ds dt \exp[i(\omega_{a\alpha}s + \omega_{b\alpha}t)]$$

$$\left\{\frac{1}{\Omega}\left[(\vec{k}_c \times \vec{k}_a)_\parallel (1 + \cos\Omega s) - \vec{k}_{c\perp} \cdot \vec{k}_{a\perp} \sin\Omega s\right] + k_{c\parallel}k_{a\parallel}\left[s + \frac{i\pi}{\Omega}\cot\frac{\pi\omega_{a\alpha}}{\Omega}\right]\right\}$$

$$\left\{\frac{1}{\Omega}\left[(\vec{k}_b \times \vec{k}_c)_\parallel (1 + \cos\Omega t) + \vec{k}_{b\perp} \cdot \vec{k}_{c\perp} \sin\Omega t\right] - k_{b\parallel}k_{c\parallel}\left[t + \frac{i\pi}{\Omega}\cot\frac{\pi\omega_{b\alpha}}{\Omega}\right]\right\}$$

$$F_{\perp\alpha}\left\{\frac{2}{\Omega^2}\left[-(k_c \times k_a)_\parallel \sin\Omega s + (\vec{k}_b \times \vec{k}_c)_\parallel \sin\Omega t - (k_a \times k_b)_\parallel \sin\Omega(s-t)\right.\right.$$

$$\left.\left. - \vec{k}_{c\perp} \cdot \vec{k}_{a\perp}(1 + \cos\Omega s) - \vec{k}_{b\perp} \cdot \vec{k}_{c\perp}(1 + \cos\Omega t) - \vec{k}_{a\perp} \cdot \vec{k}_{b\perp}(1 - \cos\Omega(s-t))\right]\right\}$$

+ 2 more terms generated by cyclic interchange of subscripts a, b, c. (32)

This coupling coefficient for a cold beam in the parallel direction is totally symmetric in the three modes, as expected for a system lacking resonant particles.

Another way to avoid resonant particles is to take three modes propagating perpendicular to the magnetic field. The most general distribution in a magnetic field is

$$f_o(\vec{v}) = f_o\left(v_\perp^2, v_\parallel\right). \tag{33}$$

The Fourier transform correspondingly is of the form

$$F_o(\vec{\beta}) = F_o\left(\beta_\perp^2, \beta_\parallel\right). \tag{34}$$

The result of substituting (34) in (25) with all $k_{\parallel}$ zero is

$$\frac{\phi_a(\rho_{b,c}+\rho_{c,b})}{\epsilon_o} = \frac{q\omega_p^2}{m}\phi_a\phi_b\phi_c \frac{4}{\sin\frac{\pi\omega_a}{\Omega}\sin\frac{\pi\omega_b}{\Omega}} \int_{-\pi/\Omega}^{\pi/\Omega}\int_{-\pi/\Omega}^{\pi/\Omega} dsdt\, \exp[i(\omega_a s+\omega_b t)]$$

$$[(\vec{k}_c\times\vec{k}_a)_{\parallel}(1+\cos\Omega s)-\vec{k}_{c\perp}\cdot\vec{k}_{a\perp}\sin\Omega s][(\vec{k}_b\times\vec{k}_c)_{\parallel}(1+\cos\Omega t)+\vec{k}_{b\perp}\cdot\vec{k}_{c\perp}\sin\Omega t]$$

$$F_o\left\{\frac{2}{\Omega^2}[-(\vec{k}_c\times\vec{k}_a)_{\parallel}\sin\Omega s+(k_b\times k_c)_{\parallel}\sin\Omega t-(k_a\times k_b)_{\parallel}\sin\Omega(s-t)\right.$$

$$\left.-\vec{k}_{c\perp}\cdot\vec{k}_{a\perp}(1+\cos\Omega s)-\vec{k}_{b\perp}\cdot\vec{k}_{c\perp}(1+\cos\Omega t)-\vec{k}_{a\perp}\cdot\vec{k}_{b\perp}(1-\cos\Omega(s-t))],0\right\}$$

+ 2 more terms given by cyclic permutation of subscripts a, b, c. (35)

This coupling coefficient for Berstein waves is totally symmetric in the three waves that interact.

To study the effect of resonant particles on the coupling coefficient, we first take the simplest case — that of waves propagating parallel to the magnetic field. The result is the same as we would get from the one-dimensional zero magnetic field problem or the three-dimensional infinite magnetic field problem.

We may derive the coupling coefficient as an integral over $\beta_{\parallel}$. Substitute (34) in (25) and set all $k_{\perp}$ to zero. We obtain

$$\frac{\phi_a(\rho_{b,c}+\rho_{c,b})}{\epsilon_o} = \frac{q\omega_p^2}{m}\phi_a\phi_b\phi_c$$

$$\left\{-\int_{-\infty}^{0}\int_{0}^{\infty} dsdt\,\exp[i(\omega_a s+\omega_b t)]\,k_{c\parallel}^2 k_{a\parallel}sk_{b\parallel}tF_o\{0,k_{a\parallel}s+k_{b\parallel}t\}\right.$$

$$+\int_{0}^{\infty}\int_{0}^{\infty} dsdt\,\exp[i(\omega_b s+\omega_c t)]\,k_{a\parallel}^2 k_{b\parallel}sk_{c\parallel}tF_o\{0,k_{b\parallel}s+k_{c\parallel}t\}$$

$$\left.-\int_{0}^{\infty}\int_{-\infty}^{0} dsdt\,\exp[i(\omega_c s+\omega_a t)]\,k_{b\parallel}^2 k_{c\parallel}sk_{a\parallel}tF_o\{0,k_{c\parallel}s+k_{a\parallel}t\}\right\} \quad (36)$$

Alternatively, by using the fact that conductivities of whatever order in the electric field are additive over particle populations, we can construct the coupling coefficient by superposing the coefficients for beams. Substitute (31) in (25), set all $k_{\perp}$ to zero, and leave the integrals in infinite interval form. The coupling coefficient for a beam with no parallel velocity spread is then

$$\left.\frac{\phi_a(\rho_{b,c}+\rho_{c,b})}{\epsilon_o}\right|_{beam} = \frac{q\omega_{p\alpha}^2}{m}\phi_a\phi_b\phi_c\left\{\frac{k_{a\|}k_{b\|}k_{c\|}^2}{\omega_{a\alpha}^2\omega_{b\alpha}^2}+\frac{k_{b\|}k_{c\|}k_{a\|}^2}{\omega_{b\alpha}^2\omega_{c\alpha}^2}+\frac{k_{c\|}k_{a\|}k_{b\|}^2}{\omega_{c\alpha}^2\omega_{a\alpha}^2}\right\}, \tag{37}$$

where

$$\omega_{p\alpha}^2 \equiv \omega_p^2 f_{\|}(v_{o\alpha}) \tag{38}$$

and

$$f_{\|}(v_{\|}) \equiv \int d\vec{v}_{\perp}\, f_o\left(v_{\perp}^2, v_{\|}\right). \tag{39}$$

Integrating over parallel velocity, we get

$$\frac{\phi_a(\rho_{b,c}+\rho_{c,b})}{\epsilon_o} = \frac{q\omega_p^2}{m}\phi_a\phi_b\phi_c(k_{a\|}k_{b\|}k_{c\|})^{-1}\int dv_{\|}\, f_{\|}(v_{\|})$$
$$\left\{\frac{k_{c\|}^3}{\left(v_{\|}-\frac{\omega_a}{k_{a\|}}\right)^2\left(v_{\|}-\frac{\omega_b}{k_{b\|}}\right)^2}+\frac{k_{a\|}^3}{\left(v_{\|}-\frac{\omega_b}{k_{b\|}}\right)^2\left(v_{\|}-\frac{\omega_c}{k_{c\|}}\right)^2}+\frac{k_{b\|}^3}{\left(v_{\|}-\frac{\omega_c}{k_{c\|}}\right)^2\left(v_{\|}-\frac{\omega_a}{k_{a\|}}\right)^2}\right\}. \tag{40}$$

The sense in which the poles of this integrand are to be circumnavigated in the complex $v_{\|}$-plane is to be determined from the regions of integration occurring in the double integrals over $\beta_{\|}$, the variable conjugate to $v_{\|}$, which constitute (36). First, suppose that

$$k_{a\|} < 0 < k_{b\|}, k_{c\|}. \tag{41}$$

Then (36) may be written

$$\frac{\phi_a(\rho_{b,c}+\rho_{c,b})}{\epsilon_o} = \frac{q\omega_p^2}{m}\phi_a\phi_b\phi_c(k_{a\|}k_{b\|}k_{c\|})^{-1}$$
$$\left\{\int_0^\infty\int_0^\infty d\beta_{\|}d\beta_{\|}' \exp\left[i\left(\frac{\omega_a}{k_{a\|}}\beta_{\|}+\frac{\omega_b}{k_{b\|}}\beta_{\|}'\right)\right]k_{c\|}^3\beta_{\|}\beta_{\|}'F_o\{0,\beta_{\|}+\beta_{\|}'\}\right.$$
$$+\int_0^\infty\int_0^\infty d\beta_{\|}d\beta_{\|}' \exp\left[i\left(\frac{\omega_b}{k_{b\|}}\beta_{\|}+\frac{\omega_c}{k_{c\|}}\beta_{\|}'\right)\right]k_{a\|}^3\beta_{\|}\beta_{\|}'F_o\{0,\beta_{\|}+\beta_{\|}'\}$$
$$\left.+\int_0^\infty\int_0^\infty d\beta_{\|}d\beta_{\|}' \exp\left[i\left(\frac{\omega_c}{k_{c\|}}\beta_{\|}+\frac{\omega_a}{k_{a\|}}\beta_{\|}'\right)\right]k_{b\|}^3\beta_{\|}\beta_{\|}'F_o\{0,\beta_{\|}+\beta_{\|}'\}\right\}. \tag{42}$$

The sense of the integrations in (42) clearly indicates that all poles in the integrand

of (40) are to be above the integration contour in the complex $v_{||}$-plane. Reversals of sign of $k_{||}$ in (41) induce corresponding reversals of integration intervals in (42). Recall that in the derivation of the coupling coefficient the convergence of the integrals (12) and (14) over the past particle histories was ensured by taking $0 < \text{Im}\ (\omega_b)$, $\text{Im}\ (\omega_c)$, and by the fact that the frequency ω_a is defined as an auxiliary quantity by (26), so that

$$\text{Im}\ (\omega_a) < 0 < \text{Im}\ (\omega_b),\ \text{Im}\ (\omega_c). \tag{43}$$

Thus we may always locate the contour correctly by first taking the mode frequencies to satisfy (43) and then choosing the contour to be the real $v_{||}$ axis. For other values of the mode frequencies we continue analytically by deforming the contour as necessary. The subscript a is used to denote the driven mode and the subscripts b and c the modes generating the nonlinear current.

It follows that the three quantities

$$\frac{\phi_a(\rho_{b,c}+\rho_{c,b})}{\epsilon_o},\ \frac{\phi_b(\rho_{c,a}+\rho_{a,c})}{\epsilon_o},\ \frac{\phi_c(\rho_{a,b}+\rho_{b,a})}{\epsilon_o} \tag{44}$$

when computed for real $\omega_a, \omega_b, \omega_c$ will differ from each other by imaginary quantities proportional to residues at the poles of the integrand in (42). The usual symmetry of coupling coefficients is consonant with the Manley-Rowe relations governing energy exchange between modes. The asymmetry displayed here is due to the presence of particles resonating with the modes. The existence of resonant-particle energy means that the sum of the mode energies alone is no longer a conserved quantity.

Similar arguments hold for coupling between modes propagating at arbitrary angles to the magnetic field. Poles of the integrand in the integral over parallel velocity now occur at all parallel velocities for which the Doppler-shifted frequency is a multiple of the cyclotron frequency. These poles are circumvented by the prescription (43), and the symmetry of the coupling coefficients (44) holds only insofar as the residues at the poles are small enough to be neglected.

References

1. R. E. Aamodt, Phys. Rev. A 138, 4513 (1965).
2. B. Coppi, M. N. Rosenbluth, and R. N. Sudan, Ann. Phys. (N.Y.) 55, 207-270 (1969).
3. Y. C. Lee and P. K. Kaw, Report MATT-860, Princeton Plasma Physics Laboratory, August 1971.
4. P. J. Catto and D. E. Baldwin, Phys. Fluids 13, 214 (1970).
5. See, for instance, D. C. Watson and A. Bers, Progress Report No. 115, Research Laboratory of Electronics, M.I.T., January 1975, pp. 172-183; also D. C. Watson, Ph.D. Thesis, Department of Electrical Engineering and Computer Science, M.I.T., January 1975.

6. WAVE-PACKET TRAPPING AND RESONANCE BROADENING IN WAVE CASCADING PROCESSES

National Science Foundation (Grant ENG75-06242)

Nathaniel J. Fisch, Abraham Bers

Introduction

In a previous report[1] we showed that resonance broadening as a rule does not occur in wave interactions because, as we reasoned, there is no mechanism that perturbs the wave modes on a time scale faster than that associated with what we have called detuning effects. The exception to this rule occurs when two of the interacting waves belong to the same wave packet in such a way that the diffusion approximation[2] can be made. This type of interaction involves a cascading of energy within one wave packet, as opposed to the transfer of energy between wave packets, so that the wave modes are more sensitive to a finite level of turbulence. We shall show that for these wave cascading processes there is a resonance broadening much like that for wave-particle interactions and, in the appropriate limit, there is a trapping of the (cascading) wave packet that is much like particle trapping.

Derivation of the Wave Diffusion Equations

We derive the wave diffusion equations directly from the coherent wave-wave equations instead of first making the random-phase approximation and then dealing only with the many-wave limit.[2] The advantage of this procedure is that the physics becomes clearer and the limits of validity of the theory can be obtained. The assumptions in making the diffusion approximation are $A_2 \gg A_1$ and $\Delta k_1 \gg k_2$ where A_i is the action amplitude of spectrum i and spectrum 1 contributes two modes to the three-wave interaction; that is, the decay condition is $k_1 = k_2 + k_3$ where k_1 and k_3 both refer to modes in spectrum 1. In Fig. X-23 we construct schematically the localization (implied by our assumptions) of wave packet 1 in the long-wavelength wave packet 2. For simplicity, we assume, at first, that there is only one mode in spectrum 2. In Fig. X-23, for simplicity, we construct only one wave packet 1, although it must be realized that, by assumption, there are many such packets situated homogeneously in the plasma. We deduce immediately that the interaction is spatially periodic, with a period $2\pi/k_2$, since wave packet 1 includes so many modes that only the envelope of the packet effectively enters into the problem. Thus the interaction of wave packet 1 with wave 2 depends only on the phase of the packet with respect to the wave trough in which it is found and not on the location of the trough. This means that in describing this interaction mathematically we may make random-phase approximations for wave packet 1 while retaining the phase information associated with wave 2.

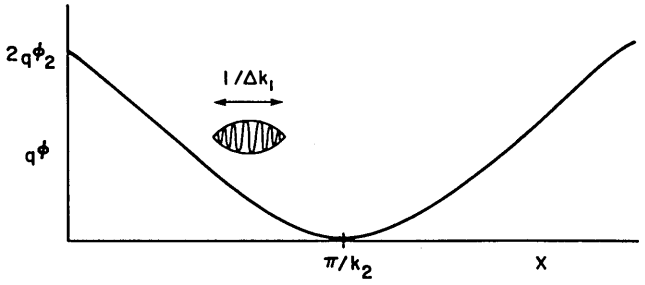

Fig. X-23. Wave-wave-packet interaction.

We may use the coherent wave-wave equations to write

$$\frac{d}{dt}\left|A_1(k_1)\right|^2 = A_1^*(k_1)\,\frac{d}{dt}A_1(k_1) + \text{c.c.}$$

$$= A_1^*(k_1) \sum_{k_1'<k_1} VA_2(k_2)\,A_1(k_1')\,\exp(i(k_2+k_1'-k_1)\,x)$$

$$-A_1^*(k_1) \sum_{k_1'>k_1} V^*A_2^*(k_2)\,A_1(k_1')\,\exp(-i(k_2-k_1'+k_1)\,x) + \text{c.c.}, \qquad (1)$$

where in short notation we write $\exp(ik_ix)$ for $\exp(ik_ix-i\omega_it)$. The first summation represents decay from a lower wave-number mode into k_1, whereas the second summation represents decay from a higher wave-number mode. We now wish to average (1) over a distance that is large compared with $1/\Delta k$, but small compared with $1/k_2$. From (1) we see that the largest contributions to the summation surviving this averaging will be at $k_1' = k_1 \pm k_2$. On the other hand, we must be sure to retain the slowly varying phase $\exp(ik_2x)$ so that the interaction will be periodic as deduced above. Thus performing an averaging operation of the type

$$\langle \exp(i(k_2+k_1'-k_1)\,x)\rangle \propto \exp(ik_2x)\;\delta(k_2+k_1'-k_1) \qquad (2)$$

on (1) results in

$$\frac{d}{dt}\left|A_1(k_1)\right|^2 = VA_2\,e^{ik_2x}\,A_1^*(k_1)\,A_1(k_1-k_2) - V^*A_2^*\,e^{-ik_2x}\,A_1^*(k_1)\,A_1(k_1+k_2) + \text{c.c.}$$

$$= VA_2\,e^{ik_2x}\left[A_1^*(k_1)\,A_1(k_1-k_2) - A_1(k_1)\,A_1^*(k_1+k_2)\right] + \text{c.c.}$$

$$= \left(VA_2\,e^{ik_2x} + \text{c.c.}\right)\left(-k_2\,\frac{\partial\left|A_1(k_1)\right|^2}{\partial k_1}\right), \qquad (3)$$

where we have expanded in a Taylor's series in k_2 to obtain the final equality. Note that the change in action in k_1-space for wave packet 1 is dependent on its slope in k_1-space as is to be expected for cascading processes. Also note that, as required by the periodicity condition, the phase $\exp(ik_2x)$ is retained in (3) so that wave packet 1 can "know" where it is (spatially) located in the trough of wave 2. In other words, wave packet 1 is unable to distinguish between a change in the phase of A_2 or simply a shift in space.

We may put (3) into a more transparent form by expanding $\partial/\partial k = (\partial v_{g1}/\partial k_1)(\partial/\partial v_{g1})$ and $d/dt = \partial/\partial t + v_{g1}(\partial/\partial x)$. Also, since $|A_1|^2$ is proportional to N_1, the action density with units $|A_1|^2/k$, N_1 obeys the same equation as $|A_1|^2$. Furthermore, since (3) is linear in A_2, we may linearly sum contributions from a number of modes in wave packet 2. Thus (3) may be written as

$$\left(\frac{\partial}{\partial t} + v_{g1}\frac{\partial}{\partial x} + F\frac{\partial}{\partial v_{g1}}\right) N_1(x, v_{g1}, t) = 0, \tag{4}$$

where F has units of force/mass and is given by

$$F = \mathrm{Re} \sum_{k_2} 2VA_2(k_2)\, k_2 \frac{\partial v_{g1}}{\partial k_1} \exp[i(k_2x - \omega_2 t)]. \tag{5}$$

Note that (4) is a Vlasov equation for N_1 in (x, v_{g1}, t)-space mathematically identical to the Vlasov equation for the particle distribution in (x, v, t)-space.[3] In fact, we may treat (4) in a manner entirely analogous to the treatment of the Vlasov equation in obtaining the quasi-linear diffusion equation. In particular, we may linearize

$$N_1 = N_{10}(v_{g1}, t) + N_{11}(x, v_{g1}, t), \tag{6}$$

where $N_{11} \ll N_{10}$ and $\langle N_1 \rangle = N_{10}$, with the angular brackets now indicating a spatial average over all of space. By treating V, and hence F, and N_{11} as small parameters, we may linearize (4) and, in the presence of a sufficiently broad spectrum 2, we may proceed[4] as in the derivation of quasi-linear wave-particle equations to obtain a diffusion equation for N_{10} given by

$$\frac{\partial}{\partial t} N_{10}(v_{g1}, t) = \frac{\partial}{\partial v_{g1}} D \frac{\partial}{\partial v_{g1}} N_{10}(v_{g1}, t), \tag{7}$$

where

$$D = \left[\frac{8\pi |V|^2 N_2(k_2)\, k_2^2 \left|\frac{\partial v_{g1}}{\partial k_1}\right|^2}{|v_{g1} - v_{g2}|}\right]_{k_2 = \omega_2/v_{g1}} \tag{8}$$

which is the same as the equation obtained by performing immediately the diffusion approximation on the weak-turbulence equations. It should be recognized that in proceeding from (4) to (7) we have assumed that N_2 is a slowly varying function of time.

Similarly, it is possible to obtain the growth rate for N_2 directly from the coherent wave-wave equations before performing the random-phase approximations. First, linearize

$$A_1 = A_{10}(k_1) + a_1(k_1, x, t) \tag{9}$$

$$A_3 = A_{30}(k_3) + a_3(k_3, x, t), \tag{10}$$

where A_1 and A_3 both belong to wave packet 1, and A_{10} is independent of time and space for homogeneous initial conditions because of the smallness of the coupling coefficient so that perturbations in A_i caused by the interaction may be lumped in $a_i \ll A_{i0}$. We can then write the coherent wave-wave equation for A_2 as

$$\frac{dA_2}{dt} = -\Sigma V^* A_{10} A_{30}^* \exp[i(\delta\omega t - \delta k x)]$$

$$-\Sigma V^* \left(A_{10} a_3^* + A_{30}^* a_1\right) \exp[i(\delta\omega t - \delta k x)], \tag{11}$$

where $\delta k = k_1 - k_2 - k_3$, and $\delta\omega = \omega_1 - \omega_2 - \omega_3$. We may argue that the first term on the right-hand side of (11) is negligible in a time-asymptotic solution (in terms of contributions to the wave energy) because of phase mixing. We can deal with the second term on the right-hand side of (11) by finding a_1 and a_3 by integrating the coherent equations for A_1 and A_3, assuming, for simplicity, homogeneous initial conditions and an interaction only in time. Then we get

$$\frac{dA_2}{dt} = +\sum V^* A_{10}\, e^{i\delta\omega t} \sum V' A_{10}'^* A_2' \left[\frac{e^{-i\delta\omega' t} - 1}{-\delta\omega'}\right] + \text{c.c.}$$

$$= \sum |V|^2 A_2 \left[\frac{1 - e^{i\delta\omega t}}{-i\delta\omega}\right]\left[|A_{10}|^2 - |A_{30}|^2\right] + \text{c.c.} \tag{12}$$

Here we noted that the double summation reduces to a single summation because of phase mixing in the cross terms ($\delta\omega \neq \delta\omega'$) in the time-asymptotic limit. We can now expand $|A_{10}|^2$ in a Taylor's series in k_2 and write the time-asymptotic solution as

$$\frac{dA_2}{dt} = A_2 \sum_{k_1} 2\pi |V|^2 k_2 \frac{\partial |A_{10}|^2}{\partial k_1} \delta(\omega_1 - \omega_2 - \omega_3)$$

$$= \frac{A_2 4\pi |V|^2}{\partial v_{g1}/\partial k} \frac{\partial N_1}{\partial k_1}. \tag{13}$$

In writing the second equality in (13) we converted the sum to an integral over k_1 and we noted that the δ-function contributed twice $\{$at $v_{g1}(\pm k_1) = \omega_2/k_2\}$. Since N_2 is proportional to A_2, we may put (13) into the form

$$\frac{dN_2(k_2)}{dt} = \gamma N_2(k_2), \qquad \gamma = 8\pi |V|^2 \frac{\partial N_1}{\partial v_{g1}}\bigg|_{v_{g1}=\omega_2/k_2} \tag{14}$$

which, together with (7), constitutes the quasi-linear equations for the wave-wave interaction.[2]

Wave-Packet Trapping

One of the major advantages of the alternative derivation of the wave diffusion equations presented here is the intermediate result (4). In the event that spectrum 2 is sufficiently coherent, (4) describes wave-packet trapping analogously to particle trapping. The coherent long-wavelength wave 2 can trap the short-wavelength wave packet by stimulating decay of high group velocity waves to low group velocity waves, thereby decelerating the packet, or vice versa for accelerating the packet. One decay process takes place at one wall of the trough, whereas the opposite decay takes place at the other wall, which results in trapping the packet. Note that this process leads to orbit secularities that can invalidate the derivation of the wave diffusion equations. In particular, note that

$$\frac{\partial N_{11}}{\partial v_{g1}} \sim Fk_2 \frac{\partial N_{10}}{\partial v_{g1}} t^2 \tag{15}$$

so that $\partial N_{11}/\partial v_{g1} \sim \partial N_{10}/\partial v_{g1}$ at time

$$t = \tau_{tr}^{w} \equiv 2\pi(k_2 F)^{-1/2} \tag{16}$$

which we may call the wave-packet trapping or bounce time analogously to the particle trapping or bounce time.

The wave conservation equation (4) contains sufficient information to allow us to deduce all details of what we have called wave-packet trapping. The mathematics is identical to that for particle trapping and it remains only to interpret the results correctly. Since we think of particle trapping in terms of forces on a particle, for illustrative purposes, we present an alternative derivation of the wave-packet trapping equations for a specific interaction from a consideration of the forces on a wave packet.

The wave cascading process that we use as an example is the generation of relativistic (phase velocity ~ c) plasma waves by a collimated beam of transverse waves. This interaction has been considered by Tsytovich,[5] who pays particular attention to the

one-dimensional problem and notes that the growth rate for the longitudinal waves has a maximum in the direction of the transverse waves. A dispersion diagram for this interaction is shown in Fig. X-24. The major result of this interaction is the nonlinear growth of the energy in the plasma waves caused by a diffusion in k-space of the transverse modes. In one dimension, the transverse wave spectrum tends to flatten toward

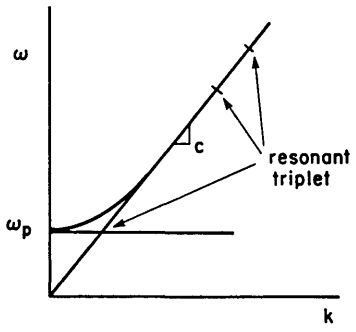

Fig. X-24.
Coupling between a longitudinal wave and a broad packet of transverse waves.

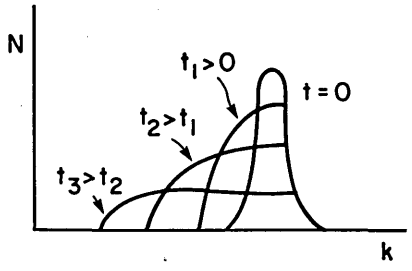

Fig. X-25.
Diffusion in k-space of the transverse wave packet.

lower k or plateau, and thus to develop a time-asymptotic distribution as shown in Fig. X-25.

The force (time averaged over the fast field variations) on the transverse wave packet by an external source may be written as the time derivative of the wave packet momentum. That is,

$$\sum_{\bar{k}_1} \frac{d}{dt}\left[\bar{k}_1 \left|A_1(\bar{k}_1)\right|^2\right] = -\mathrm{Re}\,\frac{1}{2}\left[\sum_{\bar{k}_1} \rho_{ext}\bar{E}_1^* + \sum_{\bar{k}_1} \bar{J}_{ext} \times \bar{B}_1^*\right], \tag{17}$$

where we have summed the forces on the wave modes[6] over all the modes in the packet. In (17) $|A_1|^2$ is the action of modes $[\bar{k}_1, \omega(\bar{k}_1)]$ in the wave packet, and ρ_{ext} and $\bar{J}_{ext}$ are respectively the "external" charge density and current sources. The complex electric and magnetic field amplitudes of modes $(\bar{k}_1)$ are $\bar{E}_1$ and $\bar{B}_1$. It is assumed on the left-hand side of (17) that d/dt commutes with $\sum_{k_1}$ because of our assumption $\Delta k_1 \ll k_1$. Thus the total time derivative d/dt follows the slowly varying (compared with ω_1 and k_1 oscillations) envelope of wave packet 1.

The external sources in (17) may be taken to be perturbations caused by nonlinear effects. In this interaction, the transverse modes nonlinearly excite longitudinal density and current fluctuations that drive the low-frequency wave. Each transverse mode is regenerated by the other transverse mode and the longitudinal mode, which nonlinearly

excite transverse current fluctuations. These current fluctuations can impart momentum to the transverse modes through the $\bar{J}_{ext} \times \bar{B}_1$ force as in (17). This $\bar{J}_{ext}$ may be written as

$$\bar{J}_{ext} = \sum_{k_1} \frac{4V\bar{E}_1(\bar{E}_2 \cdot \bar{k}_2) \exp[i(k_2x-\omega_2t)]}{\left|\frac{\partial\epsilon_1}{\partial\omega_1}\right| \left|\frac{\partial\epsilon_2}{\partial\omega_2}\right|^{1/2}}, \tag{18}$$

where subscripts 2 and 1 refer to longitudinal and transverse modes respectively, and V is the nonlinear coupling coefficient. Note that the coupling between the longitudinal mode and a transverse mode does not excite charge-density perturbations (ρ_{ext}) and the current-density perturbation ($\bar{J}_{ext}$) is transverse to $\bar{k}$. Thus from (17) we can see that the only momentum change in the wave packet is due to the $\bar{J}_{ext} \times \bar{B}_1$ force which is in the $\bar{k}$ direction. This must be the case, since the left-hand side of (17) has components only in the k direction. Plugging (18) into (17), we can write

$$\sum_{k_1} \frac{d}{dt}\left(k_1|A_1|^2\right) = -\mathrm{Re} \sum_{k_1} \sum_{k_1'} 2VA_2k_2A_1A_1'^{*} \exp[i(k_2x-\omega_2t)] \exp(i(k_1-k_1')x - i(\omega_1-\omega_1')t), \tag{19}$$

where A_2 is the action of the longitudinal wave. Note that in our interaction, a transverse wave decays into another transverse wave and a longitudinal wave. Since each scattering event neither creates nor destroys transverse waves, the total number (defined in terms of the action) of transverse waves is conserved. That is,

$$\frac{d}{dt} \sum |A_1|^2 = 0. \tag{20}$$

Therefore we can rewrite the left-hand side of (19) as

$$\frac{d}{dt}\left(|A_1|^2 k_1\right) = \sum |A_1|^2 \frac{dk_1}{dt} = \sum |A_1|^2 \frac{\partial k_1}{\partial v_{g1}} \frac{dv_{g1}}{dt}. \tag{21}$$

The summation over the action implies a kind of averaging or weighting. Let us define

$$(h)_{avg} \equiv \left[\sum_{k_1} |A_1|^2\right]^{-1} \sum_{k_1} |A_1|^2 h(k_1), \tag{22}$$

where h is any quantity, and $(h)_{avg}$ is taken as the average of the quantity h over the wave packet. This procedure is reasonable, since $\Delta k_1 \ll k_1$. Note that on the right-hand side of (19) the double summation reduces to a single summation because the phases of A_1 and A_1' are uncorrelated. Since $\exp(ik_2x)$ is assumed to be slowly varying compared

with $|A_1|^2$, we can replace x with $(x)_{avg}$ (where $(x)_{avg}$ is the average coordinate of the wave packet), since $|A_1|^2$ is nearly zero except at $x = (x)_{avg}$. Note that we have invoked the broadband nature of wave packet 1 ($\Delta k_1 \gg k_2$) in handling the right-hand side of (19), whereas in dealing with the left-hand side we used the narrow-band nature ($\Delta k_1 \ll k_1$). Using (21) and (22), we can now rewrite (19) as

$$\frac{d}{dt}(v_{g1})_{avg} = -\mathrm{Re}\left[2VA_2k_2\left(\frac{\partial v_{g1}}{\partial k_1}\right)_{avg} \exp\{i[k_2(x)_{avg}-\omega_2 t]\}\right]. \tag{23}$$

Note that d/dt is now defined as $\partial/\partial t + (v_{g1})_{avg}\,\partial/\partial x$, where $(v_{g1})_{avg}$ is the average group velocity and $(x)_{avg}$ is the average spatial coordinate of the wave packet. Note that $d(x)_{avg}/dt = (v_{g1})_{avg}$ so that (23) may be put in the form

$$\frac{d^2(x)_{avg}}{dt^2} = -\mathrm{Re}\left[2VA_2k_2\left(\frac{\partial v_{g1}}{\partial k_1}\right)_{avg} \exp\{i[k_2(x)_{avg}-\omega_2 t]\}\right]. \tag{24}$$

Note that (24) implies the same force/mass, F, as in (4). Here the derivation makes clear its role as a physical force on the wave packet. We may note from (24) that the force tends to restore the wave packet to the bottom of the wave trough (see Fig. X-23).

Since (24) has been solved[7] within the context of the wave-particle interaction, we simply note that the resulting trapping time τ_{tr}^{w} is as in (16) and a trapping width, $v_{tr}^{w} \equiv 2\pi/\left(k_2\tau_{tr}^{w}\right)$, may be so defined that the wave packet is likely to be trapped when

$$\left|\frac{\omega_2}{k_2} - (v_{g1})_{avg}\right| < v_{tr}^{w}. \tag{25}$$

Resonance Broadening Width

The analogy between the wave-particle interaction and the wave-wave cascading process both in the turbulent and coherent limits allows us to predict with confidence that the resonance broadening corrections to these interactions are also similar. In particular, beginning with (25) in the many-wave 2 limit, we may trace the same steps in deriving the resonance broadening widths in the wave-particle interaction to obtain

$$\delta v_{g1} = \left|\frac{D}{k_2\pi}\right|^{1/3},$$

$$\delta k_2 = \left|\frac{k_2^2 D}{\pi}\right|^{1/3} \Big/ \left|v_{g2} - \omega_2/k_2\right|. \tag{26}$$

At this point, these results can be obtained by mathematically substituting the analogous quantities into previously derived results for the wave-particle interaction. The resonance broadening widths may now be used to correct the weak-turbulence equations in a manner previously reported.[1]

For n-wave interactions, the same ideas hold. For example, it is expected that resonance broadening does not occur in four-wave interactions unless two waves, say 1 and 3, belong to the same spectrum in such a way that the diffusion approximation can be made. It then follows that this interaction, which involves the cascading of energy in wave packet 1, is analogous to nonlinear Landau damping. It can be argued, by analogy with the resonance width obtained for the nonlinear Landau damping interaction, that

$$\delta v_{g1} \sim [N_2 N_4 / |(v_{g2}-v_{g1})(v_{g4}-v_{g1})|]^{1/2}. \tag{27}$$

Note that the resonance broadening widths in (27) are proportional to N, whereas detuning widths are proportional to N^3, and hence much smaller. Higher order wave-particle or wave-wave interactions, however, do not exhibit resonance broadening. For example, for a four-wave-particle interaction (or a five-wave interaction with two waves belonging to the same wave packet) we may scale[1,4]

$$\delta v \sim \left[(N_1 \delta k_1)^{1/2} (N_2 \delta k_2)^{1/2} (N_3 \delta k_3)^{1/2}\right]^{1/2} \tag{28}$$

that scales as N^3 which is of the same order as detuning effects. Thus we have essentially categorized one-dimensional resonance broadening phenomena into two classes: interactions with resonance widths $\sim N^{1/3}$ and detuning effects $\sim N$, and interactions with resonance widths $\sim N$ and detuning effects $\sim N^3$. Higher order wave interactions in which a number of waves belong to the same wave packet or higher order wave-particle interactions in which the group velocity of some spectra equals the resonant-particle velocity, if resonance broadening occurs, reduce to one of these two classes.

References

1. N. J. Fisch and A. Bers, Progress Report No. 115, Research Laboratory of Electronics, M. I. T., January 1975, pp. 163-172.
2. V. N. Tsytovich, Nonlinear Effects in Plasma (Plenum Press, New York, 1970), Chap. V.
3. Equation 4 is a special case of the kinetic wave equation [B. B. Kadomtsev, Plasma Turbulence (Academic Press, Inc., New York, 1965)]:

   $$\left(\frac{\partial}{\partial t} + \frac{\partial \omega}{\partial k}\frac{\partial}{\partial x} - \frac{\partial \omega}{\partial x}\frac{\partial}{\partial k}\right) N(x, k, t) = 0,$$

   and can be derived by calculating $\partial\omega/\partial x$ of wave packet 1 because of the inhomogeneity of the plasma caused by wave 2. For instance, in the example considered in this

report (the generation of plasma waves by a collimated beam of transverse waves) we have $\omega_1^2 = \omega_{pe}^2 + k^2c^2$ which implies

$$\frac{\partial \omega_1}{\partial x} = \frac{q^2}{2m_e \epsilon_o \omega_1} \frac{\partial n}{\partial x} = \frac{-qk_2^2}{2m_e \omega_1} \operatorname{Re}\left[E_2 e^{ik_2x - i\omega_2 t}\right].$$

In writing the second equality we used Poisson's equation to relate the inhomogeneity of the charge density to the electric field of the plasma waves. This result is easily shown to agree with that obtained by plugging into Eq. 4 the expression for V (see, e.g., F. W. Chambers, R. J. Hawryluk, and A. Bers, Quarterly Progress Report No. 110, Research Laboratory of Electronics, M. I. T., July 15, 1973, pp. 45-53, Eq. 15).

4. N. J. Fisch, S. M. Thesis, Department of Electrical Engineering, M. I. T., January 1975 (unpublished).

5. V. N. Tsytovich, Zh. Tekh. Fiz. [Sov. Phys. – Tech. Phys.] 34, 773 (1965).

6. A. Bers, "Linear Waves and Instabilities," Massachusetts Institute of Technology Plasma Research Report PRR-7210, 1972.

7. T. O'Neil, Phys. Fluids 8, 2255-2262 (1965).

7. TEMPORALLY GROWING EIGENMODES OF A FINITE INHOMOGENEOUS PARAMETRIC SYSTEM

National Science Foundation (Grant ENG75-06242)

Frank W. Chambers, Abraham Bers

We continue our studies of parametric interactions in an inhomogeneous plasma.[1] In this report we examine the effects of a finite interaction length in one dimension. Rosenbluth and his co-workers[2,3] and Piliya[4] have shown that, in an infinite medium with a linear mismatch $\Delta k = K'x$ introduced by the density gradient, the pulse response of the system does not grow exponentially for all times; rather, saturation takes place after a gain of $e^{\pi\lambda}$, $\lambda = \gamma_o^2/(K'v_1v_2)$ has occurred. Other workers have attempted to recover the absolute instability (an exponentially growing (in time) normal mode of the system) by considering different boundary conditions for the coupled modes and different spatial profiles for the coupling coefficient. White et al.[5] considered a Gaussian profile for the coupling and found a range of half-widths for which growing modes exist, but they found no growing modes for a sufficiently long system. Nicholson and Kaufman[6] in a numerical integration allowed for fluctuations in the mismatch and recovered the absolute instability for certain amplitudes and characteristic wavelengths of the fluctuations. DuBois et al.[7] considered an arbitrarily long system with a square profile for the coupling coefficient. They investigated by WKB methods the dispersion relation of the system and found growing modes for any sufficiently long system. They did not give a description of the spatial profile of these growing eigenmodes. We shall derive

an analytical form for the mode dispersion relation and the profiles for the eigenmodes. We find the modes highly localized near the sharp boundaries assumed for the coupling coefficient. As we make the system arbitrarily long we find that these modes persist but remain tied to one or the other boundary. Since we are interested in the linear evolution of parametric instabilities to a state where nonlinear effects dominate, we thus find that the transient response away from the boundaries may be more important. The normal-mode solution is only important for very short systems or systems with the transient response effectively suppressed by the inhomogeneity. When the normal modes do become important the response is localized about the discontinuity in the coupling coefficient. To complete this work, we shall analyze the semi-infinite problem with the coupling coefficient having only one discontinuity.

We investigate the following system of coupled-mode equations[1] for the existence of exponentially growing normal modes:

$$(\partial/\partial t + v_1 \partial/\partial x + \gamma_1)\, a_1 = \gamma_o a_2^* \, e^{iK'x^2/2} \tag{1}$$

$$(\partial/\partial t + v_2 \partial/\partial x + \gamma_2)\, a_2^* = \gamma_o a_1 \, e^{-iK'x^2/2}. \tag{2}$$

For simplicity, we assume $v_1 = -v_2 = v$, that is, the modes are propagating exactly oppositely, and $\gamma_1 = \gamma_2 = 0$, that is, the modes are undamped. The coupling coefficient is assumed to have the boxed profile illustrated in Fig. X-26. The box has length ℓ and

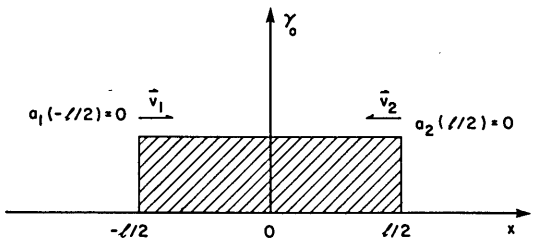

Fig. X-26.

Assumed spatial profile of the coupling coefficient γ_o and the boundary conditions on modes 1 and 2 for the finite-length inhomogeneous normal-mode problem.

the coupling vanishes outside this region. The appropriate boundary conditions are that no mode 1 or 2 propagates into the box.

We begin to solve (1) and (2) by letting $a_1 = \hat{a}_1 \exp(iK'x^2/4)$, $a_2^* = \hat{a}_2^* \exp(-iK'x^2/4)$ and eliminating $\hat{a}_2^*$ from the equations. Furthermore, we assume that the time dependence of a_1 and a_2^* is e^{pt}. This results in a single equation for $\hat{a}_1$:

$$\left\{\frac{\partial^2}{\partial x^2} + \frac{1}{4}\left(K'x - \frac{2ip}{v}\right)^2 + \left(\frac{iK'}{2} + \frac{\gamma_o^2}{v^2}\right)\right\}\hat{a}_1 = 0. \tag{3}$$

By making the substitution $X = e^{i\pi/4}\,(K'^{1/2}x - i2p/K'^{1/2}v)$, the equation becomes the parabolic cylinder equation

$$\left\{\frac{\partial^2}{\partial X^2} - \frac{X^2}{4} + \frac{1}{2} - \frac{i\gamma_o^2}{K'v^2}\right\}\hat{a}_1(X) = 0. \tag{4}$$

We choose as our solutions

$$\begin{matrix} D_\nu(X) \\ D_\nu(-X) \end{matrix} \qquad \nu = \frac{-i\gamma_o^2}{K'v^2} = -i\lambda$$

where $D_\nu(X)$ is the parabolic cylinder function (PCF), index ν, of X. We now have a general solution, a linear combination of $D_\nu(X)$ and $D_\nu(-X)$. We apply our homogeneous boundary conditions at $\pm\ell/2$, then the resulting equation for a nontrivial solution, which we shall refer to as the dispersion relation (DR) describing the growth rate Re p of the normal modes of the system, is

$$D_\nu(-X_L)\,D_{\nu-1}(X_R) = -D_\nu(X_L)\,D_{\nu-1}(-X_R)$$

$$X_L = \left(\frac{-K'^{1/2}\ell}{2} - \frac{i2p}{K'^{1/2}v}\right)e^{i\pi/4}$$

$$X_R = \left(\frac{K'^{1/2}\ell}{2} - \frac{i2p}{K'^{1/2}v}\right)e^{i\pi/4}. \tag{5}$$

Coupled with this dispersion relationship we can write the eigenvectors $\hat{a}_1$ and $\hat{a}_2^*$. We include two forms for each. When the dispersion relation is satisfied exactly the forms are equivalent; however, the numerics of the problem are quite difficult and when there is a slight numerical error in solving the DR for p one or the other forms of the eigenvector will be preferred.

$$\hat{a}_1(X) = a_o(D_\nu(-X_L)\,D_\nu(X) - D_\nu(X_L)\,D_\nu(-X)) \tag{6}$$

$$= a_o'(D_{\nu-1}(-X_R)\,D_\nu(X) + D_{\nu-1}(X_R)\,D_\nu(-X)). \tag{7}$$

$$\hat{a}_2^*(X) = a_o\,e^{i\pi/4}\lambda^{1/2}(D_\nu(-X_L)\,D_{\nu-1}(X) + D_\nu(X_L)\,D_{\nu-1}(-X)) \tag{8}$$

$$= a_o'\,e^{i\pi/4}\,\lambda^{1/2}(D_{\nu-1}(-X_R)\,D_{\nu-1}(X) - D_{\nu-1}(X_R)\,D_{\nu-1}(-X)). \tag{9}$$

In the first form in each case the form of the eigenvector guarantees that the left boundary condition at $X = X_L$ is satisfied, while the eigenvalue p is adjusted to satisfy the right boundary condition at $X = X_R$. In the second form the right-hand BC is automatically

satisfied and the eigenvalue p is adjusted to satisfy the left-hand BC.

Before proceeding, we wish to compare our procedure with that of DuBois et al.[7] The physical problem is the same for both (except that they retain damping and arbitrary group velocities) and they arrive at the same spatial differential equation but they use the approximate WKB solution rather than the exact solution. They apply the same boundary conditions to get their dispersion relation. Our approach has the advantage that we get an exact dispersion relation. Asymptotics can be applied to our solution fairly easily. We can solve the DR, Eq. 5, for p and then we can calculate the eigenvectors from Eqs. 6-9. This approach has, however, serious drawbacks. It is applicable only to the square boundary problem; we cannot easily change the profile of the coupling coefficient. The advantages of an analytical DR over a WKB DR with its implied integrations are countered by the difficulty of calculating the parabolic cylinder functions for complex index and argument. Our approach for the PCFs has been to calculate from a Taylor's series expansion for small $|X|$ and from the appropriate asymptotic series for large $|X|$.[8-11] Comparisons were made between our calculated values of $D_\nu(X)$ and tabulated values.[8,12] Agreement was good, but it must be noted that there are no tables for complex ν. Since our routines work well for real ν and the results for complex ν are reasonable, we believe the results are correct.

One set of roots of the full dispersion relation is shown in Fig. X-27. Real and imaginary p are normalized to γ_o and they are plotted as functions of the normalized system length $K'^{1/2}\ell$. This plot was carried out for λ fixed at 2.0 for comparison with the results of DuBois et al.[7] By fixing λ, we keep constant the ratio of the amplification length v/γ_o to the inhomogeneity length $K'^{-1/2}$, while varying the system length compared with these two lengths and calculating the unstable modes that are present. Later we shall discuss briefly the solutions with varying λ. For very short lengths with the system just above the usual backward-wave oscillator start of oscillation threshold[13] the roots coincide in the homogeneous and inhomogeneous cases. Here the finite-length effects dominate over the inhomogeneity effects. But when the system is longer and a second unstable p branch appears, the two solutions differ greatly. The two roots merge at $K'^{1/2}\ell = 3.7$ and take on the same Re p value with opposite Im p for increasing lengths. These modes with positive Re $p > 0$ and with Im p increasing (decreasing) linearly with ℓ are of most interest to us. To further understand these modes that persist for arbitrarily long systems, we shall calculate their eigenvectors and study the asymptotic limits of the dispersion relation and eigenvectors for large ℓ.

We note several other features in Fig. X-27. For the homogeneous case p is always real; only in the inhomogeneous case does p acquire an imaginary part corresponding to a frequency shift in the normal modes. Our scale length is approximately $2^{1/2}$ smaller than that of DuBois et al.;[7] so we believe they are in error. There are roots also for Re p in the lower right corner of the plot[7] that we have not calculated.

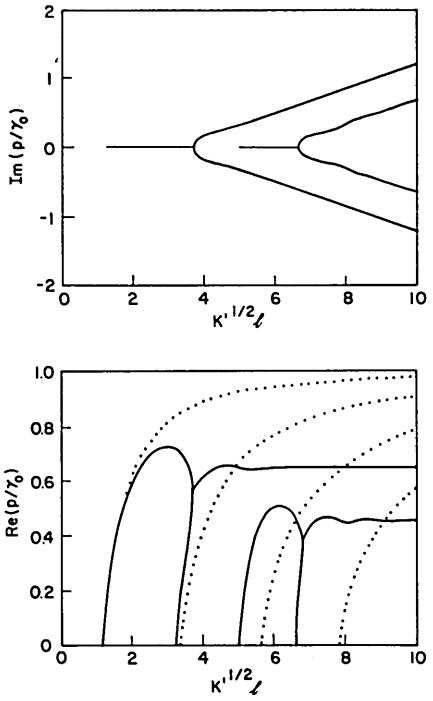

Fig. X-27.

Real and imaginary parts of the normal-mode eigenfrequency p normalized to γ_o as a function of the normalized system length $K'^{1/2}\ell$ for a fixed $\lambda = 2.0$. Dotted lines on the plot Re p indicate how the mode eigenfrequencies would appear in the absence of inhomogeneity.

To investigate the roots for large ℓ, we can apply asymptotic methods to our DR. Looking at the definitions of X_L and X_R in (5), we might first allow $|X_R| \to \infty$, $|X_L| \to \infty$ as $\ell \to \infty$. By substituting asymptotic forms for the PCF, it can be shown that there are no roots. We note, however, that both X_L and X_R depend on p; if we permit p to become arbitrarily large as ℓ increases (and this actually does happen), then we can no longer have both X_L and X_R large. If we assume one or the other large, then for the system dispersion relation for the eigenvalue p we find

$$|X_L| \gg 1 \qquad D_{-\nu}(iX_R) = 0. \tag{10}$$

$$|X_R| \gg 1 \qquad D_{\nu}(X_L) = 0. \tag{11}$$

These approximations do indeed exactly give the roots for large ℓ which are seen in Fig. X-27. The $|X_R| \gg 1$ DR yields the positive imaginary root, while the $|X_L| \gg 1$ DR yields the negative imaginary root. We note that for large ℓ there is a large frequency shift in Im p; in fact, as $\ell \to \infty$ we find that in order for X_L or X_R to remain finite Im $p \cong \pm K' \ell v/4$. The reason for this frequency shift will become apparent when we examine the physical mechanism responsible for the unstable modes.

To understand the nature of these modes physically, we have calculated their eigenvectors for several values of ℓ and p with $\lambda = 2.0$. In Fig. X-28 for $K'^{1/2}\ell = 2.0$ we see eigenmodes similar to those of the homogeneous case. We plot the magnitude of the mode amplitude against the normalized distance $K'^{1/2}x$. Note that the boundary conditions are satisfied. In Fig. X-29 we see eigenvectors for modes at $K'^{1/2}\ell = 10.0$

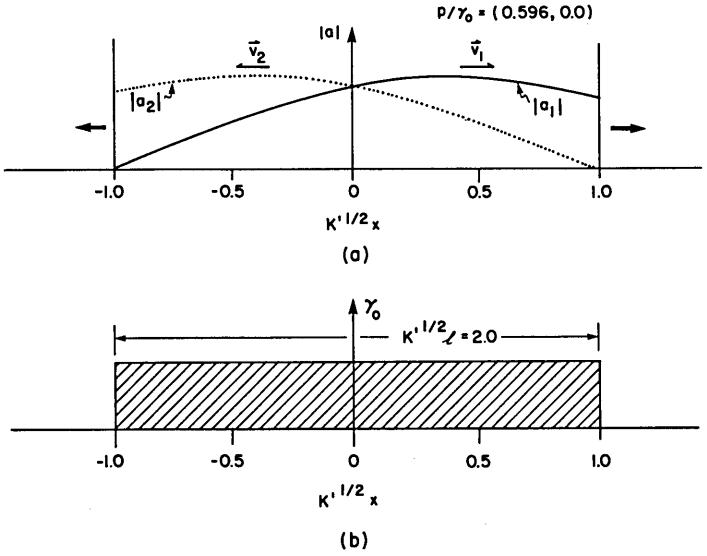

Fig. X-28.

Spatial normal-mode pattern for a finite inhomogeneous system. (a) $|a_1|$ (solid curve) and $|a_2|$ (dotted curve) for a system of normalized length $K'^{1/2}\ell$ = 2.0. For this mode λ = 2.0 and p/γ_o = (0.596;0.0) as calculated for Fig. X-27. (b) Spatial profile of the coupling that produced this eigenmode.

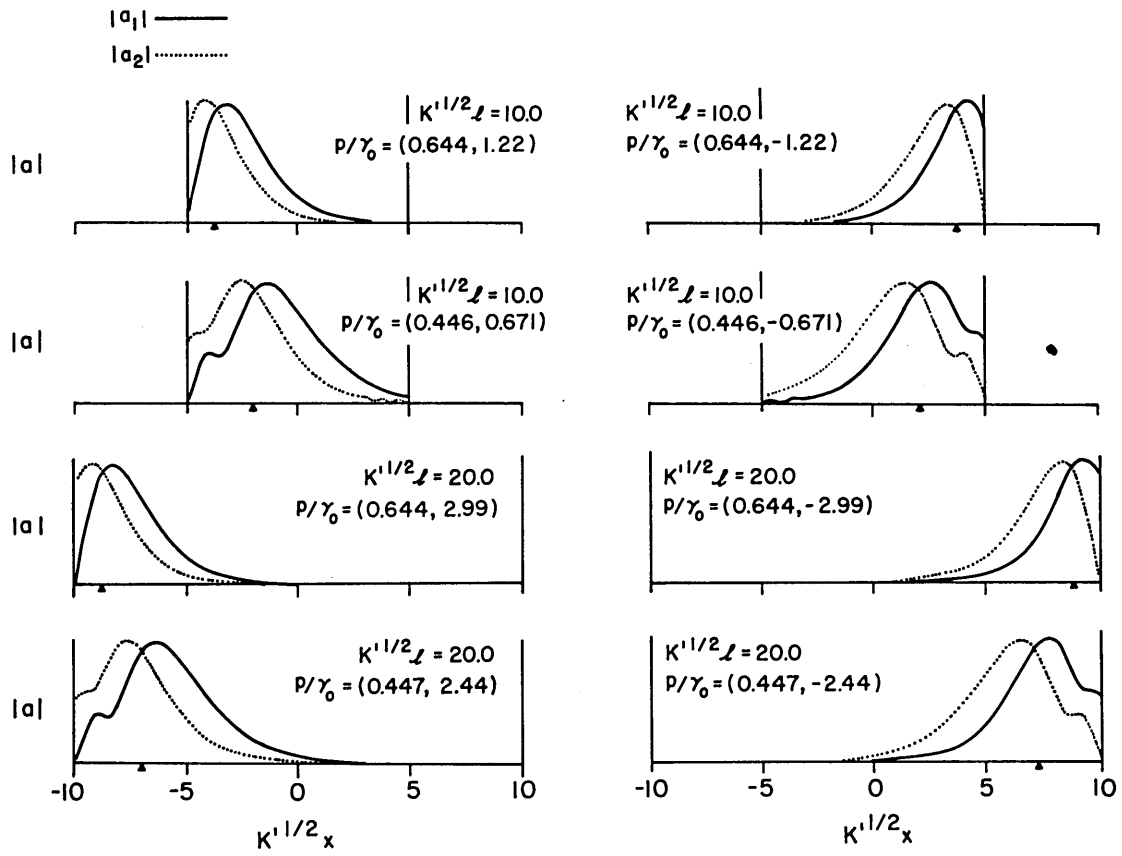

Fig. X-29. Finite-length eigenmodes $|a_1|$ (solid curve) and $|a_2|$ (dotted curve) for Im p > 0 (left) and Im p < 0 (right) for $K'^{1/2}\ell$ = 10.0 (upper) and $K'^{1/2}\ell$ = 20.0 (lower). Values of p/γ_o for each mode are given. The roots for p were calculated with λ = 2.0 (see Fig. X-27). Arrowheads in each plot indicate the exact resonance point.

and at $K'^{1/2}\ell = 20.0$ where the inhomogeneity has a large effect. With $K'^{1/2}\ell = 10.0$ we plot the two modes from Fig. X-27 with the largest real p. We plot the Im $p > 0$ root on the left and the Im $p < 0$ root on the right. The Im $p > 0$ mode is peaked near the left-hand boundary and the Im $p < 0$ mode at the right. As we proceed to $K'^{1/2}\ell = 20.0$ the eigenvectors for the two modes are presented. They have almost the same shape as before; they are merely displaced so that they hug the boundaries. At $K'^{1/2}x = 0$ the modes have very nearly zero amplitude. The eigenfunctions with lower growth rates become more complex and their widths are increased but the predominant features remain the same; the modes hug the boundaries. We are immediately led to suspect that these modes are strictly an edge effect; they are genuinely growing normal modes but their physical significance must be interpreted carefully.

To further understand this problem, we solve the semi-infinite eigenmode problem taking the boundary conditions given in Fig. X-30. This is actually a simpler problem

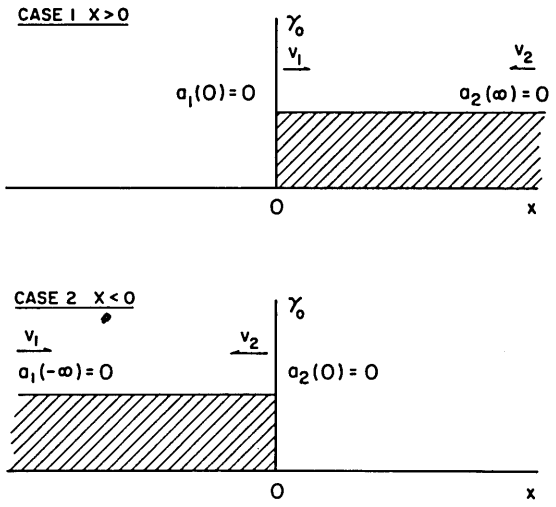

Fig. X-30.

Assumed spatial profile of the coupling coefficient γ_o and the boundary conditions on modes 1 and 2 for both semi-infinite cases. Case 1: coupling occurs for $x > 0$. Case 2: coupling occurs for $x < 0$.

to solve than the original finite-length problem. We note that requiring one of the modes to approach zero at infinity implies that the other mode will also, since from Eqs. 1 and 2 it is a linear combination of the first mode and its derivative. The solution proceeds in a manner similar to the finite-length case and we find the following dispersion relations:

$$\left.\begin{array}{ll} \text{Case 1. For } x > 0, & D_\nu(X_o) = 0 \\ \text{Case 2. For } x < 0, & D_{-\nu}(iX_o) = 0 \end{array}\right\} \quad \begin{array}{l} \nu = -i\lambda. \\ X_o = (-i2p/K'^{1/2}v)\, e^{i\pi/4}. \end{array} \qquad (12)$$

(13,

The forms of the eigenvectors are the same as those in the two-boundary problem if we pick the one that satisfies the remaining boundary condition. Thus for coupling with $x > 0$

forms (6) and (8) are appropriate, while for $x < 0$ forms (7) and (9) must be used. We note that the dispersion relations just calculated are of the same form as the asymptotic DRs (10) and (11) for the two-boundary problem discussed previously. Now we can compute the semi-infinite eigenvalues and eigenvectors for $\lambda = 2.0$. The resulting normal modes are presented in Fig. X-31. The first four eigenvectors are plotted in descending

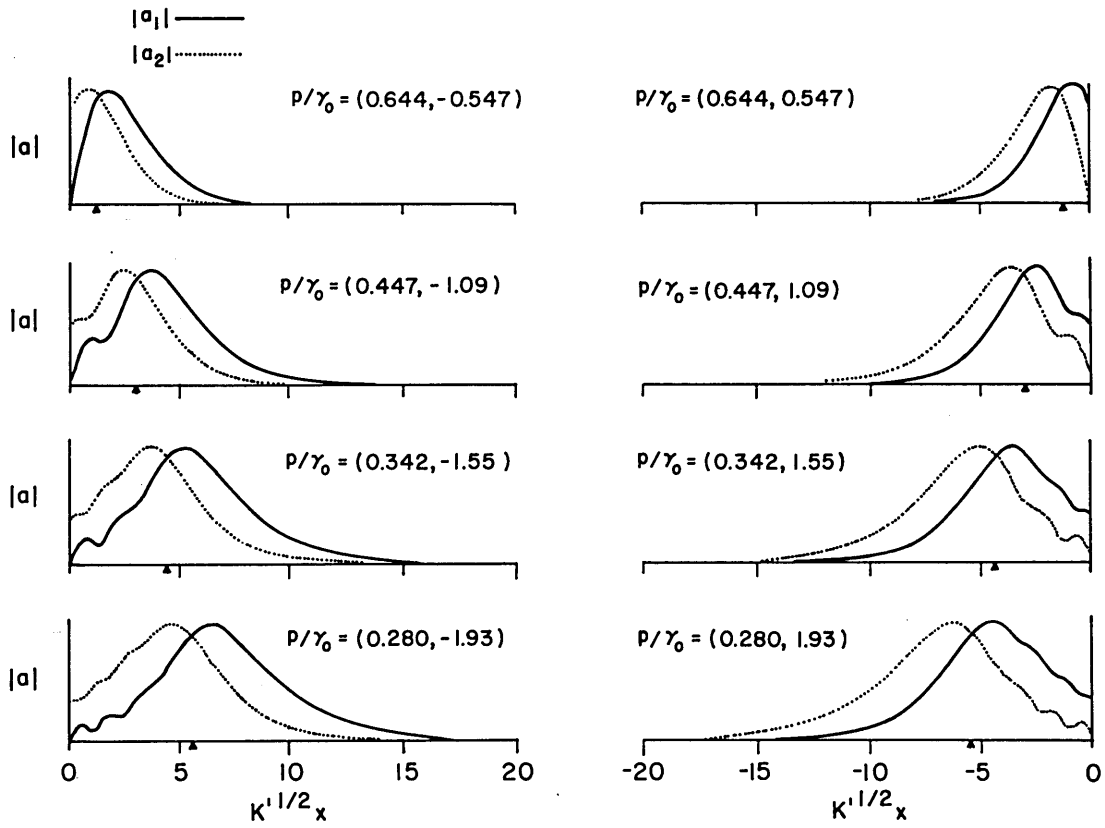

Fig. X-31. Semi-infinite eigenmodes $|a_1|$ (solid curve) and $|a_2|$ (dotted curve) for Case 1, $x > 0$ (left) and Case 2, $x < 0$ (right). The four highest Re p modes are plotted in descending order from top to bottom. Values of p/γ_0 for each mode are given. The roots for p were calculated with $\lambda = 2.0$. Arrowheads in each plot indicate the exact resonance point.

order of Re p for $x > 0$ and $x < 0$. We have essentially reproduced the finite-length two-boundary eigenvectors with no major modifications. In other words, we have shown that the finite-length growing modes for long systems are due to and attached to one or the other boundary of the coupled regions.

We shall now examine several aspects of these solutions. First, we give a physical explanation for the existence of these growing modes. We show how this result is

not inconsistent with the work of Rosenbluth who found no growing modes. Next, we explore the physical significance of the large Im p encountered with the long system lengths and discuss the extension of these results to other parameter regions. Finally, we examine the applicability of this solution to the actual physical problem of laser-pellet interaction.

The physical interpretation of these eigenmodes is straightforward. The growth occurs because at the boundary there is no out-of-phase incoming wave that might suppress the interaction. In calculating the pulse response of the infinite medium, we find that out-of-phase feedback suppresses the growth of the instability. At each boundary the feedback is suppressed and the response grows exponentially. In the case of the Gaussian profile (5) it was shown by WKB techniques that there are unstable modes when

$$v/\gamma_o < \ell_G < \gamma_o/(vK'), \tag{15}$$

where ℓ_G is the half-width of the Gaussian coupling region. We can understand this result qualitatively in terms of our present work. The first condition of (15) is simply the start of oscillation length modified for a Gaussian profile. The other condition is that the coupling possess a sufficiently steep gradient. We see that sharp edges give rise to growing modes. This calculation shows that as the edges are smoothed out the instability disappears. Similar results were found by DuBois et al.[7] Nicholson and Kaufman[6] have also found that fluctuations in the mismatch term about an assumed linear profile can cause the system to be absolutely unstable.

We shall now consider the origin of the calculated frequency shifts, the Im p, of the eigenmodes. The origin of the mismatch term is illustrated in Fig. X-32. The dispersion relations of the plasmons (EP) and the plasmons shifted by the laser frequency and wave number (EP') are plotted (Fig. X-32a) at two positions, x_1 and x_2, where the plasma density has decreased in going from position 1 to 2. The intersections on the right-hand side give rise to the two-plasmon interaction in the zero coupling limit. In the coupling-of-modes approximation we shift the origin of the ω-k plot to the intersection of interest and linearize the two mode dispersion relations of the coupled modes about this point. This linearized shifted dispersion relation at $x = x_1$ is shown in Fig. X-32b. If we look at the dispersion relations at $x = x_2$ shown in Fig. X-32c, we see that for the same frequency, $\omega = 0$, the two modes do not occur at the same k; rather, there is a mismatch which produces Δk. This linearized dispersion relation, including mismatch and coupling, is described by Eqs. 1 and 2. In Fig. X-32c we note that the two dispersion relations do intersect at a shifted $\delta\omega$ where

$$\delta\omega = v\frac{\Delta k}{2} = \frac{vK'\Delta x}{2}. \tag{16}$$

In fact, given any frequency ω, in this linearized mismatch problem we can always find an x such that the modes will be in exact resonance.

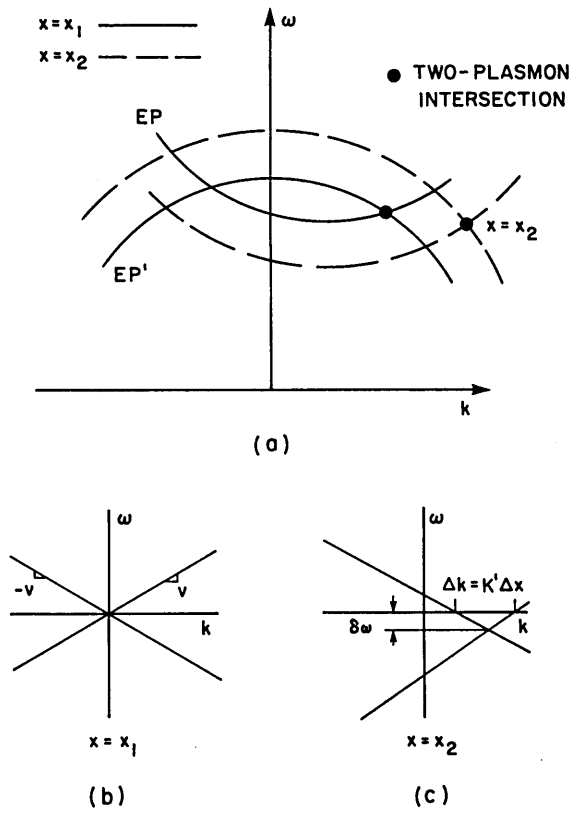

Fig. X-32. (a) An actual pair of intersecting plasmon dispersion relations ω vs k for the two-plasmon interaction plotted at different points, x_1 and x_2, in the density gradient. (b) and (c) show the coupling-of-modes approximation to the dispersion relation in (a) for each density. In (c) we find the origin of the mismatch term from the density gradient; hence, we can simply relate Δk and $\delta\omega$.

In Eqs. 1 and 2 we assumed that the frequency of the mode is the one that is in exact resonance at x = 0. Then when an eigenmode frequency with Im p ≠ 0 is calculated it indicates that for the exact phase matching to take place we should have picked another x. From Eq. 16 this normalized x is given by

$$K'^{1/2}x = -2\lambda^{1/2}\ \mathrm{Im}\ p/\gamma_o. \tag{17}$$

In Figs. X-29 and X-31 we have indicated by arrowheads the x value at which the ω and k of the eigenmode are in exact resonance. Had we chosen this point as the origin in each calculation the resulting p would have been pure real. The large values of Im p encountered in solving the DR indicate that our exact resonance point is far from the center; in fact, in all cases it is quite near the edge where the eigenmode amplitudes are largest.

We can also show this property mathematically. Since the dephasing depends on x^2, it might appear that a shift of the origin by some ℓ would completely change the problem. If we let $y = x + \ell$ in the Laplace transformed mode-coupling equations and then let

$$a_1 = \hat{a}_1 \, e^{iK'(\ell^2 - 2\ell y)/4}$$

$$a_2 = \hat{a}_2^* \, e^{-iK'(\ell^2 - 2\ell y)/4}$$

we find for a_1, a_2:

$$\left(p + v\,\frac{iK'\ell}{2} + v\,\partial/\partial y\right)\hat{a}_1 = \gamma_o \hat{a}_2^* \exp\left(\frac{iK'}{2}\,y^2\right) \tag{18}$$

$$\left(p + v\,\frac{iK'\ell}{2} - v\,\partial/\partial y\right)\hat{a}_2^* = \gamma_o \hat{a}_1 \exp\left(\frac{-iK'}{2}\,y^2\right). \tag{19}$$

Now if we just shift $p \rightarrow p' - iK'v\ell/2$ we are back to our original equations with an additional phase factor on a_1 and a_2^*. The frequency shift is the same as we have predicted before. Again, a shift in frequency can be removed by a shift in the exact resonance point.

We note from Fig. X-31 that the eigenvectors in the semi-infinite case are quite small away from the boundaries; however, since they are growing exponentially in time, they will eventually reach large amplitudes even away from the boundary (although these amplitudes will still be small compared with the amplitudes near the boundary). Far away from the edge, say at $x = \ell$, we can write for a_1 with phase factors ignored

$$a_1 \propto e^{(\mathrm{Re}\ p)t}\, D_\nu(X); \qquad X = e^{i\pi/4}(K'\ell - i2p/K'^{1/2}v)$$

$$\propto e^{(\mathrm{Re}\ p)t}\, e^{-X^2/4}$$

$$\propto e^{(\mathrm{Re}\ p)(t-\ell/v)}. \tag{20}$$

Thus the amplitude at $x = \ell$ remains exponentially small until $t > \ell/v$; that is, until a pulse originating at the boundary would propagate to ℓ. If we allow ℓ to become arbitrarily large, the normal mode produces exponential growth only after an arbitrarily long time. Until this time the infinite inhomogeneous pulse response of Rosenbluth et al.[2,3] is the appropriate solution away from the boundary. If this response brings the system into the nonlinear state, then the normal modes are unimportant.

Thus far, we have considered a system with $\lambda = 2.0$, no damping, and $v_1 = -v_2 = v$, and normal modes with varying system lengths. Recapitulating, we find 4 regions in the system length $K'^{1/2}\ell$. If this length is too short, there are no unstable modes. For

systems slightly longer than the usual backward-wave oscillator threshold we find growing modes very similar to the homogeneous, finite-length system modes. After a transition length where both finite-length effects and inhomogeneity effects are important, we find inhomogeneous normal modes that are due to, and attached to, the separate boundaries. For these systems the total length is no longer important and the semi-infinite normal-mode description suffices. We find that for other values of λ the dispersion relation exhibits similar qualitative behavior as a function of system length. Since the system is sufficiently long and inhomogeneous for the laser-pellet interaction parameters, we shall concentrate on the semi-infinite $x > 0$ problem, first for varying λ and then for varying $|v_2|/v_1 \equiv a$.

With $a = 1$, varying λ for the semi-infinite case, we find that the calculated normalized growth rate for $\lambda \lesssim 5$ is described[7] by

$$\mathrm{Re}\left(\frac{p}{\gamma_o}\right) = \left(1 - \frac{1}{\sqrt{\pi}\,\lambda^{2/3}}\right). \tag{21}$$

This form has a threshold for growing modes, $\lambda > \frac{1}{\pi^{3/4}} = 0.424$, which agrees well with the calculated value. Thus for a sufficiently inhomogeneous system the normal-mode growth is suppressed. As the inhomogeneity becomes weaker relative to the gain of the system the growth rate approaches that of the absolute instability. For all λ, however, the eigenmodes remain localized at the boundary. The modes are concentrated in x so that $K'^{1/2}x \lesssim 1$. When γ_o/v is increased with K' fixed, and hence λ increases, the growth rate increases but the width of the modes remains nearly constant. It appears physically as if the inhomogeneity were introducing a "second boundary" into the problem. If we consider the modes to be in phase at $x = 0$, then the $\exp(iK'x^2)$ in the coupling oscillates rapidly for $K'^{1/2}x > 1$, thereby effectively suppressing the coupling. This "second boundary" explains why the semi-infinite and long finite-length system problems give the same result. Furthermore, the lower limit on λ can be regarded as the condition that the backward-wave oscillator criterion be satisfied between $x = 0$ and this "second boundary." Modes 1 and 2 propagate freely away from this "bounded" interaction region and exhibit an exponential falloff in space because they originate from a source growing exponentially in time. These tails decay as $\exp\{-\mathrm{Re}\,(p)x/v\}$ (see Eq. 20) and for weakly growing modes may appear quite long.

These normal-mode solutions have been observed by Nicholson and Kaufman at the University of California, Berkeley.[14] They integrate Eqs. 1 and 2 numerically and their calculations are in excellent agreement with our analytic results both for growth rate and spatial profile. Furthermore, their numerical results can serve as a guide to how the modes scale with changing $a = |v_2|/v_1$ (v_1 and v_2 assumed opposite), since we have not done this analytically. For various integer a^{-1} we find that their program computes

growth rates given by

$$\mathrm{Re}\left(\frac{p}{\gamma_o}\right) = \frac{2|v_1 v_2|^{1/2}}{v_1 + |v_2|}\left(1 - \frac{1}{\sqrt{\pi}\,\lambda^{2/3}}\right)$$

$$= \frac{2\alpha^{1/2}}{1+\alpha}\left(1 - \frac{1}{\sqrt{\pi}\,\lambda^{2/3}}\right). \tag{22}$$

This result is intuitive, since the factor involving the α is the usual modification to the homogeneous absolute instability growth rate when the modes are not propagating exactly oppositely. Furthermore, the observed normalized mode width, determined by the Nicholson and Kaufman numerical integration, scales with α as

$$K'^{1/2}_x \propto \frac{v_1}{v_1 + |v_2|} = \frac{1}{1+\alpha}. \tag{23}$$

This result is observed for runs where $\alpha < 1$, i.e., $|v_2| < v_1$ and semi-infinite (with $x > 0$). Thus we conclude from the Nicholson and Kaufman work that the nature of these modes is independent of the requirement $\alpha = 1$. We note that the localization in x scales as $K'^{-1/2}$ in agreement with our "second boundary" argument.

Having explored thoroughly the problem of finite-length, sharp-boundary, inhomogeneous normal modes, we shall now apply our result to the laser-pellet interaction problem. Our primary objective is to determine the linear evolution of the system to the nonlinear state. Considering an initial localized excitation in space, we can use the transient response in an infinite medium to describe the time development of the system until the pulse propagates into a boundary region. In our case this is the response calculated by Rosenbluth et al.,[3] characterized by a gain of $e^{\pi\lambda}$ and a spreading of this pulse. After the pulse has encountered the boundary the dominant normal modes best describe the response. Thus if $\exp(\pi\lambda) \gg 1$ and the system is sufficiently long, the pulse response will grow to the nonlinear state before encountering the boundary. If $\exp(\pi\lambda) \ll 1$, the growing normal modes will lead to the nonlinear state. If the system is sufficiently long, these will be the localized inhomogeneous modes, and for a short system they will be the backward-wave oscillator modes. Looking directly at backscatter, we might regard the system as finite and consider the pump cutoff as one boundary and the plasma edge as the other. Because of the scale lengths involved, however, this problem is effectively semi-infinite. Considering a density scale length $L_n = 100$ μm and a neodymium laser with a 1.06 μm wavelength, we can estimate $K'^{-1/2}$ as a few microns. Actual calculations of $K'^{-1/2}$ yield results of this order.[1] Since the width of the interaction region is of the order of several hundred microns, we see that normal modes that occur will be the highly localized inhomogeneous modes at the boundary. We have found

previously[1] that the $e^{\pi\lambda}$ growth was large for the Brillouin, two-plasmon, and plasmon-phonon interactions; this indicates that for these interactions away from the boundaries the system can grow and reach a nonlinear state in the transient response. In contrast, for the Raman interaction the transient response is effectively suppressed by the inhomogeneity and the normal-mode solution becomes important. This may be the first linear step in the development of the localized nonlinear spikons or cavitons.[15] With lower powers or more inhomogeneous systems this normal-mode solution might also become important for other instabilities.

References

1. F. W. Chambers and A. Bers, "Three-Dimensional Pulse Response for Wave-Wave Interactions in the Presence of Inhomogeneity," Progress Report No. 115, Research Laboratory of Electronics, M.I.T., January 1975, pp. 121-132.
2. M. N. Rosenbluth, "Parametric Instabilities in Inhomogeneous Media," Phys. Rev. Letters 29, 565 (1972).
3. M. N. Rosenbluth, R. B. White, and C. S. Liu, "Temporal Evolution of a Three-Wave Parametric Instability," Phys. Rev. Letters 31, 1190 (1973).
4. A. S. Piliya, in Proceedings of the Tenth Conference on Phenomena in Ionized Gases, Oxford, England, 1971 (Donald Parsons Co. Ltd., Oxford, 1971), p. 320.
5. R. White, P. Kaw, D. Pesme, M. N. Rosenbluth, G. Laval, R. Huff, and R. Varma, "Absolute Parametric Instabilities in Inhomogeneous Plasmas," Nucl. Fusion 14, 45 (1974).
6. D. R. Nicholson and A. N. Kaufman, "Parametric Instabilities in Turbulent, Inhomogeneous Plasmas," Phys. Rev. Letters 33, 1207 (1974).
7. D. F. DuBois, D. W. Forslund, and E. A. Williams, "Parametric Instabilities in Finite Inhomogeneous Media," Phys. Rev. Letters 33, 1013 (1974).
8. M. Abramowitz and I. A. Stegun (Eds.), Handbook of Mathematical Functions, AMS 55, National Bureau of Standards (Government Printing Office, Washington, D.C., 1964).
9. Bateman Manuscript Project (Compilers), Higher Transcendental Functions, Vol. II, based, in part, on notes left by Harry Bateman (McGraw-Hill Book Company, Inc., New York, Toronto, London, 1953).
10. E. T. Whittaker and G. N. Watson, A Course of Modern Analysis (Cambridge University Press, London, reprint 4th ed., 1950).
11. I. S. Gradshteyn and I. M. Rhyzik, Table of Integrals, Series, and Products (Academic Press, Inc., New York, 1965). Their asymptotic series 9.246 (2) is incorrect in the $\{(p(p+1)\ldots)/(2.4z^2)\}$ term where the p should not appear.
12. I. Ye Kireyeva and K. A. Karpov, Tables of Weber Functions, Vol. I (Pergamon Press, London, New York, 1961).
13. D. L. Bobroff and H. A. Haus, "Impulse Response of Active Coupled Wave Systems," J. Appl. Phys. 38, 390-403 (1967).
14. Dwight R. Nicholson, Private communication, 1975.
15. G. J. Morales and Y. C. Lee, "Ponderomotive-Force Effects in a Non-uniform Plasma," Phys. Rev. Letters 33, 1016 (1974).